

Forschungszentrum Karlsruhe
Technik und Umwelt

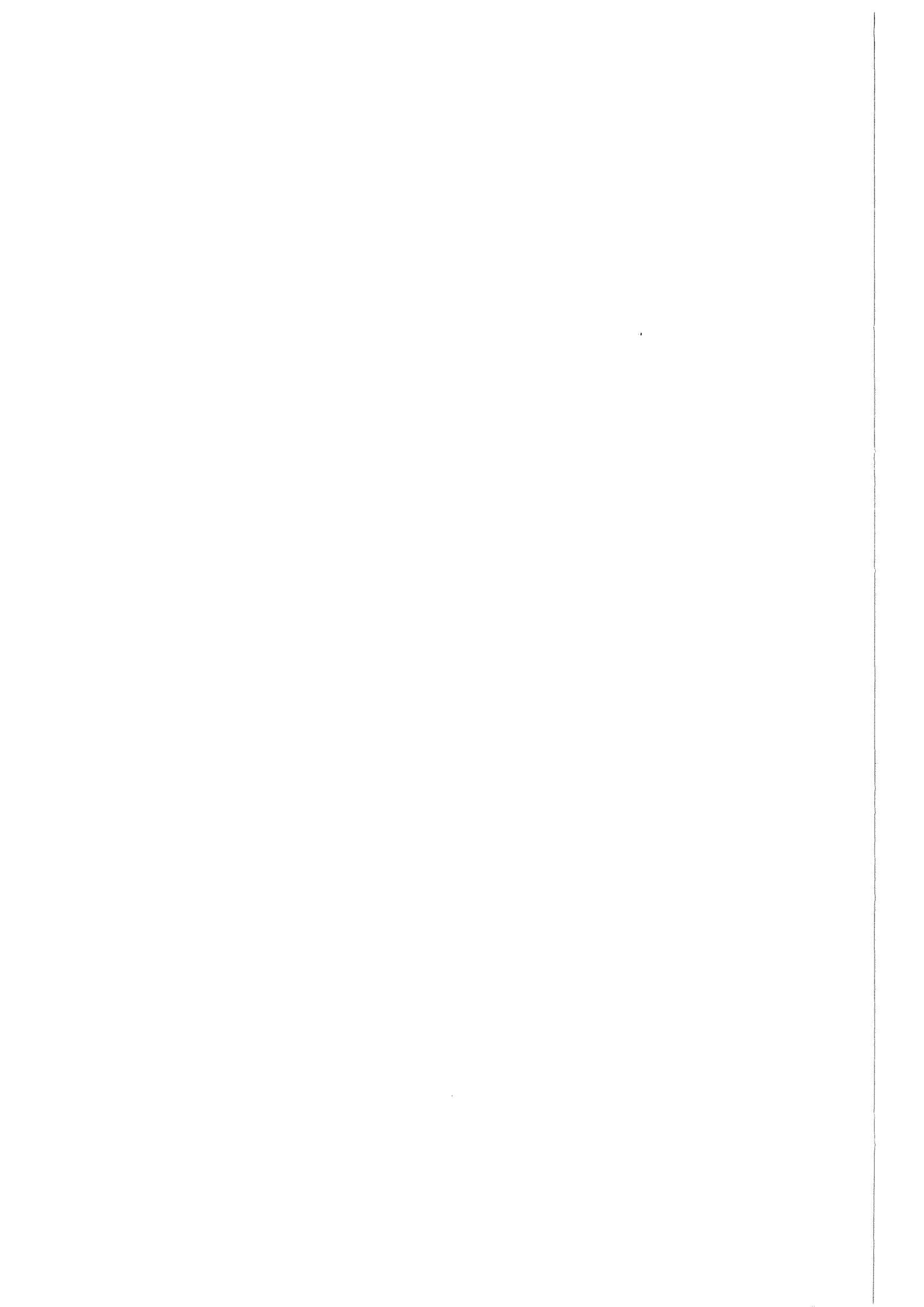
Wissenschaftliche Berichte
FZKA 6321

On the Gradient Plasticity Approach to Size Effects Part I: Reviews

**T. Malmberg, I. Tsagrakis,
I. Eleftheriadis, E. C. Aifantis**

**Institut für Reaktorsicherheit
Programm Nukleare Sicherheitsforschung**

März 2001



Forschungszentrum Karlsruhe

Technik und Umwelt

Wissenschaftliche Berichte

FZKA 6321

On the Gradient Plasticity Approach to Size Effects

Part I: Reviews

T. Malmberg, I. Tsagrakis⁽¹⁾, I. Eleftheriadis⁽¹⁾, E.C. Aifantis^{(1), (2)}

Institut für Reaktorsicherheit

Programm Nukleare Sicherheitsforschung

⁽¹⁾ Laboratory of Mechanics and Materials
Aristotle University of Thessaloniki
GR-54006 Thessaloniki, Greece

⁽²⁾ Center for Mechanics of Materials and Instabilities
Michigan Technological University
Houghton, MI 49931, USA

Forschungszentrum Karlsruhe GmbH, Karlsruhe

2001

Als Manuskript gedruckt
Für diesen Bericht behalten wir uns alle Rechte vor
Forschungszentrum Karlsruhe GmbH
Postfach 3640, 76021 Karlsruhe
Mitglied der Hermann von Helmholtz-Gemeinschaft
Deutscher Forschungszentren (HGF)
ISSN 0947-8620

On the Gradient Plasticity Approach to Size Effects

Part I: Reviews

Abstract

The influence of specimen size on the plastic deformation and failure behaviour of some metals and steels is considered. This size dependence issue relates to the question of the transferability of mechanical test results of geometrically similar scaled-down structural models to the full scale structures using similitude laws; but it concerns also the validity of small scale laboratory type test results and their use as a basis for the computational modelling of large scale components.

In Part I "Reviews" of this report a restricted review of scaled experiments at room temperature of geometrically similar specimens is given. This refers to the initiation of yielding under non-uniform states of deformation and also to the plastic deformation and fracture of smooth tensile specimens.

Among others, non-classical continuum mechanics theories have become a means to interpret size effects. Especially gradient concepts are of interest which enrich the classical plasticity theories by higher order spatial strain gradients. These model extensions implicate additional material parameters which can be associated with internal length scales characteristic for the material.

In Part I a brief review of several gradient theories of plasticity is also given, including both deformation and flow theories and a comparison of the original "symmetric stress" theory with the more recent "asymmetric stress" theory is provided.

The forthcoming Part II "Applications" exemplifies to what extend strain gradient models can describe the size influence on the deformation behaviour.

Über den Ansatz der Gradientenplastizität zur Beschreibung von Größeneffekten

Teil I: Überblicke

Zusammenfassung

Der Einfluß der Probengröße auf das plastische Deformations- und Versagensverhalten einiger Metalle und Stähle wird betrachtet. Diese Größenabhängigkeitsproblematik steht im Zusammenhang mit der Frage der Übertragbarkeit von Versuchsergebnissen an geometrisch ähnlichen, verkleinerten Strukturmodellen auf die (1:1)-Struktur unter Verwendung von Ähnlichkeitsgesetzen; sie steht aber auch im Zusammenhang mit der Frage, inwieweit kleinformartige, labortypische Versuche als Basis für die rechnerische Modellierung von Großkomponenten dienen können.

In Teil I "Überblicke" dieses Berichtes wird ein begrenzter Überblick über skalierte Versuche bei Raumtemperatur an geometrisch ähnlichen Proben gegeben. Er betrifft den Fließbeginn bei ungleichförmigen Deformationszuständen und auch die plastische Deformation und den Bruch glatter Proben im Zugversuch.

Um Größeneffekte zu interpretieren, offerieren unter anderem nicht-klassische kontinuumsmechanische Theorien neue Möglichkeiten. Insbesondere sind Gradientenkonzepte von Interesse, die die klassischen Plastizitätstheorien um räumliche Verzerrungsgradienten höherer Ordnung erweitern. Die Modellerweiterungen beinhalten zusätzliche Materialparameter, die mit materialcharakteristischen inneren Längen in Verbindungen gebracht werden können.

In Teil I wird ebenfalls ein kurzer Überblick über mehrere Theorien der Gradientenplastizität gegeben, der sowohl Deformations- wie auch Fließtheorien einschließt, wie auch einen Vergleich der ursprünglichen Theorie mit "symmetrischem Spannungstensor" mit einer neueren Theorie mit "unsymmetrischem Spannungstensor".

Der demnächst erscheinende Teil II "Anwendungen" veranschaulicht, inwieweit Verzerrungsgradientenmodelle den Größeneinfluß auf das Deformationsverhalten beschreiben können.

Contents (Part I "Reviews")

	Page
1. Introduction	1
2. Review of Experiments on Size Effects	4
2.1 Size Influence on the Initiation of Yielding Under Non-Uniform Straining	5
2.2 Similarity and Size Effects in Uniaxial Tensile Tests of Smooth Specimens	12
2.3 Similarity and Dimensional Effects in Tensile Tests of Smooth Sub-Size Specimens	33
2.4 Discussion	35
3. Review of Gradient Plasticity Theories	38
3.1 Gradient Deformation Theories	38
3.2 Gradient Flow Theories	40
Acknowledgement	50
References	51
Tables	56
Figures	69

1. Introduction

The computational assessment of the functioning or integrity of a complex structure under accident conditions may be impossible or prohibitive because of an excessive computational effort or because of insufficient knowledge of the governing physical process.

On the other hand, a full scale experiment, using the same materials as used for the prototype and accounting for the essential conditions, e.g. temperature, velocities etc., is often not realizable because of the cost or hazards. A geometrically scaled down model experiment may provide essential information if appropriate similitude laws are observed in the design and performance of this small scale experiment. Then the direct transfer of the experimental results to the full scale situation is possible using the appropriate similitude laws as transfer laws.

The derivation of the similitude laws, however, requires the knowledge of the governing physical processes. Of course, even taken this for granted, the compliance with the similitude conditions frequently cannot or can only approximately be reached.

A special situation exists for "replica models", i.e. small scale models from the same material and operated at the same temperature as the full scale structure, the prototype. If the mechanical response of the material is governed by the classical laws of elasticity and plasticity - a very often made assumption - the similitude with respect to the deformation behaviour can be assured, if - among others - the characteristic velocity (e.g. impact velocity) is the same and fracture processes can be excluded (Baker, Westine, Dodge (1991, [1.1]), Malmberg (1995, [1.2])). For many model tests (e.g. Baker et al. (1991, [1.1]), Young (1971, [1.3])) these assumptions are naturally taken for granted. This approach is based on the implicit property of the classical elasticity and plasticity laws being not dependent on an intrinsic material length.

However, there exists some experimental evidence (Section 2) of a size influence on the deformation behaviour, let alone the fracture behaviour, if scaled structures or simple specimens made from the same material are tested. This non-similarity may endanger the validity of the transfer of experimental results from small scale tests to the full scale situation.

The size effect is a subject of increasing interest due to the fact that current applications in modern technology involve a variety of length scales ranging from some tens of centimetres (nuclear reactor vessel walls) over a few millimetres (sheet metal forming) down to a few nanometers (thin film technology). Obviously, an appropriate theoretical modelling of the response is required which may depend on the specimen dimension. Several causes and competing theories are cited.

First of all pseudo effects are mentioned for instance due to

- heat to heat variation of the material where the specimens were made from
- macroscopic material inhomogeneity of the raw block of material
- surface cold work due to fabrication (cutting, turning)
- property variations due to heat treatment
- influence of non-similar testing machines for the small and the large size structure
- practical limitations on the construction of very small models and on the required decrease of the allowable tolerances.

Taking proper care of these technological effects and limitations by preventing them or reducing their influence to an acceptable degree, some basic effects are left which may be responsible for a size influence.

Viscoplasticity which, for example, becomes apparent when the flow stress is strain rate dependent may be responsible for a size influence. Similitude would require the equality of a "viscoplastic Reynolds number" (Malmberg (1995, [1.2]), Stach (1997, [1.4])). However, the use of replica models is principally in conflict with this requirement if the same characteristic velocity is used for the small and the large scale experiment. Then, generally the smaller specimen suffers less strain. The amount of this effect may be tolerable or can be estimated theoretically. On the other hand, by proper scaling of the characteristic velocity such that the strain rate is the same in both the small and the large structure, similarity (i.e. equality) of the viscoplastic strains may be obtained. However, this implies that the purely elastic deformation processes will be non-similar, which may be tolerable.

Heat conduction may induce another size-effect. Especially under dynamic plastic deformation the dissipation of the plastic work yields an increase in the temperature and a subsequent decrease in the yield stress (thermal softening). For structural steels relevant in nuclear reactor design this is especially pronounced beyond about 500 °C. It may be shown theoretically that similarity is not affected if the thermal processes are adiabatic in both the small and the large scale structure. If, however, heat conduction comes into play (the "Péclet number" is a controlling characteristic parameter), it will be more effective in the small scale replica model than in the large scale model. Thus, the thermal softening is less pronounced in the small scale and yields smaller strains.

Random inhomogeneities and related statistical theories play a prominent role when size effects are interpreted, especially in brittle fracture and fatigue. The size on these failure modes is explained by the presence of random inhomogeneities in a solid, where the weakest of these inhomogeneities determines the strength; the probability of the presence of rather weak inhomogeneities is greater the larger the structures (e.g. Weibull (1939, [1.5]), Bolotin (1969, [1.6])).

Non-classical continuum mechanics theories are a means to interpret size effects. To mention are:

- non-local (integral) concepts which involve a finite neighborhood volume integral of a state variable;
- gradient concepts which account for the influence of higher order spatial gradients in the constitutive equations;
- polar media concepts which account for additional kinematic deformation measures, their conjugated generalized stresses and additional balance equations.

These theories implicate additional parameters which can be associated with internal length scales characteristic for the material. They account for long range interactions in the material in different ways. In fact, all solid materials contain substructures (e.g. crystal lattice, inclusions, grains, grain clusters) having some characteristic lengths (the size or distance of sub-bodies). The aforementioned theoretical concepts attempt to account for this micro- or mesoscopic heterogeneity on a phenomenological level, still treating the material as a continuum.

The interaction between the geometric length of the specimen and an internal length associated with the underlying microstructure causes a size-dependent response. For example, if all geometrically similar specimens are made from the same material, then they have the same absolute grain size but larger specimens have the smaller relative grain size (Brown, Lubahn, Ebert (1947, [1.7])). It then appears that the influence of the microstructure will be primarily effective when the specimens are subject to non-uniform stress and strain fields.

Because of their relative simplicity attention is put here to concepts based on the introduction of higher order strain gradients into the constitutive equations.

Among the various higher-order gradient constitutive equations for elasticity and plasticity introduced earlier by various authors (for a brief historical account consult Aifantis (1994, [1.8])), we refer in particular to a largely overlooked paper by Shioya and Shioiri (1976, [1.9]). These authors modified the usual expression of the yield condition of classical plasticity by including the first order spatial gradient of the equivalent plastic strain normal to the yield-zone boundary. Their intention was to model the pattern formation of yielded zones associated with the phenomenon of the upper and lower yield stress in mild steel and they pointed out the scale effect introduced by the gradient term. While this work was directly motivated by the pioneering experiments of Bader and Nadai (1927, [1.10]), Nakanishi (1931, [1.11]) and others (see also Nadai (1950, [1.12])) on the formation of deformation zones during torsion, no explicit analytical relations were provided for the local loss of stability (leading to the emergence of deformation patterns) and the associated strain softening with the stabilizing role of the higher order strain gradients in obtaining a single or multiple localized shear zones. Instead, an analogy to the problem of Lüders band formation in tension was employed and the continuous distribution of dislocation theory was used in order to provide eventually numerical solutions for the plastic strain field which resembled the well-known observations. Even though questions of mesh-size dependence, convergence of solutions and other related issues, which are crucial to the current development of gradient plasticity theory, were not addressed, this work as well as the approaches of Dillon & Kratochvil (1970, [1.13]) and Dillon (1977, [1.14]) quoted in [1.8] seem to be the ones closest related to the modern treatment of the subject.

The modern treatment of gradient dependent constitutive equations in relation to loss of local stability, material softening and deformation patterning is due to Aifantis (1984, [1.15]). He extended the usual yield condition of classical plasticity by including the Laplacian of the equivalent plastic strain to dispense with the usual difficulties exhibited by the standard plasticity models when the material enters the softening regime. These difficulties, including the indetermination of the shear band thickness and the mesh-size dependence in finite element calculations, are removed by the gradient terms. The corresponding gradient coefficient, i.e. the phenomenological coefficient measuring the effect of the gradient term, turned out to relate directly to the internal length characterizing the underlying dominant microstructure, e.g. the grain size in a metal polycrystal (Mühlhaus & Aifantis (1991, [1.16]), Aifantis (1995 [1.17])).

Aifantis and co-workers [1.16 ÷ 1.31] as well as several other researchers afterwards [1.32 ÷ 1.37] have successfully employed gradient plasticity theories to discuss localization of deformation problems and to develop associated finite element codes. More recently, a different strain gradient theory of plasticity was proposed by Fleck & Hutchinson (1993, [1.38]) and Fleck, Muller, Ashbey & Hutchinson (1994, [1.39]) based on the physical concept of geometrically necessary dislocations and the structure of the Cosserat theory (polar medium concept) with "asymmetric stress". It was suggested that their theory may capture a variety of plastic deformation phenomena including size effects in micro-indentation and torsional deformation for which experimental data indicating the increase of strength with the reduction of diameter size were provided. However, no applications to localization of deformation and shear banding problems were given, and it remains to be demonstrated that their theory is well suited for such highly heterogeneous situations. On the other hand, it was shown by Aifantis (1996, [1.40]) that the original "symmetric stress" strain gradient theory can successfully be used to interpret size effects exhibited by elastic bore holes and twisted wires. It was also shown by Zhu, Zbib & Aifantis (1997, [1.41]) that the original "symmetric stress", second order gradient theory can model quite well size effects exhibited by metal matrix composites.

The objective of this report is to provide a limited review of scaled experiments of geometrically similar specimens or structures of metallic materials, to examine briefly several gradient plasticity theories and to illustrate to what extent the "symmetric stress" second order strain gradient theory can model the size effect in deformation behavior.

For this purpose the report is organized in two parts. In Part I "Reviews" the Section 2 gives an account of available experimental data on size effects of metallic specimens; this refers to the initiation of yielding under non-uniform states of deformation and to the plastic deformation and fracture of smooth tensile specimens. In Section 3 a brief review of several gradient theories of plasticity is given including both deformation and flow ones and a comparison of the original "symmetric stress" theory of Aifantis with the more recent "asymmetric stress" theory of Fleck et al. is provided.

Part II "Applications" (Malmberg et al. (2001, [1.42])) exemplifies to what extent strain gradient models can describe the size influence on the deformation behavior. This is done for simple loading configurations amenable to relatively easy theoretical treatment by fitting the models to some available experimental data and also by performing systematic parameter variations (size or internal length) to determine the relative influence of the non-classical part of the constitutive equations.

2. Review of Experiments on Size Effects

As mentioned above, classical effects – like viscosity and heat conduction – may induce a size dependence provided the same material is used in the small and in the large scale test. However, there are many examples showing a size effect in metals and steels where these mechanisms cannot serve as an explanation and where possibly the inhomogeneity of the micro-structure may induce a size dependence of the material response. To mention are, for example, the increase of the

- yield strength under monotonous straining
- hardness in the indentation tests
- endurance limit in fatigue tests
- fracture strength in brittle materials

when the size of the specimens, made from the same material, is decreased. This trend is also observed for

- particulate-reinforced metal matrix composites and
- coarse grained metals

when the particle or grain size is decreased.

By no means it is the purpose of this section to review all these various phenomena. Instead a limited discussion of size effects in plastic deformation at room temperature under monotonous quasi-static loading is aimed at: the size influence on the initiation of yielding in geometrically similar specimens under non-uniform stress distributions is considered but also attention is paid to similarity and size dependence of deformation and fracture of un-notched tensile specimens under nominally homogeneous stress conditions. The important question of the size dependence of fracture in specimens with geometric stress concentrators (e.g. notches) is beyond the scope of this review.

Before describing the results for some of the geometrically similar specimens made of the same structural material, we mention here early experiments of single size specimens on the initiation of yielding under monotonous loading of specimens subjected to non-uniform stress- or strain distributions. Such are, for example, bending of smooth beams, torsion of circular rods, tension of flat specimens with a circular bore-hole or with blunted edge notches. Frequently, steels with a pronounced upper- and lower yield stress (mild steel etc.) were used.

It was observed that the first flow lines or the first deviation from the linear force-displacement curve appeared when the elastically calculated maximum equivalent stress in the non-uniformly stressed specimen was significantly larger than the yield stress determined in a tensile test under homogeneous stress distribution. The somewhat inadequate wording "delayed yielding" was used sometimes. Early studies establishing these findings were performed by Kennedy (1923, [2.1]), Eiselin (1924, [2.2]), Scoble (1927, [2.3]), Enßlin (1928, [2.4]), Bierett (1931, [1.5]), Nakanishi (1931, [2.6]), Thum & Wunderlich (1932, [2.8]), Kuntze (1933, [2.9]), Möller & Barbers (1934, [2.10]), Siebel & Vieregge (1934, [2.11]), Föppl (1936, [2.12]), Klöppl (1936, [2.13]), Kuntze (1940 [2.15]), Föppl & Huber (1941, [2.16]), and Siebel (1948, [2.17]).

Some authors, (e.g. Kennedy [2.1]) interpret these results by assuming that the classical local yield conditions (e.g. Tresca, v. Mises), which were developed on the basis of experiments under homogeneous stress conditions, are not valid for strongly non-uniform stress distributions. They vaguely suggest¹ a supporting effect of the neighbourhood of the stress peaks ("reinforcement by under-stressed material", "micro-supporting effect") or even of the whole cross-section (here called "macro-supporting effect", Kuntze [2.15]).

The micro-supporting concept, in fact, requires the introduction of an additional material parameter with the dimension of length defining somehow the size of the supporting neighbourhood; the consequence was rarely explicitly expressed by the authors. The macro-supporting concept suggested by Kuntze [2.15], however, does not introduce a new material parameter.

The interpretation of the rise of the stress for yield initiation by the micro-supporting effect implies a size influence on the initiation of yielding such that small specimens should have a larger resistance against yield initiation than larger ones. However, Kuntze's concept is basically not capable to do so, which was not realized by this author. In fact, various results of scaled tests of geometrically similar specimens of the same material and non-uniformly stressed may show a size effect on the yield initiation with the described trend. An account of several of these studies are given in the following.

2.1 Size Influence on the Initiation of Yielding Under Non-Uniform Straining

Cook (1931, [2.7]) investigated the relation between the stress at the yield point in simple tension and for non-uniform stress distributions produced by torsion of rods, four-point-bending of bars and pressurization of thick-walled cylinders; also the stress distribution in each of the latter cases in the early stages of overstrain was considered. Systematic variation of size was done only for the cylinders. Three types of mild steel were used and the material was supplied in the form of rolled bars with a $1\frac{3}{8}$ in. diameter. To prevent cold work effects at the surface the specimens were heat treated – normalising or annealing in vacuum – after machining.

It was shown that the maximum shear stress (Tresca yield condition) at the initial yield point (defined as first deviation from linearity in the force displacement graph) is consistently higher in the cases of non-uniform stress distributions than in uniform tension; for torsion this ratio is between 1.18 and 1.23, and for flexure between 1.12 and 1.17 depending on the type of mild steel. Further, in the cylinders a pronounced scale effect was observed: Fig. 2.1 shows the ratio of the dimensionless pressure at yield versus the size (internal diameter) of the thick cylinder (ratio "external-to-internal diameter" is three). The normalizing of the yield

¹ An exception is the work of Föppl (1936, [2.12]) who suggested the fault to be related to the elasticity law. He tried to introduce a new "elastic constant" with the dimension of length; however, his concept remains confused.

pressure is done with the (upper) tensile yield stress in the transverse direction of the bar material. Evidently, the normalized yield pressure is largest for the smallest size cylinders (internal diameter 0.125 in. = 3.175 mm) and decreases exponential-like towards the 3.5-times larger cylinder. According to Cook, all results are consistent with the supposition that the initial yielding (he uses the word "dislocation") results in elastic breakdown² when the applied elastic stress state reaches a critical value of the (upper) shear stress at a certain depth in the material. Here it is not to be understood that the material in this surface layer is different from that in the interior. Using the elastic solution and the shear stress at yield in transverse tension, he estimated for steel A the depth of the surface layer to be 0.478 mm in torsion, 0.366 mm in bending and between 0.343 and 0.478 mm for three differently sized cylinders. Noteworthy, the numbers are of the same order and differences are not great! This suggests, according to Cook's somewhat misleading formulation, that "a surface layer exists having an elastic limit greater than that in the body of the metal". Naturally, then this layer thickness is characterized by a characteristic length parameter typical for the material. This concept "will account fully for the apparently increased yield points in all the cases of non-uniform stress examined, and for the scale effect observed in the cylinder tests". Cook notes that then a scale effect should also be present in torsion and bending, a matter for further investigations.

Morrison (1939, [2.14]) performed careful investigations on the criterion of yield in mild steel specimens under uniform and non-uniform stress distribution, i.e. tension, compression, pure bending, torsion, and combined tension and torsion. Testing with scaled specimens was done in tension, bending and torsion by changing the diameter of the specimens; however, there is no indication that the length was also scaled accordingly.

The material came in the form of ½-in. and 2-in. bars. By various checks the material was found to be extremely uniform, isotropic, and without difference in yield in tension and compression. Tests on material from various positions in the cross-section of the thick bar gave no appreciable variation in strength, and no differences between the two bars could be found after normalization. The preparation of the test material was done as follows. The bars were sawn into suitable lengths and normalized to remove any possible initial stresses. The machined specimens were finished by polishing and heated in a vacuum furnace (905 °C, 10 min) with long heat-up and cooling phases.

Among others, three tension tests were made on specimens ranging from 7.16 to 25.4 mm diameter (scale factor 3.55) and no dependence on the diameter was observed. Two test series, covering a range of diameters from 2.45 mm to 12.71 mm (scale factor 5.19) were done in pure bending. In the first, intermittent straining was used and the periods of rest allowed were used such that the creep was apparently almost exhausted. In the second a constant and very low rate of continuous strain ($\sim 10^{-7} \text{ s}^{-1}$ in the outer fibres) was adapted in all these tests and reading were taken at frequent instants over a period of some hours. These results are collected in Fig. 2.2 showing the dimensionless bending moment versus the angle of rotation. The normalized bending moment is equal to the normalized bending stress, i.e. the ratio of the maximum elastic bending stress and the (upper) yield stress in tension. First, it is seen that curves of the intermittent and the continuous test series agree satisfactorily. Further, it is noted that there is no sudden change in the slope of these curves as the torque is increased but clearly the normalized bending stress is larger for the small specimens than for the large specimens. The shape of the curves is affected by the size of the specimens such that larger specimens have less resistance to plastic flow.

Two series of torsion tests, covering a range of diameters from 0.1018 in. = 2.586 mm to 1.012 in. = 25.4 mm (scale factor 9.83), were performed, accompanied by tension tests of check specimens with the same heat treatment. The curves showing the normalized torque versus twist angle are collected in Fig. 2.3. Note that the normalized torque is defined by the

² This implies a sudden drop of the stress from the upper to the lower yield stress, a similar view as taken by Nakanishi (1931, [2.6]).

ratio of the maximum elastic shear stress at yield in torsion to the (upper) tensile yield stress. In contrast to the case of pure bending a distinct yield point is observed followed by a drop of the torque. This allows to plot the maximum normalized torque as a function of the diameter (Fig. 2.4) which illustrates the size effect in torsion: decreasing the diameter from 1 inch by almost a factor of 10 increases the apparent shear stress at yield by 16 %. It should be noted that the normalized torque as defined above would be a constant, i.e. 0.5774, if the v. Mises yield condition applies or 0.5 for the Tresca condition.

Morrison finally proposed a simple theory of yield for the case of non-uniform stressing. He supposed for a bending test that "yield cannot occur in an individual crystal surrounded by unyielding material but only in a number of crystals which occupy a sufficient thickness to permit of the complicated readjustment (of the crystals) which must take place before movement can occur, it is unreasonable to expect to find yield before a stress equal to the yield stress in uniform tension is applied to a depth of this magnitude. It seems reasonable to suppose that the depth might be of the order of a few crystal diameters." An elaboration of this suggestion yielded a theoretical result as shown in Fig. 2.2.

To recover the size effect approximately, the required layer thickness was estimated to be 0.005 in. = 0.127 mm, i.e. three or four crystal diameters. The approach of Morrison is very close to the explanation given by Cook (1931, [2.7]). In fact, it is also close to the concept of an "integral yield condition" studied recently by Malmberg (1995, [1.2]) for pure bending and torsion; there also it was shown that a yield condition involving a stress gradient may be viewed as an approximation for the integral condition.

Föppl & Huber (1941, [2.16]) performed a series of (partially) scaled indentation tests for a normalized structural steel St37. The indenters (stamps) were a prismatic bodies made from a tool steel, their contact surfaces being cylindrical with a radius of curvature ranging from 2 to 240 mm. The St37-test object was a rod with rectangular cross-section (width 15 mm, depth not given). An indenter of a given size was applied to the rod at various positions, each time with increased load. After the loading sequence the rod was annealed up to 200 – 300 °C, cut in the middle vertical to the contact surface. The surface of the cut was polished and etched such that the flow lines became visible. From the data the minimum load was determined under which flow lines began to appear first, defining the initiation of yielding. This procedure was repeated for the other size indenters.

From the measured minimum load for a given radius of the indenter and width of the rod-like specimen a stress-like quantity may be determined. If similarity would apply this value should be independent of the indenters radius of curvature. However, using the data the ratio of this value for a small indenter (9 mm radius) to the 26.7-times larger one (240 mm) is 1.99 and not 1. To demonstrate the non-similarity, Föppl & Huber used a different approach. Below the limit load the response is assumed to be isotropic and linear elastic such that the Hertz formulas apply. For each limit state the maximum shear stress τ_{\max} within the material below the indentation as well as the width of the elastic indentation were calculated using the measured load at yield. These results for flow line initiation are plotted in Fig. 2.5. For large radii of curvature the maximum shear stress is $\tau_{\max} = 16.4 \text{ kp/mm}^2$. According to Tresca's yield condition this corresponds to a tensile yield stress of 32.8 kp/mm^2 and according to von Mises one gets 28.4 kp/mm^2 . The actually measured tensile yield stress is 26.2 kp/mm^2 .

The general trend observed in these results is in accordance with the scaled experiments by Cook (1931, [2.7]), Morrison (1939, [2.14]) and others. The interpretation by Föppl & Huber is, however, different. They suggest that below a certain characteristic length (here 2.2 mm) the usual form of the elastic laws are not valid anymore, an idea promoted by Föppl before [2.12]; they do not make an inappropriateness of the yield condition itself responsible. It is the present authors' opinion that this conclusion cannot be obtained from the above indentation experiments. An interpretation along the lines of Cook or Morrison is more reasonable.

Richards (1954, [2.19]) carefully carried out a large number of tensile tests on three sizes of specimens (1/8 in. = 3.175 mm, 1/2 in. = 12.7 mm, 1 1/4 in. = 31.75 mm diameter, scale factor 10) made from the same bar (1 1/2 in. diameter) of the mild steel C1020. These tests are mentioned here because they are related to bending tests performed by Richards later (see below). The tensile specimens were made in accordance with ASTM specifications, and geometric similarity of their centre portions was preserved though-out. Examination of the micro-structure showed substantial uniformity across the diameter of the original bar. All specimens were annealed after machining and polishing. The annealing was done in a furnace having a controlled atmosphere (35 % H₂ and 20 % CO) so that the surfaces of the specimens would be unaffected. Examination of the micro-structure after annealing showed that grain sizes were substantially the same in various sizes of specimens and that no significant carburization had taken place in the surfaces.

All tensile tests were performed at the same constant loading rate in the elastic regime until the upper yield point (sudden load reduction). Thus, the strain rate was constant for all sizes.³ The results, individual tests and average values, are represented in Fig. 2.6 versus the normalized volume $V = \left(\frac{D}{D_1}\right)^3$ (D_1 is the minimum diameter). They demonstrate a definite dependence of the upper yield point on specimen size, following the usual trend, and a considerable scatter, especially for the small specimens is observed.

For the theoretical interpretation an analogy to Weibull's statistical theory of the weakest link in chain for brittle fracture is used. This then implies a power law dependence of the upper yield stress S_u on the volume of the specimen. A least square fit to the average data is

$$S_u = \frac{60.14}{V^{1/58}} \text{ [psi]} = \frac{\text{const}}{D^{19.3}}$$

which gives a good correlation with the mean values (Fig. 2.6). Further checks on the applicability of Weibull's theory concerning also the standard deviation was a matter of discussion of this publication [2.19].

Richards (1958, [2.20]) extended his work on the size dependence of the yield point in mild steel to the case of four-point-bending, all other influences being placed under careful experimental and statistical control.

The material was a commercial quality killed structural mild steel expected to have a pronounced upper yield point. It was obtained in the form of hot-rolled bars 1 1/2 in. diameter, all rolled from the same heat. Five different sizes of beams with rectangular cross-section ($h/b = 2.5$), the depth h ranging from 0.1585 in. to 1.000 in. (scale factor 6.3). For each size ten specimens were produced each specimen taken from the centre of the bars. The actual source of each specimen in the original stock was determined by statistical considerations to suppress influences due to macroscopic material property variation along each bar and from bar to bar.

The raw slugs were given a preliminary homogenizing anneal at 900 °C. After machining, the specimens were stress relieved by annealing at 600 °C in a salt bath to remove cold working effects due to machining.

Dimensional similarity was also realized for the loading apparatus to produce four-point-bending (Fig. 2.7). The cross-head velocity was scaled⁴ such that the maximum bending strain rate was the same for all specimens. At the chosen rate of $15 \cdot 10^{-6} \text{ s}^{-1}$ strain rate effects on the tensile yield stress do not exist. More important is, however, that the scaling of the cross-head velocity would assure the same size effect for all sizes if any visco-plasticity were present. A large number of auxiliary test were made to check basic premises. These included micro-structure examinations, macro- and micro-hardness tests, additional bending tests, etc. Most of these tests did not reveal any significant non-uniformity of the material except the bending of a series of small beams of the same size taken from different radial positions of the cross-

³ In most of the experiments described previously this is not indicated at all or only vaguely.

⁴ This is not explicitly noted in [2.20], but concluded from the choice of a constant strain rate.

section of the stock bar. The measured yield stress in bending indicate that the material at the centre of this particular bar was weaker by 7 % than that nearer the surface. Since the beams in the main tests were all taken from the centre, a decrease in yield strength towards the centre would therefore produce a corresponding increase in bending yield strength with size, if there were no true size influence.

The principal method to detect the yield point in pure bending involved the plotting of the load (or elastic bending stress) versus deflection or strain and observing the deviation from linearity. A number of strain gages were attached to the tension surface of each beam which covered as nearly as possible the entire length subjected to pure bending. A standardized testing procedure was set up and carefully followed in all tests.

The test results are collected in Table 2.1 and the decrease of the yield stress in bending as a function of size (volume) is shown in Fig. 2.8.

The ratio of the mean values of series B2 and B5 is 1.42, the associated depths being 0.251 in. and 1.000 in. (scale factor 4). This is a significant influence. Here it should be noted that these data are somewhat masked by the observed non-uniformity of the yield stress along the radius of the stock bar. If this were not present, the above ratio and the size dependence seen in Fig. 2.8 were even larger.

The statistical theory, using the Weibull interpolation, yields for the mean value of the yield stress

$$\begin{aligned}\bar{\sigma}_y &= \frac{I_m}{k^{1/m} v^{1/m}} && \text{in uniform tension} \\ \bar{\sigma}_b &= (m+1)^{1/m} \bar{\sigma}_y && \text{in pure bending} \\ I_m &= \int_0^{\infty} e^{-z^m} dz\end{aligned}$$

where k and m are material parameters and v is the volume under tension (or pure bending). Richards performed a least square fit of this power law relation which is shown in Fig. 2.8. Since the experimental data B1 were subjected to doubts, they were excluded.

It is noted that this theory implies close relations between these two loading cases, for example, the slope $1/m$ of their graphs in double-logarithmic presentation must be the same. Unfortunately tensile tests were not done for this material but were foreseen. For the bending case the slope is $\frac{1}{m} = \frac{1}{11.7} = 8.55 \cdot 10^{-2}$ with respect to the volume dependence (or $\frac{3}{m} = \frac{3}{11.7} = 25.64 \cdot 10^{-2}$ if a length dependence is used). The previous results (Richards 1954 [2.19]) for tensile tests of an (other) mild steel yields $\frac{1}{m} = \frac{1}{58} = 1.72 \cdot 10^{-2}$ which is five times smaller. The trivial conclusion is that either the mild steels used by Richards are very different or this statistical theory is insufficient to explain the results. Then it may be conjectured that in the case of non-uniform stressing an additional effect may become significant.

It is further noted that this statistical theory would yield a standard deviation whose volume dependence would follow a similar power law with the exponent $1/m$. This has not been checked by Richards. Finally, an important property of this theory should be mentioned. If the index "p" denotes a large specimen and "m" a small one, then

$$\frac{(\bar{\sigma}_y)_p}{(\bar{\sigma}_y)_m} = \frac{(\bar{\sigma}_b)_p}{(\bar{\sigma}_b)_m} = \left(\frac{v_m}{v_p} \right)^{1/m} = \left(\frac{\ell_m}{\ell_p} \right)^{3/m} = \left(\frac{1}{\lambda} \right)^{3/m}$$

where ℓ_m & ℓ_p denote corresponding lengths and λ is the scale factor. Thus, for a fixed scale factor λ the above ratio is independent of the absolute sizes of the specimens.

Finally, with respect to the size dependence of the initiation of yielding another series of experiments is briefly sketched; it concerns the initiation of yielding at stress concentrators; note that the discussion of fracture due to stress concentrations is out of the scope of this review.

Imamura & Sato (1986, [2.22]) described experimental results and a theoretical interpretation concerning the size effect on yielding in a perforated mild steel strip under tension. The flat strip specimens (Fig. 2.9) were fabricated from a 0.42 mm thickness sheet metal (mild steel, 0.10 % carbon content, average grain size 13 μm), coated with zinc. Their longitudinal direction was crosswise to the rolling direction. The width $2b$ of the strip in the gage region was 10, 20 and 30 mm and the diameter $2a$ of the central hole varied ($a/b = 0 \div 0.3$). To prevent cold work at the edge of the hole it was successively enlarged by boring in 5 to 6 steps. Finally, the zinc coating was removed by very fine emery paper. With the above data a specimen will have about 32 grains across the thickness and about 270 grains along the smallest ligament ($b - a = 3.5$ mm, $b = 5$ mm, $a = 0.3 \cdot 5 = 1.5$ mm).

Strain gages (size⁵) were attached at the edge of the hole and the average remote stress $\sigma = \frac{P}{2b-t}$ was recorded versus the strain ϵ during the quasi-static tensile tests (Fig. 2.10). No indication is given whether the strain rate or loading rate is properly scaled.

In Fig. 2.10 an elastic regime is clearly seen with a decreasing slope⁶ which is due to the choice of the stress variable. For the unperforated specimen and for the very small hole an upper and a lower yield point σ_A are found whereas for larger holes no upper yield point is seen but a deviation from linearity at reduced values $\sigma = \sigma_A$.

The lower yield stress for the homogeneous stress distribution ($a = 0$) defines the yield stress σ_y ,

$$\sigma_y = (\sigma_A)_{a=0}.$$

Three repeat tensile tests for the three specimen sizes without holes were done and the average values are

$$\begin{aligned} 2b &\approx 10, 20, 30 \text{ mm} \\ \sigma_y &= 289.6, 293.4, 304.5 \text{ MPa} \end{aligned}$$

There is a rather slight increase (5 %) in yield stress when the size is increased from 10 to 30 mm width.

With the above values "normalized yield stresses" were determined and plotted versus the relative hole size a/b with the width $2b$ as a parameter (Fig. 2.11). The main result is that for geometrically similar specimens in the plane ($a/b = \text{const.}$, but thickness t was not scaled) the absolute size (e.g. $2b$) determines the ratio σ_A/σ_y : under non-uniform stress distribution smaller specimens are significantly stronger (provided the holes are not too small) against yield, and this size effect dies out with increasing size.

Imamura & Sato interpreted their experimental results using a theory of Nakanishi & Hanada (1953, [2.18]) for the lower yield point which allows for the non-uniformity of the stress distribution. In addition, Nakanishi's concept of a material specific surface layer thickness δ , which is independent of the stress distribution, is used. This concept implies that in crystalline aggregates "the orientations are varied and plastic deformations are restrained (in a crystal) by the surrounding neighbours; as the restraint in the surface layer is weaker, the

⁵ No indication of the size of the strain gage are given. However, the size of the gage should also be scaled such that the measured quantities remain comparable for the small and the large specimen. If the same gage size is used for all sizes, size effects may disappear in the very small specimens. The qualitatively different behavior for small strip widths and very small hole sizes found by Imamura & Sato may possibly be caused by this masking effect.

⁶ Actually the stress σ is not explicitly defined in ref. [2.22]. However, the interpretation is as follows. If $\sigma_N = P/(2b-2a) \cdot t$ is the average stress in the minimum cross-section, then in the elastic range $\sigma_N = E_N \epsilon$. Thus $\sigma = \sigma_N \cdot (1 - \frac{a}{b}) = (1 - \frac{a}{b}) E_N \epsilon$. This implies in the $\sigma + \epsilon$ graph a decrease of the apparent Young's modulus $(1 - \frac{a}{b}) E_N$ with an increase of the hole-diameter and this agrees with Fig. 2.10.

stress-strain relation at that part will be different from that at the inner part; thus a sort of boundary layer must be taken into account when the stress is sharply concentrated". It appears that the combination of Nakanishi's yield point theory for non-uniform stresses and the surface layer concept is difficult to grasp since it leaves essential questions open.

Imamura & Sato were able to fit this model to their experimental results by using a single surface layer parameter $\delta = 0.08$ mm; this corresponds to about six crystal grains. Their fit is represented in Fig. 2.11 by the continuous curves. Also Nakanishi's model allows to derive an upper and lower limit for the size effect.

In the following years Imamura & Sato (1987, [2.23]) and Tamura & Sato (1992 [2.24]; 1992, [2.25]) extended this work and performed experiments on the size effect on yielding of solid mild steel cylinders with a transverse hole under compression as well as pure bending of mild steel beams of hollow circular cross-section with a transverse radial hole. Similar trends were observed and interpretations used.

The previous review makes evident that the experiments on the size dependence of the initiation of yielding in cases of non-uniform stress fields are rarely accompanied by systematic testing of smooth tensile specimens of the same material where a macroscopically uniform stress field is present. An exception are the tensile tests of Morrison (1939, [2.14]), which may be criticised because of the very few experiments and their restricted size variation, and the recent work of Imamura & Sato (1986, [2.22]). Their data for uniform stress fields show no size dependence of the yield stress, whereas Richard's data (1954, [2.19]) surely indicate this dependence accompanied with a lot of scatter. Clearly, such observations depend on the material, the way "initial yield" is defined, and the measurement technique and its accuracy.

Beyond the limitations of the above experiments, the size dependence of fully developed plastic flow in the hardening regime up to the maximum load and instability is of scientific and technological importance. However, experiments of the types described above and going clearly beyond the initiation of yielding (the bending experiments of Morrison are an exception) are difficult to find. Noteworthy in this respect are the tension and torsion experiments of very thin annealed pure copper wires (maximum diameter 170 μm ; grain size 5-25 μm), done by Fleck, Muller, Ashbey & Hutchinson (1994, [2.26]) observing a constant strain rate in all tests (Fig. 2.12). Whereas their tension tests show only some restricted size dependence with the usual trend, i.e. smaller specimens show a higher resistance against plastic flow, the size (diameter) influence is very pronounced in the non-uniform stress tests, that is the torsion test.

Also scaled fluid-structure impact tests (Stach (1997, [1.4]) showed a significant size effect: The plastic deformation was concentrated in tapered bending joints (minimum diameter 1, 4 and 10 mm, austenitic steel X5CrNi189, average grain size 30 μm) and the largest specimen showed a two- to three-times larger permanent rotation than the smallest specimens. Analysis [1.4] showed that the strain rate sensitivity is insufficient to produce this size influence. Further interpretation of the results [1.4, 2.28] revealed that this size influence should be essentially related to the initiation of yielding in the bending joints. This was confirmed by scaled quasi-static bending of the joints, performed at the Forschungszentrum Karlsruhe (Stach (1997, [2.27]), Jordan & Malmberg (1998, [2.28])): the size variation affects primarily the initiation and the small plastic strain regime (Fig. 2.13); the hardening modulus is almost not affected except for the later stages. Finally, the response of this material in scaled tests has also been investigated and a significant size effect with the same trend was observed even under these quasi-homogeneous stress conditions (for further details see Section 2.2).

In view of all these results and their limitations it appears necessary to extend the review to uniaxial tensile testing of smooth specimens of different sizes which have been done because of the basic importance of this technological test. Here tensile tests with

geometrically similar specimens are of primary interest. However, frequently the experiments refer to distorted specimens. Thus, the influence of the shape has found much more attention.

2.2 Similarity and Size Effects in Uniaxial Tensile Tests of Smooth Specimens

C. Bach (1920, [2.29]) reported about results of the experimental work by Barba (1880, [2.30]) and Bauschinger (1892, [2.31]) concerning the influence of the gage length and the diameter of circular tensile specimens:

- a slight reduction of the ultimate stress with increasing diameter is observed which may be due to a diametrical non-uniformity of the rod material the specimens were fabricated from;
- the area-reduction at fracture is independent of the diameter;
- the fracture strain increases if the gage length is kept constant but the diameter is increased;
- for geometrically similar specimens, i.e. $l/d = \text{const.}$ (l : gage length, d : diameter), the fracture strain is the same;
- the ultimate tensile stress appears to be independent of the form of the cross-section;
- the area reduction at fracture is almost independent of the shape and size of the cross-section;
- the fracture strain ϕ for a given gage length l is independent of the shape of the cross-section but increases with its size according to $\phi = a + b\sqrt{a}$ where "a" is the cross-section area;
- the fracture strains are comparable if the ratios \sqrt{a}/l are the same;
- there is no relation between area reduction and fracture strain;
- the proportional limit and the yield stress may vary considerably within a slug of material even after careful annealing such that a possible influence of shape and size is masked.

The check of the original work of Bauschinger (1892, [2.31]) reveals that the geometrically similar tensile specimens with circular or rectangular cross-section cover only a size scale of two: the circular specimens have a diameter of 10, 15 and 20 mm, whereas the width of the flat specimens is 20, 30 and 40 mm with a width-to-thickness ratio of 5/3. Barba's (1880, [2.30]) results for geometrical similar specimens with circular cross-sections, however, covered a scale range of 4 (5 to 20 mm diameter with a gage length-to-diameter ratio of 10) and 4.5 (6.9 to 31.05 mm diameter with a gage length-to-diameter ratio of 7.25).

Moore (1918, [2.32]) reviewed available test data⁷ and performed tensile tests on specimens of four grades of steel: rivet steel, two steels with about 0.35 % and 0.56 % carbon contents, and heat-treated chrome-nickel steel. Tests were made with specimens held by means of shouldered ends, with specimens held by means of threaded ends, with specimens with turned down center portions and ends held by means of wedge grips, and with specimens in the form of straight round rods. Tests were made in triplicate. The gage lengths l were 2, 4, 6 or 8 inches and the diameter were 0.5 inch and also 0.75 inch for one specimen type (Tab. 2.2). Thus, the diameters were fairly large and a size variation of geometrically similar specimens was not included in the test series although suggestively named in the title. Metallurgical data of the materials were not indicated as well as some details of the testing, e.g. strain rate or cross head speed is missing.

⁷ Among others, Moore refers to the results of Barba and Bauschinger.

From the data obtained the following results were determined for each test and averaged:

- stress at
 - proportional limit and some other elastic limit point definitions
 - yield point stretch of 0.5 % in the 2 inch gage length
 - ultimate load
- elongation at maximum load
- elongation at fracture
- reduction of area at fracture.

Except for the area reduction, details of the necking zone were not recorded. Although no conclusion can be drawn with respect to the influence of size some observations concerning the influence of shape and the ratio \sqrt{a}/l (here called "stoutness", the inverse of Moore's "slenderness") are noteworthy and are illustrated in Fig. 2.14 to 2.19. Concerning the shape of the cross-section, Moore states, in view of previous results, that "it would seem a safe conclusion that there is no great difference in results between tests made on round specimens and tests made on flat specimens whose width is not more than four times the thickness". With respect to the effect of the head of the specimen and the method of gripping in general, according to Moore, the test results showed no very marked advantage of one type or method over another.

The influence of the stoutness \sqrt{a}/l on the various "elastic limits", the yield point and the ultimate tensile strength is seen (Fig. 2.14 – 2.16), in general, to be slight. An exception is the heat-treated chrome-nickel steel which shows an increased strength for the shorter specimens.

It has been and it is still proposed to use the elongation at maximum load as a measure of ductility instead of the elongation at fracture which depends on the local elongation at the necking zone. The instant of maximum load, however, is not well marked for ductile materials. The results in Fig. 2.17 clearly lack in uniformity.

All the test data for the elongation e at fracture show that the effect of variation of the stoutness \sqrt{a}/l is very pronounced and a linear relation $e = e_0 + Q\sqrt{a}/l$ for a specific material applies (Fig. 2.18). For geometrically similar specimens one has $\sqrt{a}/l = \text{const.}$ and if this relation applies to this case too, the elongation at fracture should be size independent. This is in accordance with Bauschinger's observations for geometrically similar specimens.

Finally, all test data for the reduction of area at fracture are very slightly affected by the stoutness \sqrt{a}/l (Fig. 2.19) and the variations present do not indicate a systematic trend.

Baere & Gordon (1921, [2.33]) remarked that "the strength and the ductility of a metal as determined in a tensile tests, depend not only upon the physical properties of the metal, but also upon the form and dimension of the test bar. The extension of bars geometrically similar, but differing in dimensions, are comparable only by observing Barba's Law of Similarity – Geometrically similar bodies of the same material, under identical conditions and stress, undergo similar deformations." Since in practice it is inconvenient to prepare geometrically similar test bars, a compromise is to be established. The main object of their experiments was to determine the influence of the width of the specimen upon the strength and ductility of test bars with rectangular cross-section and constant thickness. Thus, geometrically similar specimens were not included in this test series. Specimens were fabricated from 0.25 inch (6.35 mm) and 0.125 inch (3.17 mm) mild steel plates (carbon content 0.12 ÷ 0.15 and 0.13 %) and a 0.125 inch copper plate with a uniform length of 12 inches and the ratio width/thickness ranging from 1.76 ÷ 15.39, 1.87 ÷ 29.89, and 1.90 ÷ 29.83, respectively. In all cases the same average strain rate of 1 % per minute ($1.7 \cdot 10^{-4} \text{ s}^{-1}$) was applied. Three or four nominally identical tests were performed in each case. The results show that the yield point remains practically unaffected by the width of the test bar for all three materials although the cross-section areas were increased by factors of about 8.7, 16.5

and 15.7. Also the ultimate tensile stress is little affected: in case of the two steels there is a rather slight tendency to rise as the width is increased (less than 3 %) and this effect is noticeably absent for the copper specimens. The determination of the elongation at fracture and the cross-section reduction is based on 1 inch or ½ inch markers on the central line. Unfortunately, the description of the determining procedure remains obscure such that these results will not be commented here.

An extensive study of the influence of shape and to a very limited extent also of size on the tensile properties of three aluminium sheet metals was performed by Templin (1926, [2.34]). Three different types of sheet metals have been tested:

- hard aluminium sheet (2 SH) with high tensile strength and low elongation
- soft aluminium sheet (2 SO) with low tensile strength and high elongation
- heat-treated duralumin (17S-T) with comparatively high strength and high elongation.

Only the first and main part of the investigation is sketched here; it is concerned with the effects of variation in the thickness, width and length of the uniform section, keeping the ends of the specimens 1.5 times the width and the radii of fillets equal to width. Five thicknesses, ranging from 1/64 (0.4 mm) to ¼ inch (6.35 mm) for each metal, were used and the nominal widths were 0.250, 0.375, 0.500, 0.750 inch; the length of the uniform sections were 2.25, 3.0, 4.5 inches. For all cases three nominal identical specimens were fabricated and tested giving 180 tests for each sheet metal. In all specimens the gage lengths was fixed to be 2 inches; in addition marks with staggered distances varying from ¼ to ½ inch were applied on the center line of the specimens, depending on its length.

In Fig. 2.20 the yield stress, defined as the stress at 0.5 % strain under load in the 2 inches gage, and the ultimate stress have been plotted against the cross-sectional areas. From these data it is concluded that for variations in the width to thickness ratio from 1 to 45, for cross sectional areas from 0.004 sq. in. to 0.188 sq. in. (2.58 to 121.3 mm²) and for lengths of the uniform sections from 2.25 to 4.50 inches (57.15 to 114.3 mm) no effects on the yield and ultimate stress are observed. The effects of the dimensional variations in the uniform section on the elongation at fracture using a fixed gage length of 2 inches, however, are clearly evident; this is to be expected since the non-uniform localized deformation in the necking zone (no information is given in [2.34] on this aspect) is included in the average measure of elongation. Here, only the dependence of the elongation on the cross-sectional area variation is indicated (Fig. 2.21).

Within the wide range of dimensional variations it is possible to identify several tests of different width-to-thickness ratios which relate to almost similar specimens differing by a scale factor of two only. This rather small size variation is due to the restricted length variation. The data are given in Tab. 2.3.

The test data in Table 2.3 for the yield and ultimate stress reflect more clearly than Fig. 2.20 that no systematic size effect is found and also the variation of the cross-sectional shape (defined by w/t) has no effect. The elongation at fracture within a 2 inches gage length, however, is clearly affected: increasing the size by a scale factor of 2, yields an increase in elongation for all three sheet metals. However, from the aspect of similarity this finding is not conclusive, since the gage length was not scaled like the dimensions of the specimen.⁸ Thus, the average quantity "elongation in 2 inches" does not correspond to similar parts of the geometrically similar specimens. It is noteworthy that simple considerations proof (see page 31) that the fracture elongation will increase with size when the deformations up to fracture are size independent but the gage length is held constant.

The influence of the shape variation w/t is, however, evident within the given limits: if the shape parameter w/t approaches unity (i.e. square cross-section), the elongation increases.

⁸ The ratio \sqrt{a} / ℓ_g ($a = w \cdot t$, $\ell_g = 2$ inches) was not constant as required for geometrically similar specimens.

A somewhat similar study was performed by Lyse and Keyser (1934, [2.35]), however, without variation of the specimen length. The specimens were fabricated from three rolled steel plates which were produced from the same heat. The chemical composition is reported to be 0.15 % C, 0.48 % Mn, 0.014 % P, and 0.028 % S. The plate thicknesses were 1, 0.5, and 0.25 inch. The specimens with rectangular cross-section varied in cross-section dimension from 0.25 by 0.25 inch to 1 by 4 inches. Specimens with circular cross-section with 0.25, 0.5 and 1 inch diameter were also provided. The uniform center portion of all specimens had a length of 4 inches. All specimens cut from the 0.25 inch plate had the full thickness of the plate. For the 0.5 inch plate one group of specimens had the full thickness of the plate while another group was machined down to the 0.25 inch center portion of the plate. Finally for the 1 inch plate, full thicknesses, 0.5 inch center portions and 0.25 inch center portions were used. Three specimens were produced for each kind making a total of 114 specimens.

The elongation at fracture was measured on the 2 inch portion of the uniform section. A tensometer with a 1 inch gage length was used on all specimens to determine Johnson's elasticity limit.⁹ All specimens were tested at a speed of about 0.05 inch per min. up to the total (maximum ?) load. For a 4 inch specimen this corresponds to a average strain rate of $2.1 \cdot 10^{-4}$.

It is to be expected that the elastic limit stress increases with the decrease of the plate thickness since the plates were obviously produced by successive rolling. The results for the same type of specimens but taken from the three different plates show that Johnson's limit is largest for the 0.25 inch plate and decreases significantly with the increase of thickness of the two other plates. The corresponding ultimate stresses are almost not affected. Because of this effect only a selected part of the results will be discussed here, namely the results of those specimens which stem all from the same plate, the 1 inch plate. It contains specimens with the largest variation in the cross-sectional dimensions. These selected results are collected in Table 2.4.

Within each group of Table 2.4 the cross-sections are geometrically similar and the data are arranged according to the size of the cross-section. Besides the circular and square cross-sections, rectangular cross-section with increasing width-to-thickness ratio are included.

Concerning Johnson's elastic limit, a systematic size dependence (scale factor 4 for cross-section dimensions) within each group cannot be detected. However, it appears that the non-circular specimens give the largest limit stress when the specimen cross-section includes the whole 1 inch thickness of the plate. This is probably due to some material property variation across the thickness of the plate: the material close to the plate surface has a larger yield point due to the rolling process during plate production.

Furthermore, it is seen that the shape of the cross-section has no systematic influence on the Johnson limit. To an even higher degree the ultimate stress is neither affected by the size nor by the shape.

However, the data for the area reduction decrease slightly with the four-fold increase of the cross-section dimensions; this size effect becomes more pronounced (~10 %) when the width-to-thickness ratio becomes large. On the other hand the area reduction definitely decreases with the width-to-thickness ratio.

Finally, for all shapes of the cross-sections a pronounced increase of the elongation at fracture (within a 2 inches gage length) with the size of the cross-section is found. This size influence appears to be largest for the circular cross-section. As previously, the results for the elongation at fracture within a 2 inches gage length for all specimens is not conclusive with respect to questions of similarity. Also details of the determination of this quantity as well as the area reduction are not given in ref. [2.35]. Furthermore, information about the scatter of the nominally identical tests is missing also in this reference; thus, the significance of slight effects on average values is difficult to judge.

⁹ The stress at which the rate of strain is 50 % greater than the initial rate.

Static and dynamic tensile tests were performed by Wood, Duwez and Clark (1943, [2.36]) on specimens which had different dimensions but which were geometrically similar. Similitude theory for a classical rate independent elastic-plastic material implies [1.2] that the stresses and strains at homologous points are the same if the same impact velocity is used for differently sized specimens. Of course, then the average strain rates are not the same. If the average strain rate does exert an influence due to visco-plastic material behaviour, then geometrically similar specimens should exhibit different dynamic tensile properties. On the basis of this argument Wood, Duwez, and Clark investigated whether or not geometrically similar specimens tested at the same impact velocity exhibit identical dynamic tensile properties. From the today's knowledge of size effects and their possible causes the above research program requires a carefully choice of the test matrix and its parameters. Visco-plasticity induces a size effect, but a size effect may also appear if the average strain rates are the same (scaled impact speed) or if visco-plasticity is not significant at all and the classical rate-independent elastic-plastic material models do not apply for some other reasons. Thus, the experimental program should allow to separate the visco-plastic size effect from possible other size effects.

In the following only the quasi-static tensile tests, where rate effects are probably not significant for the materials considered, are commented. Annealed (480 °C, 1 h) copper and steel were the materials used. A series of copper specimens was fabricated from a ½ inch and another one from a 1 inch round bar. The steel specimens were taken from a 1 inch diameter¹⁰ bar of SAE 1020¹¹ in the cold-rolled and annealed (875 °C, 1 h) condition. The dimensions of the specimens are given in Tab. 2.5. Two specimens were machined and tested for each case.

Each of the static stress-strain curves for the annealed copper specimens, machined from the ½ inch diameter bar, is given in Fig. 2.22 and further details are given in Tab. 2.6. Fig. 2.22 demonstrates the very good reproducibility of each of the two nominal identical tests up to fracture. The smaller 0.1 inch diameter specimen shows uniformly somewhat larger flow stresses (~800 lb./sq. in. \approx 20 % of the proportional limit) although the proportional limits and the ultimate stresses are the same. The reduction in area is also very reproducible (Tab. 2.6) and the smaller specimens show only slightly smaller values (~ 3 %). A significant difference is found in the uniform elongation and the elongation at fracture: the uniform and fracture elongation of the small specimens are about 25 % smaller compared to those of the 3.5-times larger specimens. This difference is evidently responsible for the reduced deformation energy consumption capability per unit volume of the smaller specimen (Tab. 2.6). This latter results clearly indicate that the non-similarity is restricted here to two essential aspects of the necking process, i.e. initiation and extend of the necking zone but not the final area reduction.

Wood, Duwez, and Clark associate this reduced ductility with "the non-uniform structure in the cross-section of the ½ inch bar from which the specimens were cut". In fact there is an appreciable variation in Rockwell Hardness (scale F: 1/16 inch ball indenter, maximum load 60 kp): the hardnesses in the two small specimens agree well but are a factor of more than two smaller than in the two large specimens. This may indicate a variation of material properties along the length of the ½ inch bar. However, a record of the positions in the bar where the specimen were cut from is missing.

The second series of specimens were taken from a 1 inch diameter bar. Three different sizes were used ranging from a somewhat larger minimum diameter of 0.15 inch to 0.6 inch. Fig. 2.23 shows only one of the two stress-strain curves obtained for each size since the duplicate tests did not differ by more than 500 lb./in.². The three curves almost collapse into one. However, a very slight size dependence is found in the characteristic data (Tab. 2.6): the proportional limit is not affected, however, the ultimate stress and the reduction in area increase somewhat (about 4 to 6 %) whereas the elongation decreases by about 10 % (instead

¹⁰ The 1 inch diameter is inferred from the dimensions in Fig. 2.26 (hardness versus radial distance)

¹¹ Rockwell B hardness 87 – 91; chemical analysis 0.19 % C, 1.03 % Mn, 0.018 % P, 0.029 % S, 0.34 Si

of 25 %) when the size is reduced by a factor of four. Wood, Duwez and Clark pointed out that there is an appreciable variation in hardness, also for the second set of specimens (Tab. 2.6), although the stress-strain diagrams are approximately the same over a large strain range. Also a micro-structural examination indicated the same grain size which was not reported. No explanation was given for this anomaly.

The stress-strain curves obtained for each specimen of cold rolled and annealed steel are given in Fig. 2.24 and 2.25. Evidently, each of the nominally identical tests show good reproducibility. Most important a size dependence is clearly noted for all aspects of the stress-strain curve with the same trend for both states of this material (Tab. 2.6). The percentage increase of the proportional limit and the ultimate stress are given in Table 2.7, which includes also the percentage decrease of the elongation at fracture and the area reduction when the size is decreased from 0.13 inch (7.62 mm) diameter by a factor of two only.

The most significant effect is observed for the elongation at fracture which includes the necking process, but the stress-strain graphs indicate also a comparable percental reduction of the uniform elongation. The increase in stress and the decrease in elongation, when the size is reduced, however, do not compensate in the specific deformation energy up to failure, but lead to a reduced specific energy absorption capacity of the small specimens.

The Rockwell hardness measurements for each of the specimens show very good consistency for both states of the steel (Tab. 2.6).

Searching for an explanation of the pronounced size effect, the uniformity of the hardness distributions in the cross-section of the 1 inch bar materials was investigated. The result of the superficial Rockwell hardness using the 45 T scale (1/16 inch ball diameter, major load 45 kp) is given in Fig. 2.26. For both states the hardness shows a slight minimum at the center of the rods. Outside the center very little variation is found up to a radius of 0.25 inches. The small and the large diameter tensile specimens are well within this region. The difference in the hardness for the small and the large specimen show even a slight inverse effect: the smaller specimen are somewhat "softer" than the larger specimen (Fig. 2.26), whereas the Rockwell hardness B measurements (Tab. 2.6) are almost the same. Thus, hardness differences between small and large specimens are absent or even inverse; therefore, they cannot account for the observed significant differences between the tensile properties of the various sizes of specimens. Wood, Duwez and Clark suggest "that the observed difference in tensile properties is a consequence of a non-uniform distribution of impurities in the bars On the other hand, the surface characteristics of the material may be more influential in the case of a small specimen than a large one. In such a case a greater strength at the surface could account for the observed results". Further investigations to verify one or the other hypotheses were not done.

The object of the investigation by McAdam, Geil, Woodard, and Jenkins (1948, [2.37]) was to determine the influence of a wide range of sizes of both notched and un-notched cylindrical tensile specimens on the flow and fracture stress. The annealed (~925 °C, 2 h, cooled in furnace) low carbon steel FA-17 (0.12 % C, 0.44 % Mn, 0.25 % Si, 0.020 % P, 0.021 % S) in the form of a 2 ¼ inches (57.15 mm) diameter bar was used. A few experiments were made also with large and small specimens of oxygen-free copper.

This excerpt puts attention only to the results of the un-notched, geometrically similar steel specimens. The length-to-diameter ratio was not explicitly mentioned. In Tab. 2.8 the initial specimen diameters d_0 are listed, ranging from 0.101 to 1.297 inch (2.57 to 32.94 mm), as well as the minimum diameter $2b'$ in the neck after fracture and the meridional radius of curvature r' of the neck profile at the minimum cross-section after fracture. Based on these data the area reduction ψ and the ratio $2r'/d_0$ are obtained (Tab. 2.8). If similarity of the deformations at fracture would prevail, these two dimensionless numbers would be independent of size.

However, for a 13-fold increase in size the area reduction ψ at fracture reduces by about 10 % but the relative meridional radius $2r/d_0$ increases by 66 %.

McAdam et al. performed numerous measurements of the minimum diameter during each tension test and measurements were continued to the beginning of fracture¹². The strains were expressed in terms of A_0/A , in which A_0 and A represent the initial and current cross-section areas. The true stresses S were plotted versus A_0/A , which is represented on a logarithmic scale. Fig. 2.27 gives the results for three differently sized specimens. The last point in the graphs marked by the letter "R" was determined by dividing the load at the "beginning of fracture" by the sectional area measured after fracture, and this stress is generally higher than the stress at the "beginning of fracture". It is seen that the true flow stress (beyond the maximum load) is somewhat larger for the 0.1 inch diameter specimen than for the 1.296 inch diameter specimen.

From Fig. 2.27 and other figures given in [2.37] the yield stress cannot be extracted; however, approximate data can be obtained for the true ultimate stress (true stress at maximum load marked in the figures) and the associated uniform engineering strain $\epsilon_g = A_0/A - 1$. The results are collected in Tab. 2.9.

From Tab. 2.9 it appears that the true ultimate stress and the uniform strain are almost not affected by the increase in size. However, some data in Tab. 2.9 show that the tensile properties within the original 2¼ inches diameter bar are somewhat non-uniform: the centre part has a somewhat higher strength. This can be seen in the stress-strain curves of the 0.501 inch diameter specimens (Fig. I of ref. [2.37]). Since the large specimens ($d_0 \geq 1.00$ inch) are positioned co-axially with the original bar, their flow stresses are somewhat too large compared to the smaller specimens positioned at half-radial distance. Thus, a correction of the flow stress of the 1.296 inch diameter specimen in Fig. 2.27 would shift the curve to lower values and the size influence would increase somewhat.

On the other hand, two stress-strain curves (ref. [2.37], Fig. I, 0.501 inch diameter specimen) indicate that the material inhomogeneity in the original bar may be responsible for area reductions after fracture (Tab. 2.8) of the large specimens which are somewhat too small. However, sufficient data are not available to substantiate this trend.

Miklowitz (1948, [2.38]) performed a study of the effects of geometry and size on the mode of yielding close to and beyond the ultimate load and at fracture in flat tension bars of a medium carbon steel. Results on the initiation of yielding were not reported.

The thicknesses $h_0 = 3/16, 3/8, 3/4$ inch (4.76, 9.52, 19.05 mm), corresponding to the particular specimen series A, B and C, covered a size range of 4, whereas the width-to-thickness ratios b_0/h_0 and the gage length-to-thickness ratios l_0/h_0 ranged between 1 and 10 and 5 and 50, respectively. The gage length-to-width ratio l_0/b_0 was 5 in all specimens (Fig. 2.28). Thus, specimens 1A, 3A, 5A, ... are geometrically similar to 1B, 3B, 5B, ... and 1C, 3C, 5C, This similarity includes also the transition radius R between the gage length and the specimen heads.

A rectangular grid was mechanically put on the specimens. The spacing of the grid lines differed with the size of the specimen but it is not clear whether the grid was also properly scaled. The deformation of the grid lines in the width direction after fracture allowed to calculate the engineering strain ϵ_2 in this direction. At the intersections of the lateral and longitudinal grid lines, the thicknesses h were measured with special micrometers; this measurement was used to calculate the average strain ϵ_3 in the thickness direction. A "local" strain ϵ_1 in the axial direction was calculated from ϵ_2 and ϵ_3 using the constancy of volume condition $(1 + \epsilon_1)(1 + \epsilon_2)(1 + \epsilon_3) = 1$.

¹² The "beginning of fracture" is associated with the fracture initiation at the center axes of the specimen. However, this is not immediately observable and a definition in operational terms is not given in ref. [2.37]. McAdam et al. refer to previous publications.

The medium carbon steel was an open-hearth, silicon-aluminium-killed fine grained steel (C 0.19, Mn 0.77, P 0.021, S 0.026, Si 0.17 %). No heat treatment except a stress relief was given the supplied 1 x 11 inches plates. Whether the plates came from the same heat is not recorded. Also cutting plans showing the origin of the various specimens are not indicated and tests verifying the homogeneity of the plates are not described in [2.38]. Most importantly for each type of specimen only one test was provided.

In the presentation and discussion of the results, Miklowitz puts his primary attention to the influence of geometry (i.e. the variation of b_0/h_0) which determines the constraint effect of the specimen head and which becomes more intense as the width increases. In the present report interest is restricted to the influence of size of geometrically similar specimens and only those data are extracted from [2.38] which directly refer to this aspect.

Tab. 2.10 contains the conventional ultimate stress and the engineering fracture stress and total fracture elongation in the scaled gage length l_0 . For geometrically similar specimens, e.g. (1A, 1B, 1C, $b_0/h_0 = 1$), a slight decrease of the ultimate stress with increased size is found in Tab. 2.10. However, for the other width-to-thickness ratios the trend is not so uniform. Also for the engineering fracture stress and the total elongation at fracture a significant size influence cannot be seen. Thus, it appears that Barber's law is approximately satisfied. On the other hand the influence of the width-to-thickness ratio is very pronounced for the total elongation.

Miklowitz' results allow to demonstrate the influence of specimen size by comparing the maximum strain values at fracture in the center of the neck, i.e. within the cross-shaped depressed region which is generated in the localization process (Tab. 2.11). This influence is observed especially for the maximum strain component, the calculated axial strain ϵ_1 . Although some variability is present, the general trend is evident: the "local" axial strain ϵ_1 at fracture reduces with the increase in size. The reduction may be as large as 25 %. A definite dependence on b_0/h_0 cannot be seen.

Miklowitz' work included also the determination of the axial, the lateral, and the thickness strain distribution in the axial and width direction after fracture. Unfortunately, the data for the differently sized specimens do not allow an easy comparison of these strain profiles with respect to their similarity.

The previous work was extended by Miklowitz (1950, [2.39]) to include a group of tests on round tensile bars of the same steel where the dimensions of the tensile specimens were varied under geometric similarity covering a linear size range of 1 to 16. The diameter of the specimens were 3/16, 3/8, 3/4, 3/2, and 3 inches (4.76, 9.53, 19.05, 38.1 and 76.2 mm) and the gage length was 5 times and the fillet radius 4.25 times the diameter. Two specimens for each size were cut from the same heat as the flat specimen of ref. [2.38]. Billets 4 1/2 x 4 1/2 inches (114.3 x 114.3 mm) in cross-section served the purpose. The gage sections of the specimens were marked by circumferential scratches to measure the changes in diameters; from this the cross-section average of the longitudinal engineering strain ϵ was determined using the volume conservation assumption.

The following discrete stress and strain values obtained in the tests are listed in Tab. 2.12:

- true ultimate stress at an axial strain of 0.22; since the stress-strain curves were very flat at the ultimate load, a choice had to be made;
- average true stress σ at fracture at the minimum cross-section of the neck;

- maximum true stress σ_m at fracture according to Davidenko & Spiridonova (1946, [2.40])¹³;
- axial conventional strain at the minimum cross-section of the neck at fractures calculated from $\epsilon = A_0/A - 1$.

Three groups of tests were done

- Group I: The primary test series: Scaled specimens 1 to 6.
The cutting plan of specimen 1 to 6 are indicated in Fig. 2.29a.
Specimen 7 to 10 were co-axially positioned in the billet.
- Group II: Specimen 11 and 12, fabricated from the same heat as above and co-axially positioned; a repeat of 9 and 10 two years later.
- Group III: Specimen A and B of the same size. A positioned at the centre and B at the edge of the billet to obtain information on the homogeneity.

Tab. 2.12 shows that over the 16-fold increase in size the variation of the average true ultimate stress is slight and no general trend is seen when the size is increased. On the other hand, all data related to fracture show a definite decrease when the size is increased, however, with some peculiarities.

The tests A and B, both done with the same size of specimen (0.357 inch diameter), reveal a positional influence on the tensile properties: the average true stress and the maximum true stress at fracture and especially the axial strain at fracture are larger at the rim of the billet than at the centre. On this basis Miklowitz assumes that the averages of tests A and B are the values of a specimen (of the same size) unaffected by position in the billet. Miklowitz uses this argument and some consistency checks to introduce a trend correction in Tab. 2.12 as shown by the arrows along with each value (\uparrow : shift to larger values, \downarrow : shift to lower values). This correction for positional influence yields a size effect on stress and strain data at fracture in a much more pronounced form. However, in the reviewers opinion this correction is somewhat hampered by the limited number of quality assurance tests like A and B. Additional tests could reveal further scatter of the test data not only related to the radial position of the specimen.

The size effect may be illustrated also by combining results of Group I and III such that the influence of radial position is almost eliminated: specimens 3 and B have approximately the same diameter and are both positioned at the edge of the billet, the centre of specimen 3 located $\frac{1}{2}$ in. and 1 & 2 centred 1 in. off the edges. Of course, different circumferential and different axial positions may still have an influence.

From Tab. 2.12 it is seen that the test data related to fracture of specimens 3 and B are almost the same (differences 2 % and less). The comparison of these data with those of specimen 1 & 2, which are twice as large, show a slight decrease of the stress values but a significant decrease of the conventional strain at fracture in the neck: for specimen 3 & B the strains 1.83 & 1.80 were obtained whereas 1 & 2 yielded 1.58 & 1.46.

The 3 inches specimens 11 & 12, nominally identical to 9 & 10, were tested two years later. It was felt that a premature failure of specimens 9 & 10 had occurred, recognizable by

¹³ Here

$$\sigma_m = \sigma \frac{R + 0.5a}{R + 0.25a}, \quad \sigma = \frac{P}{A}$$

- a radius of minimum cross-section in the neck
- R meridional radius of the curvature of the neck profile at and near the minimum cross-section
- $A = \pi a^2$ minimum cross-section area in the neck
- A_0 original undeformed cross-section area

the low fracture stresses and strains and the peculiarities of the fracture surface which is of cleavage type whereas the tests 11 & 12 yielded a cup and cone type fracture and definitely larger fracture stresses and strains. This suggested the search for possible metallurgical causes for the difference in fracture behaviour. Cross-sectional slides were taken within the gage length of the specimens 10 & 11 which had undergone an engineering strain of 0.20. Different methods of etching were applied which revealed a segregation zone in specimen 10. The fracture surface of specimen 10 was also coincident with a surface scratch applied for measuring purposes. This stress concentration due to the scratch might have triggered the premature fracture of specimen 10 but specimen 9, prepared with similar machined surface lines, broke in the same way, however, seemingly not influenced by a surface scratch. Therefore, Miklowitz considers the macroscopic metallurgical non-uniformity as found in specimen 10 the primary reason for the premature fracture of specimen 9 and 10 although metallurgical tests of specimen 9 were not made.

The distribution of the axial engineering strain along the neck at fracture is shown in Fig. 2.30 for the selected specimens 1, 8, 9, 11 and 12. All strain profiles have been scaled along the axial direction (abscissa) to be comparable with the 3 inches specimens. For the central section of the neck the same trend is observed as for the maximum value: the smaller the specimen the higher the strains.

For the results described so far a size effect becomes manifest only for the instant of fracture. Beyond that Miklowitz provided profiles of the axial engineering strain in the specimens 1, 8, 9, 11 and 12 at certain stress levels before fracture which show the successive development of strain distributions along the specimen starting somewhat before the ultimate load is reached and proceeding up to fracture. It would have been interesting to compare the strain profiles of the differently sized specimens at the same stress levels before complete fracture; this would allow further assessment of similarity or size effects. However, the available data are too scarce and the inherent scatter and response sensitivity beyond the ultimate loads prevents such a comparison.

Miklowitz favoured an explanation of the size effect which he used already in his previous publication [2.38]. His argument refers to the lateral constraint of the stagnant material adjacent to the thin disk of flowing material at the heart of the neck: the constraining lateral stresses increase with the diameter of the bar. However, this argument is tautological: if similarity would apply, then the restraining stresses should be the same in the small and the large specimen. If they are not the same for properly scaled specimens and loading conditions, then non-similarity and thus a size influence is present.

The objective of the experimental work of Plechanova and Ratner (1954, [2.41])¹⁴ was to study the size effect on the tensile characteristics for the two soft materials copper and aluminium and for four different steels, the specimens having been prepared by different procedures. Specimens with circular cross-sections were chosen with diameters 5, 10, 20, and 40 mm. The gage length-to-diameter ratio is not explicitly mentioned but is believed to be 5. The characteristic tensile data chosen for comparison were the proportional limit σ_{pro} , the yield stress $\sigma_{0.2}$, the ultimate engineering stress σ_u , the average true fracture stress S_R and the area reduction ψ after fracture. The uniform elongation or uniform area reduction was not recorded and no indication is given about the stress-strain curve as a whole.

The origin of the materials is not mentioned and a cutting plan is not indicated. The four alloyed (Cr, Ni)-structural steels were 30 X ГСА-GOST, 30 X ГЧА-GOST, 40 X HMA-GOST, and 18 X HBA-GOST. To check the homogeneity of some of the steel slugs, which had been tempered at high temperature, 13 Rockwell hardness measurements were made along two diameters of a cross-section and five tensile specimens (5 mm diameter) were produced from material at five positions along a diameter. The hardness data for the steels

¹⁴ For the reviewer only an abridged verbal translation of this article was available. Thus some rational reconstruction or interpretation of the results was necessary.

30 X ΓCHA, 30 X HMA, and 18 X HBA as well as all characteristic tensile data for 18 X HBA show a high degree of uniformity along the diameters; e.g., the tensile data varied by less than 3 % with respect to the maximum values.

The metal slugs were heat treated before the specimen fabrication as follows:

- (1) Copper: Annealing at 600 °C, 2 h, cooled in the furnace
- (2) Aluminium: Annealing at 360 °C, 2 h, cooled in the furnace
- (3) Steel 30 X ΓCA: Hardening & tempering at 600 °C, 2 h, cooled in air
- (4) Steel 30 X ΓCHA: Isothermal hardening in saltpeter at 320 °C
- (5) Steel 18 X HBA: Hardening & tempering at 550 °C, 2 h, cooled in air
- (6) Steel 40 X HMA: Hardening & tempering at 550 °C, 2 h, cooled in oil

All specimens were turned under the following conditions: cutting speed $v = 15$ m/min, cutting depth $t = 0.2$ mm, feed $s = 0.14$ mm/turn. The number of specimens produced and tested for each material and size is not given, thus it is believed that only single tests were performed. The cross-head speed or strain rate during the tensile tests is not reported in [2.41] but the strain rate is expected to be $10^{-4} - 10^{-3} \text{ s}^{-1}$.

The results of the tensile tests are contained in Tab. 2.13. The influence of the change in specimen size is fairly obvious and is demonstrated also in Tab. 2.14, where relative values for two scale factors $\lambda = 4$ and $\lambda = 8$ are collected, e.g. $(\sigma_{\text{pro}})_{d=20}/(\sigma_{\text{pro}})_{d=5}$ & $(\sigma_{0.2})_{d=20}/(\sigma_{0.2})_{d=5}$ etc. Considering the two soft materials copper and aluminium, the increase in diameter from 5 to 40 mm produces an extremely large reduction for the proportional limit and the 0.2 %-proof stress whereas the ultimate stress and the two fracture data are almost not affected.

The increase in size from 5 to 40 mm diameter for the steels (4), (5), and (6) has a less pronounced influence on the proportional limit (12 to 24 %). The effect on the 0.2 %-proof stress is even less (7 to 15 %). Again, the influence on the ultimate stress is very small, only a 3 %-reduction is found. Aside from the proportional limit, which is probably not a very well defined quantity, the largest decrease due to an eight-fold increase in size is found for the average true fracture stress S_R and the area reduction ψ after fracture (decrease up to 24 %). Plechanova & Ratner argue that the homogeneity observed in the supplementary hardness and tensile tests exclude the technological inhomogeneity to be a possible cause of these size effects. The question remains whether a possible surface hardening due to the turning could be a possible explanation. To test this conjecture a series of experiments was performed for the steels 30 X ΓCA, 18 X HBA, and 40 X HMA: for each of the three steels two groups of specimens of the smallest size (5 mm diameter) were prepared according to two different production sequences:

- Group I:
 - I.1 Hardening & tempering of the metal slugs at 500 °C, 2 h (30 X ΓCA & 40 X HMA) or at 550 °C, 2 h (18 X HBA)
 - I.2 Tempering of the heat treated metal slugs at 500 °C, 2 h (30 X ΓCA & 40 X HMA) or at 550 °C, 2 h (18 X HBA)
 - I.3 Turning of the specimens ($v = 15$ m/min, $t = 0.2$ mm, $s = 0.14$ mm/turn)
- Group II:
 - II.1 same as I.1
 - II.2 same as I.3
 - II.3 same as I.2

The second heat treatment and its interchange in the group II is performed to reduce or annihilate the hardening due to the cold-work at the specimen surface induced by the turning. The tensile tests with these two groups of specimens gave almost no difference (1 – 2 %) in the proportional limit and the 0.2 %-proof stress. Also the relative differences in the other tensile data are far less than the observed size influence (Tab. 2.13) when the diameter is increased from 5 to 40 mm. From the above results for the 5 mm diameter steel specimens with a different sequences in the production processes Plechanova & Ratner concluded that the surface cold-work due to turning is not significant. Thus, Plechanova & Ratner conjecture that the reduction of σ_{pro} & $\sigma_{0.2}$ with increase of size is of physical origin linked to the behaviour of the bulk material and not a surface effect; they suppose that the size effect is related to the microscopic heterogeneity of the resistance against plastic deformation in small material volumes which is of a statistical nature.

However, Plechanova & Ratner also showed for 5 mm diameter specimens made from the two (Cr, Ni)-steels 18XHBA and 40XHMA tempered at high temperatures that different treatments such as

- (A) • Partial machining of specimens from tempered material
- Finish machining by turning with slow cutting speed
($v = 1.6$ m/sec, $t = 0.2$ mm, $s = 0.2$ mm/turn)

or

- (B) • Machining of specimens and subsequent hardening and tempering
- Finish by grinding

yield an increased surface hardness (< 26 %) when procedure (A) is applied; also somewhat increased proportional limits (< 9 %) and 0.2 %-proof stresses (< 3 %) are observed. These effects are larger than those found from the tests of Group I & II above. It is the reviewers opinion that the significance of the above small variations of the two stress data would be on a better basis if more tests would have been done.

The influence of the surface properties on the tensile characteristics was also studied for the soft material copper. Departing from the presentation of Plechanova & Ratner, these data and the previous test results in Tab. 2.13 are collected in Tab. 2.15.

It is obvious from Tab. 2.15 that the various production processes (α) to (ζ) do not affect the ultimate stress σ_u , the average true fracture stress S_R and the area reduction ψ after fracture. However, the quantities characterizing initiation of non-proportionality and yielding are affected under certain conditions. The 5 mm diameter specimens subjected to the production process (α) and (β) yield approximately the same values for σ_{pro} and $\sigma_{0.2}$ although the turning processes were different: the turning of the (β)-process is much rougher in the speed and feed. Here a larger surface hardening would be expected but this is not reflected in the tensile properties; unfortunately comparable hardness values are not available.

Increasing the diameter to 40 mm in the processes (ϵ) to (ζ), again no difference is found in all the tensile characteristics although the turning data are different: in the process (ζ) the speed was reduced by almost a factor of two and the feed was ten-fold larger. Of course, because of the larger diameter any hardening at the surface is expected to be of less importance than in the small specimens.

Significant surface effects for 5 mm diameter specimens are disclosed for specimens obtained by the processes (γ) and (δ). In the (γ) process the annealing is done after the turning which is followed by a grinding. Compared to processes (β) or (α) a significant reduction of σ_{pro} and $\sigma_{0.2}$ is obtained. The annealing should reduce cold work effects due to manufacture of the original copper bar but also due the surface hardening induced by the turning and the grinding abrades a thin cold-worked surface layer; it appears that this is of minor importance for the tensile test.

A significant surface hardening is obtained if the annealing and specimen fabrication by turning (e.g. process (β) or (α)) is followed by shot peening (process (δ)): compared to process (β) σ_{pro} and $\sigma_{0.2}$ increase by 30 and 37 % whereas the micro-hardness increases by 25 %.

From the comparison of specimen types (γ) and (ζ) the following conclusion may be drawn if the following assumptions are made: the comparison of the tensile data for the types (γ) and (ζ) indicates that the significant size effect found for copper (Tab. 2.13) is primarily due to a surface effect for this soft material. This statement is based on the assumption that the subsequent annealing after fabrication (process (γ)) annihilates the surface hardening in the 5 mm diameter specimen; further, the surface hardening in the process (ζ) is not effective because of the much larger diameter and the difference of σ_{pro} and $\sigma_{0.2}$ for these two differently sized specimens is much smaller than those given in Tab. 2.13.

Plechanova & Ratner measured also the cup and cone fracture areas and found that the ratio of the central fracture area (bottom of the cup) to the total area in the broken neck increases considerably in the steel whereas it remains constant for copper when the size is increased from 5 to 40 mm diameter.

Cechulin (1954, [2.42]) performed an extensive experimental study on the size effect in tensile tests of pure iron (Armco type) and various steels varying the size up to a scale factor of 13.3. The diameters of the circular specimens were 1.5, 3, 6, 15, and 20 mm. The gage length-to-diameter ratio was 5 and the similarity included the radius in the transition region as well as the specimen heads, except the very small specimens where the heads were somewhat larger. All specimens were taken along the rolling direction of the raw material and small as well as large specimens were cut from positions having the same distance from the surface of the metal blocks. Further details on the original material are not given. Also no indication is given on the homogeneity of the material.

The materials chosen were

- (1) Technically pure iron (Armco type)
- (2) Low carbon steel St3-GOST
- (3) Cr Ni steel 30XH3-GOST
- (4) Cr Ni steel 37XH3A-GOST, Brinell hardness $H_B = 241$
- (5) Cr Ni steel 37XH3A-GOST, Brinell hardness $H_B = 293$
- (6) Cr Ni steel 37XH3A-GOST, Brinell hardness $H_B = 352$
- (7) Cr Ni steel 40XH-GOST

For each material and each size 6 to 10 specimens were fabricated. The cross-head speed of the tensile testing machines was 0.02 mm/sec and was the same for all specimen sizes¹⁵. The author states that increasing the strain rate by a factor of about 10 due to the decrease in size will have a minor effect on the ultimate stress and area reduction (<1 %)

The results for the mean values of the conventional ultimate stress σ_B , the yield stress σ_T and the uniform area reduction ψ_g for the various materials as functions of the specimen diameters are shown in Fig. 2.31. The full scale range of 1.5 to 20 mm diameter was covered only for the rather soft materials, i.e. pure iron and the low carbon steel St3. It is seen that none of the above characteristic tensile data depend on the specimen size.

The size-independence of the yield stress is in contrast to the results of Plechanova & Ratner (1954, [2.41]); there a strong increase of the yield stress with a decrease in diameter was found especially for the soft materials. However, the size-independence of the conventional ultimate stress is observed again. The frequently found relation between hardness of a material and its yield and ultimate stress is realized again for the steel 37XH3A.

¹⁵ This corresponds to an average strain rate of about $3 \cdot 10^{-3} \text{ s}^{-1}$ for the smallest specimen.

An important result is the size-invariance of the uniform area reduction which corresponds to the area reduction at ultimate load; this implies also a size-invariance of the uniform elongation. Beyond the data in Fig. 2.31 Chechulin points to the fact that the engineering stress-strain curves for four different sizes from 1.5 to 10 mm diameter agree except in the softening region close to fracture.

Here, however, the reader expects more differentiated statements: it is almost unbelievable that no scatter is present in 6 to 10 nominally identical tensile tests of very different sizes. Unfortunately, the question of the variability of these tests is not even mentioned in [2.42].

The size influence becomes evident when those tensile data are investigated which characterise the instant of fracture, i.e. the area reduction ψ after fracture and average true fracture stress S_R . For the materials (1), (2), (3) and (7) the decays of the area reductions with increasing size are shown in Fig. 2.32(a) and for the material 37XH3A with different hardnesses ((4), (5) and (6)) the area reductions are plotted in Fig. 2.32(b). The average true fracture stress is presented in Fig. 2.33. Except for an anomalous maximum for the pure iron (1) and the low carbon steel St3 (2) at small specimen sizes, all data show a quasi-exponential or linear decay with increasing size. Chechulin relates this anomaly to the irregular shape of the fractured cross-section, which appears if the material is coarse grained, and to the usual procedure the area reduction is determined (measurement of two orthogonal diameters only). Cutting the specimens in the fractured neck and determination of the area of the irregular cross-section yields a more accurate value for the area reduction. With these data the dashed curves become valid and the anomaly disappears.

Fig. 2.32(b) shows the influence of changes in the hardness on the size dependence of the area reduction at fracture for the steel 37XH3A. The increase in hardness does not only reduce the area reduction for a given size but also shifts the size influences to larger sizes. The size dependence of S_R and ψ for the three hardnesses allows to plot the average true fracture stress S_R as a function of the area reduction ψ with the diameter representing the curve parameter. Chechulin obtains, within the size range of 1.5 to 15 mm diameter, three linear relations with positive slope, the large specimens being at the lower and the small specimens at the upper end.

Davidenko (1960, [2.43]) called attention to the question of the size influence on the mechanical properties of solids. Among the different publications which followed the editorial appeal, only the results of Chechulin (1961, [2.44]) are related to the topic discussed here. Chechulin clearly distinguishes between the three stages of the mechanical response where the size effect may become important: (a) Effects on the proportional limit, the hardness etc. i.e. before the first cracks appear, (b) the dependence of the limiting plasticity or the beginning of cracking on the specimen size, and (c) the differences between the rupture processes taking place in small and large specimens after the appearance of the first cracks. Chechulin further elaborates somewhat on plausible explanations of the size effects like statistical and energy theories.

To clarify the dependence of the appearance of the first crack on the size of the samples, tensile tests on geometrically similar 3 mm and 15 mm diameter specimens of 37XH3A steel, heat treated to obtain three different hardnesses, were performed. Details of the origin, fabrication, other geometrical data and testing conditions are not given. The results are collected in Tab. 2.16. The 15 mm specimens were all ruptured and here δ and ψ denote the elongation and area reduction after rupture. On the contrary, the 3 mm specimens were tested only until the neck was fully developed but not ruptured; thus, δ and ψ here relate to a state just before rupture.

As seen from the average values in Tab. 2.16 the $\sigma_{0.2}$ -proof stress and the ultimate stress σ_B are not affected by the change in size, irrespective of the hardness level. Of course, the hardness has an influence on these data. Unfortunately, no data for the uniform elongation are available. Also a more complete picture could be obtained if all the individual test data were

given. It is noteworthy that the deformation measures δ and ψ of the unbroken 3 mm-specimens are practically the same as those of the broken 15 mm-specimens. Chechulin notes: "If the first crack were to be produced during the same strain stage in large and in small test pieces, then the necked, but not ruptured 3 mm-specimens should have a well developed crack". The x-ray investigations and the metallographic inspections of axially cut specimen showed, however, a complete absence of cracks. A microscopic crack was detected only in one 3 mm-specimen whose area reduction exceeded that of the ruptured 15 mm-specimens. These tests demonstrate that cracks appear in small specimens at a later stage than in geometrically similar large test specimens.

The influence of size on the tensile properties of the carbon steel Ck15 was tested by Schneeweiß (1966, [2.45]) using proportional specimens with diameters 3.5, 6, 10, 14, and 30 mm (scale factor 8.6). The ratio gage length-to-diameter was 10 and all other dimensions were also properly scaled except some deviations in the threads. The specimens were taken from a 90 mm diameter bar with a length of three meters. It was divided in eight sections, each section for one specimen type, and their sequence is indicated in Tab. 2.17. Thus all small specimens are taken from two adjacent sections at one end. No heat treatment was given to the specimens. A relatively large number of nominally identical test were performed. The average test results are indicated in Tab. 2.17 and Fig. 2.34. Young's modulus E , as well as the upper and the lower yield stress σ_{so} and σ_{su} do not show any systematic dependence on the size. The ultimate stress σ_B and the corresponding true ultimate stress S_B show a slight decrease of 3.8 % and 5.1 %, respectively, over the whole scale range when the size is increased.

Schneeweiß believes that this size effect is caused by the different heat-up due non-adiabatic heating by plastic deformation: the heat conduction plays a more important role for the smaller specimens and reduces the temperature increase, thus the thermal softening effect is less pronounced than in the large specimens. Certainly, this is a phenomenon to be considered but quantitative estimates of its influence are entirely missing in [2.45].

The uniform elongation was obtained by two different methods: measurements of the strain distribution (outside the necked region) which yields δ_g' and using the total elongations δ_{10} and δ_5 after fracture which gives approximately $\delta_g'' = 2 \delta_{10} - \delta_5$. Their average value is denoted by δ_{gm} . These various data are contained in Tab. 2.17 and Fig. 2.34.

The elongations at fracture δ_{10} and δ_5 as well as the area reduction ψ at fracture and the true fracture stress S_R show a definite decrease with increasing size (Fig. 2.34): over the whole range of sizes the relative decreases are 8.6 %, 7 % and 7.5 % for δ_{10} , δ_5 and ψ and 28 % for S_R . The uniform elongations δ_g' and δ_g'' (Fig. 2.35) as well as their average (Fig. 2.34) appear to have a maximum at $d_0 = 6$ mm diameter, however, the scatter for the 3.5 mm diameter specimens is large and the two methods give somewhat different results. Here it would be necessary to know the actual measurements and their scatter band to make a reliable judgement whether a size dependence of δ_g' and δ_g'' is significant within the range of the 3.5 to 14 mm diameter specimens. Schneeweiß states that the observed size dependence of the elongations at fracture is mainly due to the size dependence of the uniform strain. This is comprehensible for the regime $d_0 = 14$ to 30 mm but not for the smaller specimens. Here it seems that the dependence is more related to the size dependence of the necking process.

The dependence of the tensile characteristics of geometrically similar steel specimens of different purities was studied by Buch (1969, [2.46]): a conventional cast (K) and a electrode-slag remelting (E) of the structural steel 36CrNiMo4, two melts I & II of different purities of the structural steel X20Cr13, and the ball bearing steel 100Cr6 in the form of two melts (K) and (E) were used. The specimen diameters were 3, 4, and 5 mm for the first two steels whereas for the ball bearing steel specimens 3, 5, and 10 mm diameter were used. In all cases the gage length-to-diameter ratio was 5.

The impurity content was determined as the relative area fraction of the non-metallic inclusions found in longitudinal or transverse cuts. The amount of impurities larger than 5 μm of the (K)-cast of the CrNiMo-steel is about two times larger than for the (E)-cast (0.0708 % and 0.0330 %, longitudinal cuts). Impurities larger than 30 μm were much less present (0.0172 % and 0.0010 %). For the melt II of the X20Cr13 steel the impurity content was also about two times larger than in melt I.

Aside from the conventional tensile characteristics like ultimate stress σ_B , elongation at fracture δ_5 and area reduction ψ at fracture also the true fracture stress σ_R ¹⁶

$$\sigma_R = \sigma_0 \left(1 + \frac{a}{4R} \right)$$

a: radius of minimum cross-section in the neck

R: meridional radius in the neck profile

$\sigma_0 = \sigma_1 - \sigma_2$: difference in principle stresses (at the surface $\sigma_0 = \sigma_1$)

was determined. They are collected in Tab. 2.18 for the first two steels. The "L" and "Q" letters refer to the orientation of the specimens in the raw block of material ("L": longitudinal, "Q": transverse). Since the number of tests and the amount of scatter for each parameter case are not indicated in [2.46], it is likely that only single tests for each case were performed. Also the values of R at fracture are not given whereas the radius a can be calculated from ψ . Unfortunately, the yield stress as well as uniform elongation were not recorded.

For the conventional melt (K) of the 36CrNiMo4-steel the ultimate stress clearly reduces by about 10 % for both the "L" and "Q" directions when the diameter is increased from 3 to 5 mm.

The elongation at fracture δ_5 and the area reduction ψ are also reduced especially for the "Q"-direction (decrease of $\psi_Q \approx 23$ %). This trend is also found in the true fracture stress σ_R ("L" direction ≈ 20 %, "Q"-direction 16 %).

For the electrode-slag remelt (E) of the 36CrNiMo4-steel with two times less impurity content the ultimate stresses for both directions are almost the same when the diameter is increased. This is also true for the deformation measures δ_5 and ψ in the "Q"-direction whereas these measures are somewhat larger (around 5 %) for the smaller specimens of the "L"-direction. Again the true fracture stress σ_R is found to decrease ("L"-direction ≈ 24 %, "Q"-direction ≈ 9 %) when the diameter increases from 3 to 5 mm.

The melt II of the X20Cr13-steel with the higher impurity content gives even a slight increase (≈ 7 %) of the ultimate stress for the "L"-directions whereas a very slight decrease is observed for the "Q"-direction when the diameter is increased from 3 to 5 mm. The elongation δ_5 and the area reduction at fracture ψ reduce with the increase in size especially for the "Q"-direction. For melt I with less impurity content the size influence on these data is generally reduced.

Results for the ball bearing steel 100Cr6 show an increase in the fracture deformation measures δ_5 and ψ as well as the true fracture stress σ_R when the diameter is decreased from 10 to 3 mm. From Fig. 2.36 it is seen that the size influence is largest for small diameters. The influence of the different melts (impurity is not recorded) is very moderate. The significance of the observed trends is difficult to judge since it appears that only single tests for each case have been done.

Sato and Terazawa (1971, [2.47]) investigated the effects of sizes and shapes of various round and sheet type tensile specimens (specified in the Japanese Industrial Standard (JIS) Z2001) on the tensile properties of several aluminium alloys. Whereas the 0.2 %-proof stress $\sigma_{0.2}$ and the ultimate stress σ_B were almost not affected, the elongation at fracture was

¹⁶ This is an approximation of Davidenko's formula, footnote 13.

depending on the slenderness ratio L_0/\sqrt{A} (L_0 : gage length, A : undeformed area of the cross-section) and to some extent also on the constraining effects of the end-sections of the specimen outside the gage length L_0 . These latter influences were the primary interest of the above authors. To be more specific we restrict attention to the results of the specimens with circular cross-sections. The geometry of the specimens, according to the Japanese Industrial Standard, is given in Tab. 2.19. All the specimens 14 A1 to 14 A4 show geometrical similarity within the gage section L_0 . The specimens 14 A2, 14 A3 and 14 A4, however, have a higher degree of similarity, since it extends over the whole length L_c of the uniformly reduced cross-section. In any case the diameters range only from 14 to 22 mm which represents a very limited change of size (scale factor $\lambda = 1.57$). The chemical composition of the three aluminium alloys 1100, 2017 and 5056 is put together in Tab. 2.20.

The specimens were manufactured from round bars of 35 mm diameter. All specimens were marked at distinct points along a meridional line at the surface within the gage length L_0 and beyond, including the region of the reduced cross-section and the fillet radius. This allows to determine the axial strain distribution. The number of nominally identical tests is not explicitly stated in [2.47] but some of the results are said to be the averages of three tests.

Fig. 2.37 demonstrates the insensitivity of the 0.2 %-proof stress $\sigma_{0.2}$ and of the ultimate stress σ_B . Unfortunately, the uniform elongation is not recorded in [2.47]. The elongation at fracture δ , referred to the various gage lengths L_0 of the different JIS-specimens, are shown in Fig. 2.38. For the probes No. 14A2, 14A3 and 14A4 which are geometrically similar within the reduced section length L_c and where L_c is considerably longer than the gage length L_0 ($L_0/D = 5$, $L_c/D \approx 7$) the elongations at fracture show almost no difference for each one of the materials. The specimen JIS No. 4 which has the smallest slenderness ratio ($L_0/\sqrt{A} = 4.03$) yields the largest fracture elongation for all three materials.

The influence of the choice of the gage length is also shown in Fig. 2.39. The distinct marks along the various specimens allow to choose different reference lengths L_0^* ($0.8 D \leq L_0^* \leq 7.3 D$) such that the fracture is positioned at their centre, and the average axial strain (the fracture strain δ^*) in these sections can be calculated. Fig. 2.39 shows the dependence of the fracture strain δ^* on the choice of the reference length L_0^* for the different specimen types, which may be smaller or larger than the standard reference (gage) length L_0 . The very strong dependence of the fracture strain δ^* on the magnitude of the reference length L_0^* , giving the largest values for small ratios L_0^*/\sqrt{A} , is evident. Of course, the largest value corresponds to the average strain over the smallest gage length L_0^* enclosing the minimum cross-section of the fractured neck. In fact, the curves in Fig. 2.39 represent integrals of the local strain distribution $\epsilon_{(x)}$ along the length of the specimen:

$$\delta^* = \frac{1}{L_0^*} \int_0^{L_0^*} \epsilon_{(x)} dx.$$

For the specimens JIS No. 14A2 to 14A4 the results collapse almost into one curve; here $L_c/D \sim 7$. Holding the gage section the same but reducing the straight section length from $L_c/D \sim 7$ to $L_c/D \sim 5.5$ (specimen JIS No. 14A1), this yields a reduction of the fracture strains δ^* . Obviously, this influence is due to the increase of the constraining effect of the material outside the gage section, especially the region of the fillet radius. This effect is largest for the soft aluminium alloy 1100. Therefore, for probes of circular cross-section Sato & Terazawa consider the desirable relation between the reduced section length L_c and the gage length L_0 to be $L_c \geq L_0 + 2D$. Accordingly the probes JIS No. 4 & 10 are not appropriate and for the probe JIS No. 14A ($L_0/D = 5$) the use of a large reduced cross-section length $L_c/D = 7$ is proposed. For $(L_c - L_0) < 2D$ constraint effects of the specimen ends will affect the fracture elongations.

Certainly, the end effects are influences which must be properly accounted for. However, even then the fracture strain is not an intrinsic material property as it appears to be at some

instances in the presentation of Sato & Terazawa; even without end effects it is depending on the geometry of the gage section, i.e. the slenderness ratio L_0/\sqrt{A} . The conclusion one may draw from the results for the geometrically similar specimens JIS No. 14A2 to 14A4, not affected by end effects and shown in Fig. 2.39, are that the dimensionless average strain functions δ^* vs. L_0^*/\sqrt{A} are size independent within the range of diameters from 14 to 22 mm. Thus, then the definition of δ^* implies also that the local axial strain distributions ϵ are independent of the specimen size.

The axial strain distribution curves for JIS No. 14A ($L_c = 7D$) specimens of the three aluminium alloys are illustrated in Fig. 2.40. It is noteworthy that the alloys 2017 and 5056 show a pronounced necking zone of length l_n which is well within the gage section $L_0 = 5D$; the uniform straining outside the neck is also well established and it extends beyond the marks of the gage length. However, for the soft alloy 1100 the neck extends almost over the whole gage length and a zone of uniform straining is difficult to identify. This behaviour implies that the constraining end effects will affect the necking process; thus, a reduction of the straight section length L_c will decrease the straining in the neck. This explains the L_c/D -sensitivity of the δ^* -function for the alloy 1100 in Fig. 2.39.

Matic, Kirby, and Jolles (1988, [2.48]) proposed and used a hybrid computational experimental approach for the identification of material constitutive parameters. The experimental basis was the load-deformation response beyond the onset of necking of tensile specimens with different dimensions. By this procedure, the parameters for the NiCrMo-steel HY-100 were determined, in the context of a standard incremental rate-independent elastic-plastic model as provided by the ABAQUS finite-element code. Here the computational aspects, and basic premises are not commented; attention is put only to the experimental investigations.

A family of unscaled tensile specimens was designed to obtain data on the effect of "size and geometry" for the HY-100 steel. Three different gage section diameters $d_0 = 7.6, 12.7$ and 17.8 mm (0.30, 0.50 and 0.70 inch) and four different gage lengths $L_0 = 12.7, 25.4, 38.1,$ and 50.8 mm (0.50, 1.00, 1.50, 2.00 inches) were used to generate 12 different specimen geometries. The corresponding gage length-to-diameter ratios are given in Tab. 2.21.

In the following, the letters (a), (b), (c) and (d) will be used to identify a specimen type: for example, in the letter pair (a, b) the first letter refers to the diameter d_0 and the second one to the gage length L_0 . Obviously, specimens with strict geometrical similarity, which implies $L_0/d_0 = \text{const.}$ within the gage section, are not included in this family. In all specimens a transition section was existing between the gage section and the 25.4 mm diameter grip section; the transition section's cross-sectional area was double the gage sectional area such that elastic response was ensured for this material outside the gage section. The origin of the material and the assurance of its homogeneity are not reported in [2.48]. Also no indication of the cutting plan for the 36 specimens and the fabrication procedure of the specimens are given.

All tests were performed under stroke control at a rate of 1.27 mm/min. A clip-on extensometer was used to measure the elongation of the specimen in the gage length. Without halt of the tests photographs of the specimen's gage section were taken close to the occurrence of the ultimate load and subsequently in intervals to obtain full-field information of the necking process. The corresponding load displacement data were marked so that the photographs could be matched with the elongation. Typically, 12 photographs were taken for each specimen. Three tests were performed for each specimen type and all test run up to failure. Matic et al. state that the load elongation curves of each of the three nominally identical tests are "essentially identical", but this is not demonstrated by presenting individual data of nominally identical tests.

The above results may be considered as a confirmation of the macroscopical homogeneity of the material the specimens were made from, if the various nominally identical specimens were randomly distributed in the raw material and not taken from a small section.

The corresponding engineering stress-strain curves for each of the specimen types are plotted in Fig. 2.41. It is not clear whether each curve represents a typical test result for each of the 12 specimen types or whether each curve is an average of the three nominally identical tests. It is also not assured whether the curves are very precise graphical reproductions of one or the other data set. Thus, the conclusions the reader can draw from Fig. 2.41 are subject to uncertainty.

From Fig. 2.41 it is seen that the yield stress and the ultimate stress are independent of the diameter and independent of the gage length, except specimen type (c, a) (Fig. 2.41c, curve (a)). Here yield stress and ultimate stress are increased and this specimen is specified by a very small ratio $L_0/d_0 = 0.713$. The uniform elongations (engineering strain at ultimate stress) appear to be roughly the same in Fig. 2.41b & c (specimens diameter 12.7 & 17.8 mm), except specimen (c, a). But in Fig. 2.41a, containing the specimens with the smallest diameter (7.6 mm), the uniform elongation decreases with increasing gage length. Thus, even excluding specimen (c, a), similarity of stress-strain curves up to the ultimate stress is not found over the whole range of ratios $L_0/d_0 = 1 \div 6.68$ and diameters $d_0 = 7.6 \div 17.8$ mm.

Identifying the end points in the graphs as the instants of fracture, the engineering fracture stress is approximately the same for the specimens with smaller diameters (Fig. 2.41a & b; except specimen (a, b) with a somewhat higher stress). However, in Fig. 2.41c, where the specimens with the largest diameter are collected, the fracture stress seems to decrease with increasing gage length. Clearly, for all diameters the elongation at fracture decreases with increasing length, a very well known result related to the localized necking process (see e.g. Moore [2.32]).

Within the family of specimens one may identify three pairs of specimen types which are roughly geometrically similar, i.e. which have approximately the same ratio L_0/d_0 . They are (c, b) & (a, a), (b, b) & (c, c), and (c, d) & (b, c).

From Fig. 2.41 the corresponding elongation at fracture ε_f can be determined and they are listed in Tab. 2.22. The scale factor λ_d of the diameter is also indicated.

From Tab. 2.22 it is noted that the elongations at fracture ε_f of the roughly similar specimens are approximately the same and thus satisfy a similarity condition. This complies with results of Barba and Bauschinger described earlier. However, the scale factors involved are rather small. From Tab. 2.22 it is also seen that a decrease in the ratio L_0/d_0 yields an increase in the total elongation at fracture. This is also in agreement with observations made by Moore and others mentioned previously. Although full-field photos were taken geometric information on the successive neck formation, and the final neck geometry is not reported in [2.48], not even the area reduction after fracture. Some verbal statements are made by Matic et al. such as: "The geometric similitude of the neck geometry over all specimens, with the exception of the specimen with the smallest L_0/d_0 ratio of 0.71 is consistent with the increase in global specimen ductility as the specimen gage section is decreased for a constant specimen diameter." This is a meagre argument.

Matic et al. remark also: "Geometric similitude is in evidence for all but the specimens... . Further examination of this geometric similitude in the neck profile tends to support a view that the length of the neck remains a constant multiple of the original specimen diameter...". A measure characterising the neck profile is the distance between the inflection points adjacent to the minimum cross-section in the neck. With regard to an experimental assessment of the similitude of the neck deformation for sufficiently long specimens under the same stress the above statements are essentially insufficient because of their qualitative and vague description.

However, using the available data and an approximate and simple consideration, the following statement with respect to the geometric similarity of the neck can be made. It is assumed that a finite necking region $L_n < L_0$ exists characterized by an average axial engineering strain ϵ_n . Before neck formation the uniform plastic strain at maximum load is ϵ_g which does not change outside the necked section when the neck is formed. If ϵ is the total strain in the gage length, then the total extension of the gage section is

$$\epsilon L_0 = \epsilon_g (L_0 - L_n) + \epsilon_n L_n$$

or

$$\epsilon = \epsilon_g + \frac{L_n}{L_0} (\epsilon_n - \epsilon_g).$$

Among others, similarity implies that ϵ_g is size invariant and ϵ_n is independent of the size for the same stress level. If the specimen is sufficiently long, the end effects do not effect the neck length L_n and L_n scales with the diameter, i.e. $L_n/d_0 = \hat{c} = \text{const}$. Thus the total strain

$$\epsilon = \epsilon_g + \frac{d_0}{L_0} \hat{c} (\epsilon_n - \epsilon_g).$$

In terms of the initial circular cross-section S_0 the diameter is $d_0 = \sqrt{4/\pi} \sqrt{S_0} = 1.13 \sqrt{S_0}$ and the total elongation reads

$$\begin{aligned} \epsilon &= b + c \frac{\sqrt{S_0}}{L_0} \\ b &= \epsilon_g \\ c &= \hat{c} \sqrt{4/\pi} (\epsilon_n - \epsilon_g). \end{aligned}$$

A linear relation between elongation ϵ and the "stoutness" $\sqrt{S_0}/L_0$ has been derived for the instant of fracture independently by Barba (1880, [2.30]), Bauschinger (1892, [2.31]), Martens (1989, [2.49]) and Unwin (1904, [2.50]), and it was considered to be valid also for non-circular cross-sections. But, according to Beare & Gordon (1921, [2.33]), experiments showed that it is satisfied only in the case of bars of compact section (circular, square, rectangular) with width-to-thickness ratios not greater than about 4 (see Moore (1918, [2.32]) mentioned above).

The above relation implies that for specimens with the same diameter and a decreasing gage length the fracture strain increases. Fig. 2.41 confirms this qualitatively and Fig. 2.39, obtained by Sato and Terazawa (1971, [2.47]) for aluminium alloys, shows this trend very clearly.

For geometrically similar specimens the ratio $\sqrt{S_0}/L_0$ is constant and the total strain ϵ is the same for the small and the large specimen at the same engineering stress level. In principle this can be checked by comparing the engineering stress-strain curves in Fig. 2.41 of the specimens which are roughly geometrically similar (Tab. 2.22): these curves should be roughly congruent, especially in the softening part. The reviewers, however, considered only the instant of fracture and the corresponding strains ϵ_f are collected in Tab. 2.22. As already mentioned the total fracture strains compare reasonably well. As seen from Fig. 2.41, also the fracture stresses are approximately the same for the roughly geometrically similar specimens except for the pair (c, b) & (a, a) which has the largest geometrical scale factor. This mismatch in the fracture stress signals non-similarity. The similarity obtained for the specimen pairs (b, b) & (c, c) and (c, d) & (b, c) appears to be not very convincing since the scale factor is rather small ($\lambda = 1.4$). In any case similarity considerations require also a quantitative comparison of the neck profiles which is not given by Matic et al. in [2.48].

In Section 2.1 the size dependence of quasi-static bending tests (austenitic steel X5CrNi189; Stach (1997, [2.27]), Jordan & Malmberg (1998, [2.28])) were mentioned. The response of this material in scaled tensile tests has also been investigated subsequently by Malmberg, Aktaa & Schlossmacher (1999, [2.62]) at the Forschungszentrum Karlsruhe. In conjunction with the above mentioned bending specimens, geometrically similar uniform tension specimens with 1.5 and 15 mm diameter (gage length-to-diameter ratio 5) were carefully machined by turning from a single stock bar of 30 mm diameter and 1800 mm length. Three large and 9 small tension specimens were obtained from the central section around the axis of the bar. Each of the three sets of three specimens (triple set) were arranged within the 15 mm diameter core. The three large specimens were taken from three positions, periodically distributed along the bar, 600 mm apart, and the three triple sets of small specimens were arranged similarly along the bar. After machining three specimen sets of both sizes were prepared: (i) as fabricated, (ii) stress annealed for 40 min. at 650°C in air to reduce surface cold working due to machining, and (iii) solution annealing for 4 h at 1050°C in vacuum. Each set contained, of course, one large specimen and three small specimens, each of them from three different positions along the bar 600 mm apart. All tensile tests were performed at a constant quasi-static strain rate of 10^{-3} s^{-1} ; thus, the cross head speed was scaled according to the size of the specimens to obtain approximately the same rate influence on the flow stress. Thus, three nominally identical 1.5 mm diameter specimen were tested for each state whereas only a single 15 mm diameter specimen was available. A very large size effect is observed for state (i) and also (ii) (see Fig. 2.42a & b). The small specimens show a significantly increased initial and subsequent flow stress (at 2 % strain about 27 % increase in the "as fabricated" condition) but the hardening rate is almost not affected. Also the scatter of the tests for the small specimen is rather small, thus material heterogeneity is negligible along the bar. Comparing the results of the 15 mm diameter specimen of state (i) and (ii), the stress annealing has almost no effect but the 1.5 mm diameter specimen show a slightly reduced flow stress due to stress annealing (e.g. at 5 % strain the flow stress is reduced by about 5 %). The small effect of this heat treatment may be an indication that a surface effect induced in the small specimens due to machining might possibly not have been fully annihilated by this heat treatment and therefore, this effect may still be one cause for the observed size effect. Micro-structural investigations and micro-hardness tests, however, did not provide direct hints for an explanation. In any case the large effect is likely related to the size of the 1.5 mm diameter which is considerably smaller than the minimum diameters of the tensile test series discussed so far. On the other hand, in the solution annealed state (iii) the flow stress is reduced considerably, but more important, the size effect is not observed, instead a slightly reduced initial yield strength of the small specimens is found. This treatment implies a transformation of the micro-structure, among others, the dissolution of carbon precipitates on the grain boundaries which are responsible for the strength. The absence of a size effect for this state appears to contain a clue for the presence of a size effect in the other states. However, whether this is related to a surface effect or to the bulk properties of the different micro-structures is unresolved.

2.3 Similarity and Dimensional Effects in Tensile Tests of Smooth Sub-Size Specimens

The development of fission and fusion reactor materials requires the investigation of the effects of irradiation damage on the material properties. The radiation facilities impose severe restrictions on the size and the thickness of the test specimens. Very small flat specimens have been designed and manufactured with varying thickness (typically ~20 to 400 μm and more), the thinnest specimen having only a few grains across the thickness. Tension tests have been performed under non-irradiation conditions to investigate the transition of the mechanical response from thin foil to polycrystalline bulk behaviour.

It cannot be the purpose of this review to elaborate on this topic in any detail because the minimum dimensions are outside the range of our present interest. Nevertheless, some of the important results are briefly sketched.

Among others, Miyazaki, Shibata and Fujita (1979, [2.51]) investigated the 0.2%-yield stress and the flow stress at 5, 10, and 20 % strain of polycrystalline Al, Cu, Cu-13 at% Al and Fe as a function of the grain size and the specimen thickness. The materials were heavily cross-rolled at room temperature which was followed by annealing in order to avoid the rolling texture. Controlled grain sizes were in the range from 16 to 180 μm in all the specimens. The thickness of the flat specimens (width 6 mm, gage length 12 mm) was changed by chemical- and electro-polishing and ranged from 0.045 to 1.840 mm for each grain size d . The tensile tests show for all materials that, for a given grain size, the yield and flow stresses decrease with decreasing specimen thickness t if the specimen thickness is smaller than a critical value, independent of the amount of strain (Fig. 2.43); this suggests a critical ratio¹⁷ $(t/d)_c$. Beyond this critical thickness a saturation is obtained. However, if the grain sizes d are decreased, the critical thickness is decreased or remains approximately constant.

Thus, the critical ratio $(t/d)_c$ is not independent of the grain size but decreases if the grain size is decreased.

Miyazaki et al. associate this with the fact that the slip mode in individual grains of polycrystals are strongly affected by the interaction with adjacent grains. This interaction is considered to reach widely beyond the first nearest-neighbour grains so that the flow stress decreases with decreasing specimen thickness when the number of grains contained along the thickness direction becomes smaller than a critical value (see [2.51] and the references cited therein).

Igata, Miyahara, Uda, and Asada (1983, [2.53]) determined the mechanical properties of thin foil specimens (width: 4 mm, uniform length: 15 mm, thickness: 18 to 350 μm) of types 304 and 316 austenitic stainless steels at room temperatures at a constant strain rate of $4.5 \cdot 10^{-4} \text{ s}^{-1}$. Tension specimens were cut from as-received foils and were not deburred by chemical- or electro-polishing. Solution treatments were done at various temperatures from 1050 to 1300 $^{\circ}\text{C}$ for 8 to 80 min in argon to change the average grain size. According to Igata et al., there were no other micro-structural differences, such as dislocation density or the precipitation of carbides, between the specimens besides the differences in grain size. The 0.2 % proof stresses of SS 304 and 316 were shown to be grain size and specimen thickness dependent (Fig. 2.44). The 0.2 % proof stress of the SS 304 bulk material (thickness: 3.2 mm) follows the Hall-Petch relation (linear $(d^{1/2})$ -dependence on grain size). For specimens below a critical thickness the proof stresses are shifted to lower values. This is sketched in Fig. 2.44 which shows the relation between the proof stresses and the number of grains across the thickness t/d (for a given grain size). Above a critical value $(t/d)_c$ (about 4 for SS 304 and 6 for SS 316) the proof stress of the thin specimens becomes equal to that of the bulk material.

¹⁷ The value t/d is the average number of grains across the thickness.

The total elongation at fracture of SS 304 is not grain size dependent but for SS 316 it increases definitely with a decrease in grain size for each specimen thickness (Fig. 2.46). For a given grain size the total elongation decreases strongly for both materials when the thickness is decreased (other dimensions held constant).

The work hardening exponent n of the true stress – true strain relation $\sigma = k \epsilon^n$ increases slightly with grain size for SS 304 and a given specimen thickness; for SS 316 it is almost independent of the grain size over a wide range. For a given grain size the hardening exponent decreases when the specimen thickness is decreased for both SS 304 and especially SS 316. For very small thicknesses (~0.02 mm) the exponent n comes down to 0.2 from 0.3 at the largest thickness.

Related comparisons for SS 316 have been performed by Rickerby, Fenici, Jung, Piatti, and Schiller (1983, [2.54]). Among others, Rickerby et al. compared characteristic tension data of thin, flat specimen (width: 2 mm, uniform length: 11 mm, thickness: 0.2 mm, grain size: 35 μm) obtained by Kraaij (1980, [2.55]) with corresponding results by Matteazi et al. (1981, [2.56]) of standard ISO type specimens with circular cross-section (diameter: 4 mm, gage-to-diameter ratio 5, grain size ~ 45 μm); this comparison covered a large temperature range from room temperature to 800 °C.

The thin flat specimens with longitudinal axes parallel to the rolling direction were cut from cold-rolled sheet, the material being in a solution annealed condition. The larger specimens with circular cross-section were machined directly from as-received, solution-annealed material without any intermediate cold rolling. It is not reported whether the two material sources came from the same heat. The tests at elevated temperature were performed in a pure argon atmosphere with an average plastic rate of about 10^{-3} s^{-1} which was maintained during uniform elongation in all cases.

Experimental data for the 0.2 % proof stress ($\sigma_{0.2}$), the ultimate tensile stress (σ_{uts}), the uniform elongation (ϵ_u) and the elongation at fracture ϵ_f were recorded (Fig. 2.47 & 2.48). A striking feature of the $\sigma_{0.2}$ and σ_{uts} values of the two different specimens is their closeness over the entire temperature range (Fig. 2.47) It is noted that the values for the thin flat specimens are slightly below the data of the circular diameter specimens.

This appears to be in accordance with the thickness effect found previously ([2.51], [2.53]): according to Igata et al., six or even more (compare Fig. 2.45b) grains across the thickness are necessary for SS 316 to obtain bulk material data; the flat specimens used here correspond to 5.7 grains across the thickness.

For the thin flat specimens the uniform elongations ϵ_u practically coincide with the elongations at fracture ϵ_f (Fig. 2.48). This suggests that an extended necking process is not possible if only a few grains are located along the minimum dimension of the cross-section. Instead, the 4 mm diameter specimen necks down to fracture with a fracture strain much larger than the uniform elongation. The comparison of the uniform elongations of both specimen types shows again an approximate agreement, except at the highest temperature. The difference seen could be properly judged if the number of repeat tests and their scatter would have been indicated in [2.56].

2.4 Discussion

The objective of the previous sections was to provide a restricted review of mechanical tests with geometrically similar laboratory type specimens of different sizes but of a relatively simple shape and made of metallic materials, especially steel. Results of tests of complex scaled down component type models and their comparison with the corresponding full scale component were not considered here. Motivated by the results of scaled fluid-structure impact experiments performed at the Forschungszentrum Karlsruhe (Stach (1997, [1.4]), Jordan & Malmberg (1998, [2.28])) and by certain hints found in the published literature (quoted by Malmberg (1995, [1.2])) the review concentrated on the initiation of yielding under non-uniform states of deformation and subsequently on the plastic deformation and fracture of un-notched tensile specimens. The latter review provides also the necessary basic information for the tensile test program of smooth geometrically similar specimens within the EU-Project REVISA [2.57, 2.58]. Experimental results demonstrating similarity or size dependence of plastic deformations going beyond yield initiation up to fracture under moderately non-uniform deformation (e.g. bending or torsion) appear to be very rare. On the other hand, the important question of the size dependence of deformation and fracture in specimens with strongly non-uniform stress or strain distributions, for example induced by stress concentrators (e.g. notches), has found more attention but is not included here.

Furthermore, the review was restricted essentially to the experimental findings. Their theoretical interpretations were addressed only when appropriate; in fact, this is still a very intricate issue.

The topic of size dependence of plastic deformation and ductile fracture is almost not existing in the standard text books on plasticity. Thus, most of the older literature was found by groping the way from one publication to a previous one. Some of the more recent publications were found by a computer supported search using relevant data banks (e.g. METADEX) but the outcome was meagre.

The phenomenon of the increased yield stress (sometimes called "delayed yielding") under non-uniform stress distribution compared with the yield under quasi-homogeneous stress distributions (tensile tests) has found considerable attention in the past. It is observed especially for steels with a pronounced upper and lower yield stress (e.g. mild steel). Various authors have related this to the formation of flow layers of finite thickness or to the supporting effect of the neighbourhood of the stress peaks, their thickness or size characterized by an intrinsic material length. This interpretation of the rise of the yield stress implies a size influence on the initiation of yielding of geometrically similar specimens under macroscopically non-uniform stress such that small specimens should have a greater resistance against yield initiation than larger ones. However, a size dependence in tests of geometrically similar tensile specimens with nominally homogeneous stress distribution should not occur if this interpretation is the sole explanation of the "delayed yield" phenomenon.

The review evaluated a set of publications related to the size effect on the initiation of yielding in geometrically similar specimens of the same material under non-uniform stress. Experiments involved thick cylinders under internal pressure, beams with circular or rectangular cross-section under pure bending, torsion of circular rods and wires, flat strips with a central circular bore-hole under tension and indentation tests. Typical dimensions (diameter or depth) ranged from a few mm (<5 mm) to dimension up to 10-times larger. An exception is the indentation test of Föppl & Huber (1941, [2.16]) and the torsion tests of very thin wires (Fleck et al. (1994, [2.26])), the latter being somewhat out of the range of conventional engineering interest. Qualitatively all tests showed a decrease of the yield stress when the specimen size is increased and the decrease is quasi-exponential. Because of the

limited range of size the experiments do not allow to ascertain that a finite stress level is reached for the large dimensions.

In several but not all size effect studies a careful assessment of technological influences has been done by special specimen preparations and accompanying testing, such that pseudo size effects have been reduced or eliminated. Otherwise differences in the material of the small and the large samples compared may induce or mask size effects and thus interfere with true size effects corresponding to deviations of the similitude of the physical processes (Fridman (1961, [2.59])). Although the definition and determination of yield initiation is non-trivial and may be subject to ambiguities, it appears that the observed size effects are experimentally well established in qualitative terms. The question whether the rise of the yield stress with reducing the size is solely related to the non-uniformity of the stress (or strain) distribution, can be tested by accompanying tensile tests with geometrically similar un-notched tensile specimens of the same material. This has been done only by a few authors, Morrison (1939, [2.14]), Imamura & Sato (1986, [2.22]), Fleck et al. (1994, [2.26]) who did not observe any significant dependencies. However, Richards (1954, [2.19]) did find a size dependence of the upper yield stress of a mild steel in uniform tension with the usual trend.

On the other hand frequently the opinion is expressed that true size effects in ordinary tensile tests of ductile engineering materials are so small that they are difficult to detect (e.g. Shearin, Ruark & Trimble (1948, [2.60])). Therefore, an additional review was performed to assess the influence in the testing of smooth tensile specimens (quasi-homogeneous stress distribution).

Sixteen references related to this topic were reviewed, about 2/3 of them were published before 1960. Various data were recorded and investigated such as the proportional limit, the stress at 0.2 % or 0.5 % strain, the ultimate stress and uniform strain, the elongation at fracture in a scaled or fixed gage length, as well as the engineering or true fracture stress and also the local axial strains and area reduction at the minimum cross-section of the neck after fracture. Usually, only a part of this spectrum is reported in each of the publications and intermediate values or the whole stress-strain curve is rarely included. Quantities of interest are also the plastic working per unit volume up to maximum stress and up to fracture but only one of the reviewed publications puts attention to the size dependence of these integral measures (Wood et al. (1943, [2.36])). Also in one case only (McAdam et al. (1948, [2.37])) the meridional curvature of the neck profile after fracture and its dependence on the size of the specimen was documented. In addition the follow-up of the evolution of the profile of the neck in the softening regime is a very rare event and the available informations (Miklowitz (1950, [2.39]), Matic et al. (1988 [2.48])) do not allow quantitative statements with respect to the influence of size.

In the early years of systematic tensile testing Barba's law: "Geometrically similar bodies of the same material, under identical conditions and stress, undergo similar deformations", is not only based on the results of Barba (1880, [2.30]) but also Bauschinger (1892, [2.31]) and it reflects the state of knowledge at that time; in fact, later testing with smooth specimens made of various materials and with larger size ranges have confirmed this partially. Thus, the ultimate tensile strength is the quantity for which the least size influence is observed: usually no or only a slight decrease with increasing size (diameter) is found (e.g. 5 % for a diameter range of 3.5 to 30 mm; Schneeweiß, (1966, [2.45])). However, Buch (1969, [2.46]) recorded a significant increase of the size dependence in cases when the impurity content was doubled (10 % decrease of the ultimate stress if the diameter is increased from 3 to 5 mm). This result and even more the influence of the impurity content on quantities related to fracture makes evident that size dependence and microscopic heterogeneity are strongly interrelated, i.e. it increases with increase in heterogeneity.

Also the yield stress, 0.2 %-proof stress or the stress at 0.5 % strain is frequently found to be not affected by the change in diameter but there are definite exceptions which show a

decrease when the diameter is increased (Richards (1954, [2.19]), Plechanova & Ratner (1954, [2.41])). For the four different steels studied by Plechanova & Ratner (1954, [2.41]) the decrease of the 0.2 %-proof stress may be as much as 15 % when the diameter is increased from 5 to 40 mm; a larger influence is found for the proportional limit. Experimental evidence [2.41] supports the suggestion that this size dependence may not be generated due to a surface hardening induced by the machining of the specimens. The uniform elongation is rarely recorded and if results are notified no effect is found. However, the data of Schneeweiß (1966, [2.45]) indicate a slight decrease for larger diameters between 14 and 30 mm.

Much attention has been put to the percentage elongation after fracture, an average strain within a finite gage length and depending on the choice of the gage length. For varying sizes (cross-sections) but fixed gage length a pronounced increase with increase in size has been found. On the other hand, changing the cross-section area S_0 and the gage length L_0 , the fracture elongation frequently is found to be an approximately linear function of the ratio $\sqrt{S_0} / L_0$. This may be proved theoretically if one assumes that the necking process follows Barba's similarity law. These simple theoretical considerations also show that for geometrically similar tensile specimens with properly scaled gage lengths the fracture elongation should be size independent. In fact, several authors have reported this (e.g. Bauschinger (1892, [2.31])). However, the results of Schneeweiß (1966, [2.45]) show an undoubted decrease of about 7 % (relative) for the elongation δ_5 when the size of the specimen is increased by a factor of 8.6 (diameter increase from 3.5 to 30 mm). This clearly indicates that the neck geometry at fracture does not follow similarity laws.

Generally, size influences emerge if 'local' quantities at the minimum cross-section of the neck are considered such as the percentage area reduction or the local axial strain, the meridional curvature of the neck as well as the true average fracture stress (load at fracture/minimum cross-section) or the true fracture stress (corrected stress according to Davidenko & Spiridonova (1945, [2.40])). In Fig. 2.49 experimental results for the reduction of area of circular tension specimens extracted from the reviewed publications, are collected. It is noteworthy that in the semi-logarithmic presentation a roughly linear decrease of the area reduction with diameter is observed and that the mean slopes are roughly comparable. Even the somewhat irregular results of Miklowitz (1950, [2.39]), which covers the very large scale range of 16, fits into this qualitative picture if the inhomogeneity of the raw material is accounted for (see Tab. 2.12). A definite exception is the result of Wood et al. (1943, [2.36]) for steel which opposes this trend; also the other tensile characteristics obtained by Wood et al. do not follow the usual trend. The inhomogeneity of the raw material was made responsible but a proof was not given. Also the recent tension test results for a stainless steel at room temperature by Malmberg, Aktaa & Schlossmacher (1999, [2.62]) represent an exception. Significantly larger flow stresses of the very small specimens (1.5 mm diameter) are observed than the 10-times larger specimen (at 2 % strain an increase of about 20 % is seen) although the specimens were stress annealed. This large effect is certainly related to the fact that the small specimens are much smaller (in diameter) than all the other tension specimens discussed so far. But whether the effect is related to surface or bulk properties is not clear; micro-structural investigations gave no indications. However, it is important to note, that a complete restructuring by solution annealing annihilated this trend largely.

In summary most of the experimental evidence does support Barba's law of similarity if the ultimate stress is considered and to some extent also the yield or proof stress at small plastic strains; it applies also frequently to the elongation at fracture if the gage length is properly scaled. However, the local data at the minimum section of the neck after fracture are size dependent with the tendency that larger specimens endure less local strain at fracture and the true fracture stress reduces with size. Thus, it appears that the size dependence at the centre of the neck does not sufficiently contribute to show up in the global measure of the fracture elongation.

An analogous behaviour has been demonstrated theoretically for a tapered tension rod using a gradient plasticity model (Tsagrakis et al. (1998, [2.61])); see also Part II, Section 3): The size influence is more readily detectable when local strains, determined in regions of intensive strain non-uniformities, are used as deformation measures than approaches which use averages on extended spatial domains.

The initiation of a crack in the tensile specimens cannot be detected usually. There remains the question whether the size dependence of the neck formation is only related to the final phase when cracks have formed and propagate or also to the precursor stage: initiation of necking localization by geometrical instability and damage yet without the presence of cracks. The authors are aware of only the publication by Chechulin (1961, [2.44]): his tests demonstrate that cracks appear in small specimens at a later deformation stage than in geometrically similar large test specimens. This result indicates that already the precursor stage, the formation, growth and coalescence of voids which finally yields microscopic cracks, are subjected to size influences.

Although it is beyond the present engineering scope, the literature survey very briefly referred also to some similarity and dimensional effects in tensile tests of rather thin tensile specimens (thin foil specimens), the thinnest specimen having a few grains across the thickness. Qualitatively new effects occur, the most noteworthy being the decrease of the yield and flow stresses with decreasing specimen thickness t if the specimen thickness is smaller than a critical value which depends on the grain size d (critical number of grains across the thickness $(t/d)_c$). Above this critical value (4 to 6 for 304 and 316 stainless steel) constant bulk values are approached. It should be noted that this behaviour is in contrast to size dependencies of the yield and 0.2 % proof stress found in smooth specimens for different steels, their minimum cross-section dimension being in the mm-range

3. Review of Gradient Plasticity Theories

It is well known that the classical mathematical theories of plasticity can be divided roughly into two types: deformation theories and flow theories. The deformation theories are characterized by constitutive equations that relate the instantaneous strain to the stress in a uniquely determined way or vice versa. Flow theories, however, are characterized by relations between increments or rates of stress and strain, which are homogeneous of degree one in the rate terms and thus are independent of the time scale. In general, flow theories describe better plastic deformation phenomena involving loading and unloading, while deformation plasticity is mathematically more convenient and also sufficient for proportional loading configurations and they are suitable for providing insight.

Accordingly, gradient plasticity theories can be formulated as “deformation” or “flow” type theories as discussed in detail below.

3.1 Gradient Deformation Theories

Model 1 [Aifantis (1984, [3.1]; 1987, [3.2])]

The simplest form of the gradient modification of plasticity theory involves one extra term proportional to the Laplacian $\nabla^2(\cdot)$ of the equivalent plastic strain ε in the yield condition in the form

$$\sigma = \kappa(\varepsilon) - c\nabla^2 \varepsilon , \quad (3.1)$$

where the equivalent stress σ and the equivalent plastic strain ε are defined by

$$\sigma = \sqrt{\frac{3}{2} S_{ij} S_{ij}} \quad , \quad \varepsilon = \sqrt{\frac{2}{3} \varepsilon'_{ij} \varepsilon'_{ij}} \quad , \quad (3.2)$$

with $\kappa(\varepsilon)$ denoting the usual homogeneous flow stress, $c = c(\varepsilon)$ being the gradient coefficient, S_{ij} meaning the deviatoric stress tensor and ε'_{ij} denoting the deviatoric strain tensor which for incompressible plastic deformation ($\varepsilon_{kk} = 0$) equals the strain tensor ε_{ij} . Thus, from (3.2) we can obtain the variation $\delta\varepsilon$ of ε with respect to the variations of the strain tensor ε_{ij} , i.e.

$$\delta\varepsilon = \frac{\partial\varepsilon}{\partial\varepsilon_{kl}} \delta\varepsilon_{kl} = \frac{2}{3} \frac{1}{\varepsilon} \varepsilon_{kl} \delta\varepsilon_{kl} \quad . \quad (3.3)$$

By assuming the equivalent work condition

$$S_{ij} \delta\varepsilon_{ij} = \sigma \delta\varepsilon \quad , \quad (3.4)$$

which in view of (3.3) gives

$$S_{ij} \delta\varepsilon_{ij} = \sigma \frac{2}{3} \frac{1}{\varepsilon} \varepsilon_{kl} \delta\varepsilon_{kl} \Rightarrow \left(S_{ij} - \frac{2}{3} \frac{\sigma}{\varepsilon} \varepsilon_{ij} \right) \delta\varepsilon_{ij} = 0 \quad , \quad (3.5)$$

for all variations $\delta\varepsilon_{ij}$, one can determine the deviatoric stress tensor $S_{ij} = \sigma_{ij} - \frac{1}{3} \sigma_{mm} \delta_{ij}$ in terms of strain as

$$S_{ij} = \frac{2}{3} \frac{\sigma}{\varepsilon} \varepsilon_{ij} = \frac{2}{3\varepsilon} \left[\kappa(\varepsilon) - c \nabla^2 \varepsilon \right] \varepsilon_{ij} \quad . \quad (3.6)$$

From Eq.(3.6)₁ we can deduce that

$$S_{ij} S_{ij} = \left(\frac{2}{3} \frac{\sigma}{\varepsilon} \right)^2 \varepsilon_{ij} \varepsilon_{ij} \quad , \quad (3.7)$$

which in view of (3.2)₂, gives (3.2)₁. This confirms the consistency of the definitions.

The classical mechanical balance equations are assumed to be not affected by this modification, but additional boundary conditions are required.

Model 2 [Fleck and Hutchinson (1993,[3.3])]

In contrast to the previous ‘‘symmetric stress’’ gradient deformation theory of plasticity, Fleck et al [3.3] have proposed recently a Cosserat type ‘‘asymmetric stress’’ theory summarized below. With the definitions of σ_{ij} denoting the symmetric part of the stress tensor, τ_{ij} denoting the anti-symmetric part of the stress tensor, m_{ij} denoting the deviatoric part of the couple stress tensor, and the standard expressions $\varepsilon_{ij} \equiv (u_{i,j} + u_{j,i})/2$ for the infinitesimal strain tensor and χ_{ij}

$\equiv e_{ikl} \varepsilon_{jl,k}$ for the infinitesimal curvature tensor, the appropriate balance equations expressing equilibrium of forces and momentum read $\sigma_{ji,j} + \tau_{ji,j} = 0$ and $\tau_{jk} = -e_{ijk} m_{pi,p} / 2$, respectively.

Next, the strain energy density w of a homogeneous isotropic solid is assumed to depend only upon a gradient dependent equivalent strain measure $\bar{\varepsilon}$, which is defined as

$$\bar{\varepsilon} = \sqrt{\varepsilon^2 + l^2 \chi^2} \quad , \quad \varepsilon = \sqrt{\frac{3}{2} \varepsilon_{ij} \varepsilon_{ij}} \quad , \quad \chi = \sqrt{\frac{3}{2} \chi_{ij} \chi_{ij}} \quad , \quad \varepsilon_{kk} = 0 \quad , \quad (3.8)$$

where l is a material length scale. Then, an overall equivalent stress measure $\bar{\sigma}$ is defined as the work conjugate of $\bar{\varepsilon}$, with

$$\bar{\sigma} = \frac{dw(\bar{\varepsilon})}{d\bar{\varepsilon}} \quad , \quad (3.9)$$

and thus, $\bar{\sigma}$ is a unique function of $\bar{\varepsilon}$, i.e. $\bar{\sigma} = \kappa(\bar{\varepsilon})$. The work done on the solid per unit volume equals the increment in strain energy, i.e.

$$\delta w = S_{ij} \delta \varepsilon_{ij} + m_{ji} \delta \chi_{ij} \quad , \quad (3.10)$$

which for independent variations of $\delta \varepsilon_{ij}$ and $\delta \chi_{ij}$, gives

$$S_{ij} = \frac{\partial w}{\partial \varepsilon_{ij}} = \frac{\partial w}{\partial \bar{\varepsilon}} \frac{\partial \bar{\varepsilon}}{\partial \varepsilon_{ij}} = \bar{\sigma} \frac{\partial \bar{\varepsilon}}{\partial \varepsilon_{ij}} = \frac{2 \bar{\sigma}}{3 \bar{\varepsilon}} \varepsilon_{ij} = \frac{2 \kappa(\bar{\varepsilon})}{3 \bar{\varepsilon}} \varepsilon_{ij} \quad , \quad (3.11a)$$

$$l^{-1} m_{ji} = \frac{\partial w}{\partial \chi_{ij}} = \frac{\partial w}{\partial \bar{\varepsilon}} \frac{\partial \bar{\varepsilon}}{\partial \chi_{ij}} = \bar{\sigma} \frac{\partial \bar{\varepsilon}}{\partial \chi_{ij}} = \frac{2 \bar{\sigma}}{3 \bar{\varepsilon}} l \chi_{ij} = \frac{2 \kappa(\bar{\varepsilon})}{3 \bar{\varepsilon}} l \chi_{ij} \quad . \quad (3.11b)$$

On combining Eqs.(3.8) and (3.11) we obtain the following expression for the gradient counterpart of the equivalent stress measure $\bar{\sigma}$

$$\bar{\sigma} = \sqrt{\sigma^2 + l^{-2} m^2} \quad , \quad (3.12)$$

where the quantities σ and m are von Mises type stresses defined by $\sigma = \sqrt{3 S_{ij} S_{ij} / 2}$ and $m = \sqrt{3 m_{ij} m_{ij} / 2}$, respectively.

Appropriate boundary conditions are to be added to close the problem.

3.2 Gradient Flow Theories

Model 3 [Aifantis (1984, [3.1]; 1987, [3.2])]

The simplest form of flow theory of gradient plasticity is also based on the gradient modification of the expression for the flow stress $\tau = \kappa(\gamma^p)$ to include the Laplacian $\nabla^2(\cdot)$ of the equivalent plastic strain, i.e. $\nabla^2 \gamma^p$. The corresponding form of the gradient dependent yield condition is

$$F = \tau - (\kappa(\gamma^p) - c\nabla^2\gamma^p) = 0 , \quad (3.13)$$

where the equivalent shear stress τ and equivalent shear strain rate $\dot{\gamma}^p$ are defined as usual by

$$\tau = \sqrt{\frac{1}{2}S_{ij}S_{ij}} \quad , \quad \dot{\gamma}^p = \sqrt{2\dot{\epsilon}_{ij}^p\dot{\epsilon}_{ij}^p} \quad . \quad (3.14)$$

The flow rule deriving from the yield condition (3.13) reads

$$\dot{\epsilon}_{ij}^p = \dot{\gamma}^p \frac{\partial F}{\partial \sigma_{ij}} = \frac{\dot{\gamma}^p}{2\tau} S_{ij} \quad , \quad (3.15)$$

giving the expression for the plastic strain increment. The relevant elastic strain increment $\dot{\epsilon}_{kl}^e = \dot{\epsilon}_{kl} - \dot{\epsilon}_{kl}^p$ is determined by Hooke's law which is written in the form $\dot{\sigma}_{ij} = C_{ijkl}^e (\dot{\epsilon}_{kl} - \dot{\epsilon}_{kl}^p)$, in which C_{ijkl}^e denotes the fourth-order isotropic tensor of elastic constants given as $C_{ijkl}^e = \mu(\delta_{ik}\delta_{jl} + \delta_{il}\delta_{jk}) + \lambda\delta_{ij}\delta_{kl}$, where μ, λ are Lamé's constants.

The plastic multiplier $\dot{\gamma}^p$ in the flow rule (3.15) satisfies the following loading-unloading conditions

$$\dot{\gamma}^p = \begin{cases} \dot{\gamma}^p & \text{if } F = 0 \text{ \& } \sigma_{ij}\dot{\epsilon}_{ij}^p > 0 \text{ (loading) or } \sigma_{ij}\dot{\epsilon}_{ij}^p = 0 \text{ (neutral loading) ,} \\ 0 & \text{if } F < 0 \text{ (elasticity) or } F = 0 \text{ \& } \sigma_{ij}\dot{\epsilon}_{ij}^p < 0 \text{ (unloading) ,} \end{cases} \quad (3.16)$$

and is determined by the consistency condition

$$\dot{F} = 0 \quad , \quad (3.17)$$

which, in view of (3.13), gives

$$\frac{S_{ij}}{2\tau} \dot{\sigma}_{ij} - \frac{\partial \kappa(\gamma^p)}{\partial \gamma^p} \dot{\gamma}^p + c\nabla^2\dot{\gamma}^p = 0 \quad , \quad (3.18)$$

where $c = \text{constant}$ is assumed. With the aid of Hooke's law and (3.15) eq.(3.18) reads

$$\dot{\gamma}^p - \frac{c}{H} \nabla^2\dot{\gamma}^p = \frac{1}{H} \frac{S_{ij}}{2\tau} C_{ijkl}^e \dot{\epsilon}_{kl} \quad , \quad (3.19)$$

where $H \equiv h + S_{ij} C_{ijkl}^e S_{kl} / 4\tau^2 = h + \mu$ and $h = \partial \kappa(\gamma^p) / \partial \gamma^p$.

Eq.(3.19) is a differential equation for $\dot{\gamma}^p$ in contrast to the classical plasticity case ($c \equiv 0$) where $\dot{\gamma}^p$ is determined from an algebraic equation. Below, we discuss briefly various procedures for evaluating (3.19) in relation to the solution of elasto-plastic boundary value problems.

(i) The method of Mühlhaus and Aifantis (1991, [3.4]) : Here $\dot{\gamma}^p$ is treated as an additional independent variable and (3.19) as an additional field equation, whereas necessary extra boundary conditions are deduced from an appropriate variational principle. To this end, the following total potential $\Psi(\dot{u}_i, \dot{\gamma}^p)$ is defined

$$\Psi(\dot{u}_i, \dot{\gamma}^p) = \frac{1}{2} \int_B \left(\dot{\epsilon}_{ij} - \dot{\gamma}^p \frac{S_{ij}}{2\tau} \right) C_{ijkl}^e \left(\dot{\epsilon}_{ij} - \dot{\gamma}^p \frac{S_{kl}}{2\tau} \right) dV + D[\dot{\gamma}^p] - \int_{\partial_t B} t_i \dot{u}_i dA, \quad (3.20)$$

with $D[\dot{\gamma}^p] = \frac{1}{2} \int_B \{ h(\dot{\gamma}^p)^2 + c(\nabla \dot{\gamma}^p)(\nabla \dot{\gamma}^p) \} dV$. The applied tractions t_i act on the surface $\partial_t B$ and geometrical boundary conditions are prescribed on $\partial_u B = \partial B - \partial_t B$; body forces are ignored. By assuming that upon equilibrium $\delta\Psi$ is stationary with respect to arbitrary infinitesimal variations of $[\dot{u}_i, \dot{\gamma}^p]$ and with $\delta\dot{u}_i = 0$ on $\partial_u B$ and with $\dot{\gamma}^p \geq 0$, the stationary condition

$$\delta\Psi = 0, \quad (3.21)$$

yields the following relations

$$\int_B \dot{\sigma}_{ij,j} \delta\dot{u}_i dV - \int_{\partial_t B} [\dot{\sigma}_{ij} n_j - t_i] \delta\dot{u}_i dA = 0, \quad (3.22a)$$

$$\int_B \left\{ \frac{S_{ij}}{2\tau} C_{ijkl}^e \dot{\epsilon}_{kl} - H\dot{\gamma}^p + c\nabla^2 \dot{\gamma}^p \right\} \delta\dot{\gamma}^p dV = 0, \quad (3.22b)$$

$$\int_{\partial_{ep} B} \{ c\nabla \dot{\gamma}^p \} \cdot \mathbf{n} \delta\dot{\gamma}^p dA = 0 \quad \Rightarrow \quad \frac{\partial \dot{\gamma}^p}{\partial \mathbf{n}} = 0 \quad \text{or} \quad \delta\dot{\gamma}^p = 0, \quad \text{on} \quad \partial_{ep} B \quad (3.22c)$$

where \mathbf{n} is the unit outward normal vector on the elastic-plastic interface $\partial_{ep} B$. It is noted that (3.22a) leads back to the stress equilibrium relations and the standard traction type boundary condition. Equation (3.22b) leads back to the consistency condition, while (3.22c) derives non-standard boundary conditions along the elastic-plastic interface $\partial_{ep} B$. The second of these conditions ($\delta\dot{\gamma}^p = 0$) is automatically satisfied at the elastic-plastic boundary in the interior of the body. When the spread of the plastic zone extends to an external boundary of the body either of conditions (3.22c) may be imposed. The above equations provide the basic structure for implementing the present gradient flow theory of plasticity into finite element formulations.

(ii) The method of Zbib and Aifantis (1989, [3.5]) : By formally writing (3.19) as

$$\dot{\gamma}^p = \frac{1}{H} \frac{S_{ij}}{2\tau} C_{ijkl}^e \dot{\epsilon}_{kl} + \frac{c}{H} \nabla^2 \dot{\gamma}^p, \quad (3.23)$$

and observing (3.15), Hooke's law takes the form

$$\dot{\sigma}_{ij} = C_{ijkl}^{ep} \dot{\epsilon}_{kl} - c^* C_{ijkl}^e S_{ij} , \quad (3.24)$$

where

$$\left. \begin{aligned} \dot{c}^* &= \frac{\langle 1 \rangle}{H} \frac{c}{2\tau} \nabla^2 \dot{\gamma}^p , \\ C_{ijkl}^{ep} &= C_{ijkl}^e - C_{ijkl}^p = C_{ijkl}^e - \frac{\langle 1 \rangle}{H} C_{ijqp}^e \frac{S_{qp}}{2\tau} \frac{S_{mn}}{2\tau} C_{mnkl}^e , \end{aligned} \right\} \quad (3.25)$$

with the symbol $\langle 1 \rangle$ defined as usual by

$$\langle 1 \rangle = \begin{cases} 1 & \text{if } F = 0 \quad \& \quad \dot{\gamma}^p > 0 , \\ 0 & \text{if } F < 0 \quad \text{or} \quad \{ F = 0 \ \& \ \dot{\gamma}^p \leq 0 \} . \end{cases} \quad (3.26)$$

Then the problem can be solved numerically, e.g. using FEM equipped with a return mapping algorithm. In such a method, (3.24) replaces the equation $\dot{\sigma}_{ij} = C_{ijkl}^{ep} \dot{\epsilon}_{kl}$ of classical plasticity, while the plastic corrector at the current iteration k of a typical time step $[t, t+\Delta t]$ takes the form

$$[\Delta \gamma^p]_k = (\gamma^p)_k - (\gamma^p)_{k-1} = \left[\frac{F + c \nabla^2 (\Delta \gamma^p)}{H} \right]_{k-1} , \quad (3.27)$$

replacing the plastic corrector $[\Delta \gamma^p]_k = [F/H]_{k-1}$ of classical plasticity. Thus, at the beginning of each iteration increment we solve for the strain gradient $g = c \nabla^2 \gamma$ at each integration point. In particular, the equation $g = c \nabla^2 \gamma$ is solved implicitly using Galerkin's method (e.g., see [3.6]) by assuming $g = [N]\{g\}$, $\gamma = [N]\{\gamma\}$, where $[N]$ is the shape function matrix. This leads to $[L]\{g\} = -c[M]\{\gamma\}$, where $[M] = \int_V [grad N]^T [[grad N] dV$ and $[L] = \int_V [N]^T [[N] dV$ and the integral boundary condition (3.22c)₁ has been used.

(iii) The method of Vardoulakis et al. (1995, [3.7] and [3.8]) : By making use of the approximation

$$\frac{1}{1 - \frac{c}{H} \nabla^2} \approx 1 + \frac{c}{H} \nabla^2 + \mathcal{O}\left(\frac{c^2}{H^2}\right) \doteq 1 + \frac{c}{H} \nabla^2 , \quad (3.28)$$

and neglecting non-linear and gradient terms of $[(1/H)(S_{ij}/2\tau)]$, eq.(3.19) takes the form

$$\dot{\gamma}^p \doteq \frac{\langle 1 \rangle}{H} \frac{S_{ij}}{2\tau} C_{ijkl}^e \left(1 + \frac{c}{H} \nabla^2 \right) \dot{\epsilon}_{kl} . \quad (3.29)$$

Then, in view of Hooke's law and (3.15), we obtain

$$\dot{\sigma}_{ij} = C_{ijkl}^{ep} \dot{\epsilon}_{kl} - C_{ijkl}^p \left(\frac{c}{H} \nabla^2 \dot{\epsilon}_{kl} \right) . \quad (3.30)$$

One may define a double stress tensor \dot{m}_{ijk} such that

$$\dot{m}_{ijk} = C_{jkmn}^p \frac{c}{H} \dot{c}_{imn} , \quad (3.31)$$

where .

$$\dot{c}_{imn} = \partial_i \dot{\epsilon}_{mn} . \quad (3.32)$$

On combining (3.32) and (3.31), we obtain

$$\partial_m \dot{m}_{mij} = C_{ijkl}^p \frac{c}{H} \nabla^2 \dot{\epsilon}_{kl} . \quad (3.33)$$

From the virtual work equation (neglecting inertia and body forces) we have

$$\int_B [C_{ijkl}^{ep} \dot{\epsilon}_{kl} \delta \dot{\epsilon}_{ij} + \dot{m}_{ijk} \delta \dot{c}_{ijk}] dV = \int_{\partial B} [\dot{t}_i \delta \dot{u}_i + \dot{m}_i D \delta \dot{u}_i] dA , \quad (3.34)$$

where $D \equiv n_k \partial_k$ denotes the derivative in a direction normal to the boundary with local unit outward normal \mathbf{n} (the boundary is assumed to be smooth) and $D_k \equiv (\delta_{kl} - n_k n_l) \partial_l$. By applying the divergence theorem to (3.34), after some algebraic manipulations we obtain

$$\begin{aligned} \int_B [\dot{\sigma}_{ij,j} \delta \dot{u}_i] dV &= \int_{\partial B} \{ [n_k n_j \dot{m}_{kji} - \dot{m}_i] D \delta \dot{u}_i \} dA \\ &+ \int_{\partial B} \{ [\dot{\sigma}_{ij} n_j - n_k D_j \dot{m}_{kji} + (n_k n_j D_l n_l - D_j n_k) \dot{m}_{kji} - \dot{t}_i] \delta \dot{u}_i \} dA . \end{aligned} \quad (3.35)$$

In these equations \dot{t}_i and \dot{m}_i are rates of surface tractions and double forces, respectively and as we can deduce from (3.35), they are related to $\dot{\sigma}_{ij}$ and \dot{m}_{ijk} by the following boundary conditions

$$\left. \begin{aligned} \dot{t}_i &= \dot{\sigma}_{ij} n_j - n_k D_j \dot{m}_{kji} + (n_k n_j D_l n_l - D_j n_k) \dot{m}_{kji} , \\ \dot{m}_i &= n_k n_j \dot{m}_{kji} , \end{aligned} \right\} \text{ on } \partial_t B, \quad (3.36)$$

On the complementary part $\partial_u B$ of the boundary the velocity \dot{u}_i as well as its normal derivative should be given, i.e.

$$\dot{u}_i = \dot{w}_i , \quad D \dot{u}_i = \dot{r}_i \quad \text{on } \partial_u B. \quad (3.37)$$

Equation (3.34) provides the basis for the finite element formulation of the problem.

(iv) The method of de Borst et al. (1992, [3.9]; 1993, [3.10]): Various attempts have been developed for incorporating the original symmetric stress theory of gradient plasticity into finite elements formulations. Thus, de Borst et al [3.9, 3.10] have treated $\dot{\gamma}^p$ as an additional independent variable and (3.19) as additional field equation which is assumed to be satisfied in a weak sense, i.e.

$$\int_B \left\{ \frac{S_{ij}}{2\tau} C_{ijkl}^e \dot{\epsilon}_{kl} - H\dot{\gamma}^p + c \nabla^2 \dot{\gamma}^p \right\} \delta \dot{\gamma}^p dV = 0 . \quad (3.38)$$

It is further assumed that the fields $\dot{\gamma}^p$ and $\nabla^2 \dot{\gamma}^p$ are discretized as follows

$$\dot{\gamma}^p = \mathbf{q}^T \hat{\Gamma} \quad , \quad \nabla^2 \dot{\gamma}^p = \mathbf{p}^T \hat{\Gamma} \quad , \quad (3.39)$$

where $\hat{\Gamma}$ denotes the nodal values of $\dot{\gamma}^p$ and

$$\mathbf{q} = [q_1, \dots, q_n]^T \quad , \quad \mathbf{p} = [\nabla^2 q_1, \dots, \nabla^2 q_n]^T \quad , \quad (3.40)$$

with q_i denoting the shape functions (C^1 - continuous) used for the interpolation of $\dot{\gamma}^p$. This formulation is identical to the one arised upon application of the variational principle for gradient plasticity mentioned above (Mühlhaus et al. [3.4]).

(v) The method of Li and Cescotto (1996, [3.11]): More recently, Li et al. [3.11] proposed a 2D incremental solution within a finite element formulation as follows. For an arbitrary integration point k , (3.19) written in incremental form, gives

$$(\Delta \gamma^p)_k - \frac{c}{H} \nabla^2 (\Delta \gamma^p)_k = \left[\frac{1}{H} \frac{S_{ij}}{2\tau} C_{ijnl}^e (\Delta \epsilon_{nl}) \right]_k \quad , \quad (3.41)$$

where $\nabla^2 (\Delta \gamma^p)_k$ is calculated by adopting the following approximation

$$\nabla^2 (\Delta \gamma^p)_k = \sum_{m=1}^{N_k} g_{km} (\Delta \gamma^p)_m \quad , \quad (3.42)$$

with N_k denoting the number of neighbouring integration points of k , including k . Next, for the determination of the coefficients g_{km} , a complete 2nd order polynomial in two coordinates is assumed to represent the function of $\Delta \gamma^p$ around point k , i.e.

$$\Delta \gamma^p = \alpha^T \mathbf{v} \quad , \quad (3.43)$$

where $\alpha = [\alpha_1, \alpha_2, \alpha_3, \alpha_4, \alpha_5, \alpha_6]^T$ and $\mathbf{v} = [1, x, y, x^2, xy, y^2]^T$. By minimizing the *Error* = $\sum_{m=1}^{N_k} [\Delta \gamma^p - (\Delta \gamma^p)_m]^2$, the vector α is obtained as

$$\alpha = \mathbf{D}^{-1} \sum_{m=1}^{N_k} (\Delta \gamma^p)_m \mathbf{v}_m \quad , \quad (3.44)$$

where \mathbf{v}_m is the vector \mathbf{v} at the m th neighbouring integration point and

$$\mathbf{D} = \begin{bmatrix} \Sigma 1 & \Sigma x_m & \Sigma y_m & \Sigma x_m^2 & \Sigma x_m y_m & \Sigma y_m^2 \\ & \Sigma x_m^2 & \Sigma x_m y_m & \Sigma x_m^3 & \Sigma x_m^2 y_m & \Sigma x_m y_m^2 \\ & & \Sigma y_m^2 & \Sigma x_m^2 y_m & \Sigma x_m y_m^2 & \Sigma y_m^3 \\ & & & \Sigma x_m^4 & \Sigma x_m^3 y_m & \Sigma x_m^2 y_m^2 \\ \text{Sym} & & & & \Sigma x_m^2 y_m^2 & \Sigma x_m y_m^3 \\ & & & & & \Sigma y_m^4 \end{bmatrix} \quad (3.45)$$

is the sum $\sum_{m=1}^{N_k} [\mathbf{v}_m \mathbf{v}_m^T]$. Then, it follows that the coefficients g_{km} should be given by

$$g_{km} = \mathbf{g}^T \mathbf{v}_m, \quad (3.46)$$

where

$$\mathbf{g}^T = 2(\text{4th row of } \mathbf{D}^{-1} + \text{6th row of } \mathbf{D}^{-1}). \quad (3.47)$$

It is remarked that the coefficients g_{km} only depend on the coordinates of the neighbouring integration points. The choice of these points is based on the mesh topology. Generally the integration points of the neighbouring elements are used.

It is also assumed that the consistent tangent constitutive relation of the point k will be given in the form

$$(\dot{\sigma}_{pq})_k = \sum_{m=1}^{N_k} C_{pqnl}^{ep} (\dot{\epsilon}_{nl})_m, \quad (3.48)$$

replacing the equation $(\dot{\sigma}_{pq})_k = C_{pqnl}^{ep} (\dot{\epsilon}_{nl})_k$ of classical plasticity. Then the problem can be solved as in classical plasticity (e.g. using FEM and a return mapping algorithm). In this case, the plastic corrector of a given point k at the current iteration i of a typical time step $[t, t+\Delta t]$ takes the form

$$[\Delta \gamma_k^p]_i = \frac{[F_k]_{i-1} + c \sum_{m=1, m \neq k}^{N_k} g_{km} (\Delta \gamma_m^p)_i}{[H_k - c g_{kk}]_{i-1}}, \quad (3.49)$$

replacing the plastic corrector $[\Delta \gamma_k^p]_i = [(F/H)_k]_{i-1}$ of classical plasticity. Then (3.49) can be solved by a Newton iterative procedure.

Model 4 [Fleck and Hutchinson (1993,[3.3])]

For completeness we conclude this section with a summary of the gradient flow theory with “asymmetric stress” as proposed recently by Fleck and Hutchinson [3.3]. The appropriate differential equations expressing equilibrium of forces and momentum are identical to those of the gradient deformation model 2 mentioned above, i.e $\sigma_{ji,j} + \tau_{ji,j} = 0$ and $\tau_{jk} = -e_{ijk} m_{pi,p} / 2$, respectively.

The starting point of this theory is the definition of a 13-dimensional stress vector $\tilde{\Sigma} = (S_{ij}, \Gamma^{-1} m_{ji})$ comprising the five components of the deviatoric symmetric stress tensor S_{ij} and the eight components of the deviatoric couple stress tensor $\Gamma^{-1} m_{ji}$, and the definition of the 13-dimensional plastic strain rate vector $\dot{\tilde{E}}^p = (\dot{\epsilon}_{ij}^p, l \dot{\chi}_{ij}^p)$ comprising the five components of the plastic strain rate tensor $\dot{\epsilon}_{ij}^p$ and the eight components of the plastic curvature tensor $l \dot{\chi}_{ij}^p$.

Then the yield condition is written as

$$\Phi(\tilde{\Sigma}, \dot{\tilde{E}}^p) = \Sigma_e - Y = 0, \quad (3.50)$$

where Y denotes the uniaxial flow stress and Σ_e is the overall effective stress:

$$\Sigma_e = \sqrt{\frac{3}{2} \tilde{\Sigma} \cdot \tilde{\Sigma}} = \sqrt{\frac{3}{2} S_{ij} S_{ij} + \frac{3}{2} l^{-2} m_{ij} m_{ij}} = \sqrt{\sigma_e^2 + l^{-2} m_e^2}, \quad (3.51)$$

and the associate flow rule reads

$$\dot{\tilde{E}}^p = \frac{1}{h(\Sigma_e)} \frac{\partial \Phi}{\partial \tilde{\Sigma}} \dot{\Sigma}_e, \quad (3.52)$$

with the hardening rate h being chosen so that the uniaxial homogeneous tensile response is reproduced.

The plastic work rate per unit volume is

$$\dot{w}^p = S_{ij} \dot{\epsilon}_{ij}^p + m_{ji} \dot{\chi}_{ij}^p = \tilde{\Sigma} \cdot \dot{\tilde{E}}^p. \quad (3.53)$$

On substitution of the flow rule (3.52) into (3.53) we obtain $\dot{w}^p = \Sigma_e \dot{E}_e^p$, where the overall effective plastic strain rate is defined as $\dot{E}_e^p \equiv \dot{\tilde{E}}^p / h$. Using this definition, (3.52) gives, via (3.50) and (3.51),

$$\dot{E}_e^p = \sqrt{\frac{2}{3} \dot{\tilde{E}}^p \cdot \dot{\tilde{E}}^p} = \sqrt{\frac{2}{3} \dot{\epsilon}_{ij}^p \dot{\epsilon}_{ij}^p + \frac{2}{3} l^2 \dot{\chi}_{ij}^p \dot{\chi}_{ij}^p} = \sqrt{(\dot{\epsilon}_e^p)^2 + (l \dot{\chi}_e^p)^2}, \quad (3.54)$$

where $\dot{\epsilon}_e^p = \sqrt{\frac{2}{3} \dot{\epsilon}_{ij}^p \dot{\epsilon}_{ij}^p}$ is the effective plastic strain rate and $\dot{\chi}_e^p = \sqrt{\frac{2}{3} \dot{\chi}_{ij}^p \dot{\chi}_{ij}^p}$ is the effective plastic curvature rate.

Using the definition of the plastic strain rate vector $\dot{\tilde{E}}^p = (\dot{\epsilon}_{ij}^p, l \dot{\chi}_{ij}^p)$, the flow rule (3.52) can be decomposed in the following equations

$$\dot{\varepsilon}_{ij}^p = \frac{3}{2h} \frac{S_{ij}}{\Sigma_e} \dot{\Sigma}_e \quad ; \quad l \dot{\chi}_{ij}^p = \frac{3}{2h} \frac{l^{-1} m_{ij}}{\Sigma_e} \dot{\Sigma}_e \quad . \quad (3.55)$$

The rate of the overall effective stress $\dot{\Sigma}_e$ can be obtained as the rate form of (3.51),

$$\dot{\Sigma}_e = \frac{3}{2} \frac{S_{ij}}{\Sigma_e} \dot{S}_{ij} + \frac{3}{2} \frac{l^{-1} m_{ji}}{\Sigma_e} l^{-1} \dot{m}_{ji} \quad . \quad (3.56)$$

Then the elastic strain rate state is assumed to be related to the stress rate state. For obtaining such a relation one can introduce a strain gradient theory of elasticity starting with the definition of an elastic strain energy density w^e of the form

$$w^e = \mu \varepsilon_{ij}^e \varepsilon_{ij}^e + \frac{1}{2} \lambda (\varepsilon_{kk}^e)^2 + l_{el}^2 \mu \chi_{ij}^e \chi_{ij}^e \quad , \quad (3.57)$$

The elastic work per unit volume equals the increment in elastic strain energy,

$$\delta w^e = \sigma_{ij} \delta \varepsilon_{ij}^e + m_{ji} \delta \chi_{ij}^e \quad . \quad (3.58)$$

Using (3.57), (3.58) enables one to determine the stress state in terms of the elastic strain state as

$$\sigma_{ij} = \frac{\partial w^e}{\partial \varepsilon_{ij}^e} = C_{ijkl}^e \varepsilon_{kl}^e \quad ; \quad l^{-1} m_{ji} = \frac{\partial w^e}{\partial \chi_{ij}^e} = J_{ijkl}^e l \chi_{kl}^e \quad , \quad (3.59)$$

or in a rate form

$$\dot{\sigma}_{ij} = C_{ijkl}^e \dot{\varepsilon}_{kl}^e \quad ; \quad l^{-1} \dot{m}_{ji} = J_{ijkl}^e l \dot{\chi}_{kl}^e \quad , \quad (3.60)$$

where the elastic moduli C_{ijkl}^e and J_{ijkl}^e are given as

$$C_{ijkl}^e = \mu (\delta_{ik} \delta_{jl} + \delta_{il} \delta_{jk}) + \lambda \delta_{ij} \delta_{kl} \quad . \quad (3.61)$$

and

$$J_{ijkl}^e = 2\mu \left(\frac{l_{el}}{l} \right) \delta_{ik} \delta_{jl} \quad , \quad (3.62)$$

with μ , λ denoting Lamé's constants. The internal length l_{el} is assumed to have no physical significance and is introduced in order to partition the curvature tensor χ_{ij} into its elastic part $\chi_{ij}^e = e_{imk} \varepsilon_{kj,m}^e$ and plastic part $\chi_{ij}^p = e_{imk} \varepsilon_{kj,m}^p$. Therefore, one has to take $l_{el} \ll l$ so that the dominant size effect is associated with the plastic rather than elastic strain gradients.

Remarks to the Flow Gradient Plasticity Model 4

a) One could alternatively write a general flow rule

$$\dot{\tilde{E}}^p = \dot{\Lambda} \frac{\partial \Phi}{\partial \tilde{\Sigma}}, \quad (3.63)$$

where $\dot{\Lambda} \geq 0$ is the commonly known plastic multiplier. Then defining an overall effective plastic strain rate \dot{E}_e^p such that

$$\dot{w}^p = \tilde{\Sigma} \cdot \dot{\tilde{E}}^p = \Sigma_e \dot{E}_e^p, \quad (3.64)$$

we can deduce that $\dot{\Lambda} = \dot{E}_e^p$.

b) From eq. (3.57) we can deduce that Fleck et al. [3.3] have added the term $l_{el}^2 \mu \chi_{ij}^e \chi_{ij}^e = l_{el}^2 \mu (\varepsilon_{ij,k}^e \varepsilon_{ij,k}^e - \varepsilon_{ij,k}^e \varepsilon_{ik,j}^e)$ to the expression for the elastic strain energy density of classical elasticity. For example, the contribution of this term in the case of an elastic torsion problem is

$$l_{el}^2 \mu \chi_{ij}^e \chi_{ij}^e = l_{el}^2 \mu \frac{3}{2} \varphi^2, \quad (3.65)$$

and in the case of an elastic pure bending problem is

$$l_{el}^2 \mu \chi_{ij}^e \chi_{ij}^e = l_{el}^2 \mu k^2 (1 + \nu^2). \quad (3.66)$$

In a different way, Altan & Aifantis [3.12] added the term $c \left[\mu \varepsilon_{ij,k}^e \varepsilon_{ij,k}^e + \frac{1}{2} \lambda \varepsilon_{ii,k}^e \varepsilon_{jj,k}^e \right]$ to the expression for the elastic strain energy density of classical elasticity. In the case of an elastic torsion problem and an elastic pure bending problem, this term gives

$$c \left[\mu \varepsilon_{ij,k}^e \varepsilon_{ij,k}^e + \frac{1}{2} \lambda \varepsilon_{ii,k}^e \varepsilon_{jj,k}^e \right] = c \mu \varphi^2, \quad (3.67)$$

and

$$c \left[\mu \varepsilon_{ij,k}^e \varepsilon_{ij,k}^e + \frac{1}{2} \lambda \varepsilon_{ii,k}^e \varepsilon_{jj,k}^e \right] = c k^2 \left[\mu (1 + 2\nu^2) + \frac{1}{2} \lambda (1 - 2\nu)^2 \right], \quad (3.68)$$

respectively.

Acknowledgement: This work was financially supported by the EU under the project "Reactor Vessel Integrity in Severe Accidents (REVISA)", contract FI4S-CT96-0024. The enduring support of the Department of Library and Communication-Services of the Forschungszentrum Karlsruhe is gratefully acknowledged. Also the authors want to express their special thanks to Mrs. Schröder and Mrs. Röser (FZK-PAE) for translating Russian and French articles and Dr. Bottoni for translations from the Japanese. The support of Dr. Jordan is also appreciated. The authors are also indebted to Dr. Göller, Dr. Jordan, and Dr. Krieg (all FZK-IRS) for their painstaking proof reading of large parts of the final version. Last but not least, Mrs. Mäule, secretary of the Institut für Reaktorsicherheit, deserves our particular thanks for typing and correcting several versions of a part of this report.

References Part I, Section 1

- [1.1] Baker, W.E., Westine, P.S., Dodge, F.T.: *Similarity methods in engineering dynamics (Theory and practice of scale modeling)*, Rev. Ed., Elsevier, Amsterdam-Oxford-New York-Tokyo, 1991
- [1.2] Malmberg, T.: Aspects of similitude theory in solid mechanics, Part 1 Deformation behavior, *Forschungszentrum Karlsruhe, Scientific Report FZKA 5657*, Dec. 1995
- [1.3] Young, D.F.: Basic principles and concepts of model analysis, *Experimental Mechanics*, vol. 11, pp. 326-336, July 1971
- [1.4] Stach, T.: Zur Skalierung von Modellversuchen zum Aufprall flüssiger Massen auf deformierbare Strukturen, *Forschungszentrum Karlsruhe, Scientific Report FZKA 5903*, May 1997
- [1.5] Weibull, W.: A statistical theory of the strength of materials, *Proc. Roy Swedish Inst. Eng. Res.*, Stockholm, No. 151, 1939
- [1.6] Bolotin, V.V.: *Statistical methods in structural mechanics*, Holden-Day Inc., San Francisco-Cambridge-London-Amsterdam, 1969
- [1.7] Brown, W.F., Lubahn, J.D., Ebert, L.J.: Effects of section size on the static notch bar tensile properties of mild steel plate, *Welding J.*, vol. 26, pp. 554-s – 559-s, 1947
- [1.8] Aifantis, E.C.: Spatio-temporal instabilities in deformation and fracture, in: *Computational material modeling* (Noor, A.K., Needleman, A., eds.), ASME AD-Vol42/PVP-Vol. 294, pp. 199-222, 1994
- [1.9] Shioya, T., Shioiri, J.: Elastic-plastic analysis of the yield process in mild steel, *J. Mech. Phys. Solids*, vol. 24, pp. 187-204, 1976
- [1.10] Bader, W., Nadai, A.: Die Vorgänge nach dem Überschreiten der Fließgrenze in verdrehten Eisenstäben, *VDI-Zeitschrift*, vol. 71, no. 10, pp. 317-323, 1927
- [1.11] Nakanishi, F.: On the yield point of mild steel, *Report of the Aeronautical Research Inst., Tokyo Imperial Inst.*, vol. 6, pp. 83-140, 1931
- [1.12] Nadai, A.: *Theory of flow and fracture of solids*, McGraw-Hill Book Comp., New York-Toronto-London, 1950
- [1.13] Dillon, O.W., Kratochvil, J.: A strain gradient theory of plasticity, *Int. J. Solids Structures*, vol. 6, pp. 1513-1533, 1970
- [1.14] Dillon, O.W.: Strain gradients in plasticity, *Acta Mechanica*, vol. 26, pp. 189-200, 1977
- [1.15] Aifantis, E.C.: On the microstructural origin of certain inelastic models, *J. Mat. Engng. Tech.*, vol. 106, pp. 326-330, 1984
- [1.16] Mühlhaus, H.B., Aifantis, E.C.: A variational principle for gradient plasticity, *Int. J. Solids Structures*, vol. 28, no.7, pp. 845-857, 1991
- [1.17] Aifantis, E.C.: Pattern formation in plasticity, *Int. J. Engng. Sci.*, vol. 33, pp. 2161-2178, 1995
- [1.18] Aifantis, E.C.: The physics of plastic deformation, *Int. J. Plasticity*, vol. 3, pp. 211-247, 1987
- [1.19] Aifantis, E.C.: On the role of gradients in the localization of deformation and fracture, *Int. J. Engng. Sci.*, vol. 30, pp. 1279-1299, 1992
- [1.20] Aifantis, E.C.: Gradient effects at macro, micro, and nano scales, *J. Mech. Behavior of Materials*, vol. 5, pp. 355-375, 1994
- [1.21] Triantafyllidis, N., Aifantis, E.C.: A gradient approach to localization of deformation-I. Hyperelastic materials, *J. of Elasticity*, vol. 16, pp. 225-238, 1986
- [1.22] Zbib, H.M., Aifantis, E.C.: On the structure and width of shear bands, *Scripta Met.*, vol. 22, pp. 703- 708, 1988
- [1.23] Zbib, H.M., Aifantis, E.C.: On the localization and postlocalization behavior of plastic deformation, I, II and III, *Res. Mechanica, Int. J. Struct. Mech. Mater. Sci.*, vol. 23, pp. 261-277, 279-292 and 293-305, 1988
- [1.24] Zbib, H.M., Aifantis, E.C.: A gradient-dependent flow theory of plasticity: Application to metal and soil instabilities, *Appl. Mech. Rev.*, vol. 42, pp. 295-304, 1989
- [1.25] Zbib, H.M., Aifantis, E.C.: On the gradient-dependent theory of plasticity and shear banding, *Acta Mech.*, vol. 92, pp. 209-225, 1992
- [1.26] Vardoulakis, I., Aifantis, E.C.: Gradient dependent dilatancy and its implications in shear banding and liquefaction, *Ingenieur Archiv.*, vol. 59, pp. 197-208, 1989

- [1.27] Vardoulakis, I., Aifantis, E.C.: A gradient flow theory of plasticity for granular materials. *Acta Mechanica*, vol. 87, pp. 197-217, 1991
- [1.28] Vardoulakis, I., Mühlhaus, H.B., Aifantis, E.C.: Continuum models for localized deformations in pressure sensitive materials, In: *Computer Methods and Advances in Geomechanics* (eds. G. Beer et al.), Balkema Publ., Rotterdam (1991) 441-448.
- [1.29] Mühlhaus, H.B., Aifantis, E.C.: The influence of microstructure-induced gradients on the localization of deformation in viscoplastic materials, *Acta Mechanica* 89, 217-231 (1991).
- [1.30] Oka, F., Yashima, A., Adachi, T., Aifantis, E.C.: A gradient dependent viscoplastic model for clay, In: *Constitutive Laws for Engineering Materials-Theory and Applications* (Desai, C.S. et al., eds.), ASME press, New York, pp. 313-316, 1991
- [1.31] Oka, F., Yashima, A., Adachi, T., Aifantis, E.C.: Instability of gradient dependent viscoplastic model for clay saturated with water and FEM analysis, *Appl. Mech. Rev.*, vol. 45, pp. 140-148, 1992
- [1.32] de Borst, R., Mühlhaus, H.B.: Gradient-dependent plasticity: Formulation and algorithmic aspects, *Int. J. Numer. Meth. Eng.*, vol. 35, pp. 521-539, 1992
- [1.33] Sluys, L.J., de Borst, R., Mühlhaus, H.B.: Wave propagation, localization and dispersion in a gradient dependent medium, *Int. J. Solids Structures*, vol. 30, pp. 1153-1171, 1993
- [1.34] Vardoulakis, I., Frantziskonis, G.: Micro-structure in kinematic hardening plasticity, *Eur. J. Mech. A/Solids*, vol. 11, pp. 467-486, 1992
- [1.35] Sulem, J., Vardoulakis, I., Papamichos, E.: Microstructure and scale effect in granular rocks, In: *Continuum Models for Materials with Microstructure* (Mühlhaus, H.B., ed.), John Wiley & Sons, New York, pp. 201-237, 1995
- [1.36] Vardoulakis, I., Sulem, J.: Second-grade plasticity theory for geomaterials, in: *Bifurcation analysis in Geomechanics* (Vardoulakis, I., Sulem, J., eds.), Blackie Academic & Professional, New York, pp. 382-425, 1995
- [1.37] Li, Xikui, Cescotto, S.: Finite element method for gradient plasticity at large strains, *Int. J. Num. Meth. Engng.*, vol. 39, pp. 619-633, 1996
- [1.38] Fleck, N.A., Hutchinson, J.W.: A phenomenological theory for strain gradient effects in plasticity, *J. Mech. Phys. Solids*, vol. 41, no.12, pp. 1825-1857, 1993
- [1.39] Fleck, N.A., Muller, G.M., Ashby, M.F., Hutchinson, J.W.: Strain gradient plasticity: Theory and experiment, *Acta Metall. Mater.*, vol. 42, no.2, pp. 475-487, 1994
- [1.40] Aifantis, E.C.: Higher order gradients and size effects, in: *Size-Scale Effects in the Failure Mechanisms of Materials and Structures* (Carpinteri, A., ed.), E & FN Spon, 2-6 Boundary Row, London, pp. 231-242, 1996
- [1.41] Zhu, H.T., Zbib, H.M., Aifantis, E.C.: Strain gradients and continuum modeling of size effect in metal matrix composites, *Acta Mechanica*, vol. 121, pp. 165-176, 1997
- [1.42] Malmberg, T., Tsagrakis, I., Eleftheriadis, I., Aifantis, E.C.: On the gradient plasticity approach to size effects, Part II: Applications, INV-REVISA(00)-P005, June 2000; Revised Version: Milestone Report INV-REVISA(00)-P006, March 2001; *Forschungszentrum Karlsruhe, Scientific Report FZKA 6322*, March 2001

References Part I, Section 2

- [2.1] Kennedy, A.B.W.: Experiments on the yield point of steel under transverse tests, *Engineering*, June 15, pp. 736 – 738, 1923
- [2.2] Eiselin, O.: Untersuchungen am einfach gelochten Zugstab, *Bauing.*, vol. 5, pp. 247 – 281, 1926
- [2.3] Scoble, W.A.: Reinforcement by under-stressed material, *Engineering*, Jan. 21., pp. 65 – 67, 1927
- [2.4] Enßlin, M.: Die Grundlagen der theoretischen Festigkeitslehre, *VDI-Zeitschrift*, vol. 27, no. 45, pp. 1625 – 1633, 1928
- [2.5] Bierett, G.: Ein Beitrag zur Frage der Spannungsstörungen in Bolzenverbindungen, *Mitt. der deutschen Mat.-Prüf.-Anst.*, Sonderheft 15, Berlin 1931
- [2.6] Nakanishi, F.: On the yield point of mild steel, *Report of the Aeronautical Research Inst., Tokyo Imperial Univ.*, vol. 6, pp. 83 – 140, 1931

- [2.7] Cook, G.: The yield point and initial stages of plastic strain in mild steel subjected to uniform and non-uniform stress distributions, *Phil Trans. Roy. Soc., A*, vol. 23, pp. 103 – 147, 1931
- [2.8] Thum, A., Wunderlich, F.: Die Fließgrenze bei behinderter Formänderung, *Forschung auf dem Gebiet des Ingenieurwesens*, vol. 3, no. 6, pp. 261 – 270, 1932
- [2.9] Kuntze, W.: Ermittlung des Einflusses ungleichförmiger Spannungen und Querschnitte auf die Streckgrenze, *Stahlbau*, Jg. 6, Heft 7, pp. 49 – 52, 1933
- [2.10] Möller, A., Barbers, J.: Über röntgenographische Messungen elastischer Spannungen, *Mitteilungen Kaiser-Wilhelm Inst. für Eisenforschung*, Düsseldorf, vol. 16, no. paper 247, pp. 21 – 31, 1934
- [2.11] Siebel, E., Vieregge, H.F.: Über die Abhängigkeit des Fließbeginns von Spannungsverteilung und Werkstoff, *Mitteilungen Kaiser-Wilhelm Inst. für Eisenforschung*, Düsseldorf, Band 16, Lieferung 21, Abhandlung 270, pp. 225 – 239, 1934
- [2.12] Föppl, L.: Eine neue elastische Materialkonstante, *Ing. Arch.*, vol. 7, pp. 229 – 236, 1936
- [2.13] Klöppel, K.: Gemeinschaftsversuche zur Bestimmung der Schwellzugfestigkeit voller, gelochter und genieteter Stäbe aus St37 und St52, *Stahlbau*, 9. Jg., Heft 13/14, pp. 97 – 112, 1936
- [2.14] Morrison, J.L.M.: The yield of mild steel with particular references to the effect of size of specimen, *Proc. of the Inst. of Mech. Eng.*, vol. 142, pp. 193 – 223, Nov. 1939 – March 1940
- [2.15] Kuntze, W.: Mechanische Eigenschaften metallischer Systeme, §21 Ungleichmäßiger Spannungszustand, pp. 305 – 312, from: *Handbuch der Metallphysik*, vol. 21, part 2, G. Masing ed., Leipzig 1940
- [2.16] Föppl, L., Huber, K.: Der Gültigkeitsbereich der Elastizitätstheorie, *Forschung auf dem Gebiete des Ingenieurwesens*, vol. 12, no. 6, pp. 261 – 265, 1941
- [2.17] Siebel, E.: Neue Wege der Festigkeitsrechnung, *VDI-Zeitschrift*, vol. 10, no. 5, pp. 135 – 139, 1948
- [2.18] Nakanishi, F.: Hanada, M., et al: Yield point of mild steel under sharply concentrated stress, (Japanese), *Trans. of the Japan Soc. of Mech. Eng.*, vol. 19, no. 87, pp. 14-18, 1953 (see also [2.21])
- [2.19] Richards, C.W.: Size effect in the tension test of mild steel, *Proc. Am. Soc. Test. Mat.*, vol. 54, pp. 995 – 1000, 1954
- [2.20] Richards, C.W.: Effect of size on the yielding of mild steel beams, *Proc. Am. Soc. Testing Mat.*, vol. 58, pp. 955 – 970, 1950
- [2.21] Publishing committee: *Selected papers of F. Nakanishi*, Department of Aeronautics, The University of Tokyo, June 1966
- [2.22] Imamura, S., Sato, Y.: The size effect on yielding of a mild steel strip with a hole under tension, (Japanese), *Trans. Japan Soc. Mech. Eng.*, (Ser. A), vol. 52, no. 477, pp. 1440-1444, 1986
- [2.23] Imamura, S., Sato, Y.: The size effect on yielding of a mild steel with a transverse hole under compression, (Japanese), *Trans. Japan Soc. Mech. Eng.*, (Ser. A), vol. 53, no. 489, pp. 911-915, 1987
- [2.24] Tamura, K., Sato, I.: Yielding on mild steel beam of hollow circular cross section with a radial hole (1. Report, Experiments), (Japanese), *Trans. Japan Soc. Mech. Eng.*, (Ser. A), vol. 58, no. 547, pp.426-430, 1992
- [2.25] Tamura, K., Sato, I.: idem (2. Report, Explanation of Experiments) (Japanese), *Trans. Japan Soc. Mech. Eng.*, (Ser. A), vol. 58, no. 547, pp. 431-435, 1992
- [2.26] Fleck, N.A., Muller, G.M., Ashbey, M.F., Hutchinson, J.W.: Strain gradient plasticity: Theory and Experiment, *Acta Metall. Mater.*, vol. 42, no. 2, pp. 475-487, 1994
- [2.27] Stach, T.: Unpublished Report, Forschungszentrum Karlsruhe, Oct. 1997
- [2.28] Jordan, T., Malmberg, T.: Size effect on liquid impact and resulting structural response, in *Severe Accidents and Topics in the the NESC Project* (Bhandari, S., ed.), presented at *1998 ASME/JSME Joint Pressure Vessel and Piping Conference*, San Diego, California, July 26-30, 1998, ASME PVP-Vol. 362, pp.33-38, 1998
- [2.29] Bach, C.: *Elastizität und Festigkeit* (8th edition), Springer Verlag, Berlin, 1920
- [2.30] Barba, J.: Resistance des materiaux. Epreuves de resistance a la traction. Etude sur les allègements des mataux apres rupture, *Memoires et compte rendu des travaux de la Société des Ingénieurs Civil*, part 1, pp. 682-714, 1880

- [2.31] Bauschinger, J.: Mitteilung XXV – Über den Einfluß der Gestalt der Probestäbe auf die Ergebnisse der Zugversuche mit denselben, *Mitteilungen aus dem mechanisch-technischen Laboratorium der Königl. Technischen Hochschule in München*, 21, 43 p. 23 graphs, 1892
- [2.32] Moore, H.F.: Tension tests of steel with test specimens of various size and form, *Proc. ASTM*, 18, part I, pp. 403-421, 1918
- [2.33] Baere, T.H., Gordon, W.: The influence of width of the specimen upon the results of tensile tests of mild steel and rolled copper, *Engineering*, 112, pp. 389-391, 1921
- [2.34] Templin, R.L.: Effects of size and shape of test specimen on the tensile properties of sheet metals, *Proc. ASTM*, 26, part 2, pp. 378-398, 1926
- [2.35] Lyse, I. Keyser, C.C.: Effect of size and shape of test specimens upon the observed physical properties of structural steel, *Proc. ASTM*, 34, part 2, pp. 202-210, 1934
- [2.36] Wood, D.S., Duwez, P.E., Clark, D.S.: The influence of specimen dimensions and shape on the results of tensile impact tests, *Natl. Defense Research Committee Armor and Ordnance Report*, No. A-237 (OSRD No. 3028), Dec. 1943
- [2.37] McAdam, D.J., Geil, G.W., Woodard, D.H., Jenkins, W.D.: Influence of size and the stress system on the flow stress and fracture stress of metals, Am. Inst. Mining & Metal. Eng., Technical Publ. No. 2373, Class E, *Metals Technology*, pp. 1-19, June 1948
- [2.38] Miklowitz, J.: The influence of the dimensionless factors on the mode of yielding and fracture in medium-carbon steel – I, The geometry and size of the flat tensile bar, *Trans. ASME, J. of Appl. Mechanics*, 70, pp. 274-287, Sept. 1948
- [2.39] Miklowitz, J.: The influence of the dimensionless factors on the mode of yielding and fracture in medium-carbon steel – II, The size of the round tensile bar, *Trans. ASME, J. of Appl. Mechanics*, pp. 159-168, June 1950
- [2.40] Davidenko, N.N., Spiridonova N.T.: Analysis of the state stress in the neck of a tension test specimen, *Proc. ASTM*, vol. 46, pp. 1147-1158, 1946
- [2.41] Plechanova, N.G., Ratner, S.J.: Size influence on plastic materials, (Russian), *Zhur. Tekh. Fiz.*, 23, 3, pp. 445-453, 1954
- [2.42] Chechulin, B.B.: Influence of specimen size on the characteristic mechanical values of plastic fracture, (Russian), *Zhur. Tekh. Fiz.*, 24, 6, pp. 1093-1100, 1954
- [2.43] Davidenko, N.N.: Effect of the dimension factor on the mechanical properties of specimens, *Industrial Laboratory (engl. transl. of Zavodskaya Laboratoriya)*, 26, 3, pp. 338-339, 1960
- [2.44] Chechulin, B.B.: On the size effect, *Industrial Laboratory (engl. transl. of Zavodskaya Laboratoriya)*, 26, 9, pp. 1192-1194, 1961
- [2.45] Schneeweiß, G.: Influence of specimen size on tensile characteristics and on tendency to brittle fracture of steel, (German), *Materialprüfung*, 8, 11, pp. 410-416, 1966
- [2.46] Buch, A.: Effect of specimen diameter on the tensile characteristics of small steel specimens of different purity, (German), *Materialprüfung*, 11, 2, pp. 54-58, 1969
- [2.47] Sato, S., Terazawa, K.: Studies on sizes and shapes for tensile test specimens, (Japanese), *J. Japan Inst. Light Metals*, vol. 21, no. 4, pp. 175-182, 1971
- [2.48] Matic, P., Kirby III, G.C., Jolles, M.I.: The relation of tensile specimen size and geometry effects to unique constitutive parameters for ductile materials, *Proc. Roy. Soc. London*, A 417, pp. 309-333, 1988
- [2.49] Martens, A.: *Handbuch der Materialkunde für den Maschinenbau*, Springer Verlag, Berlin, 1898
- [2.50] Unwin, W.C.: Tensile tests of mild steel and the relation of elongation to the size of the test bar, *Proc. of the Inst. of Civil Eng.*, 155, paper no. 3452, pp. 170-233 & plates, 1904
- [2.51] Miyazaki, S., Shibata, K., Fujita, H.: Effect of specimen thickness on mechanical properties of polycrystalline aggregates with various grain sizes, *Acta Metallurgica*, 27, pp. 855-862, 1979
- [2.52] Cowin, W.R., Lucas, G.E., ed.: *The use of small scale specimens for testing irradiated material*, Symp. Albuquerque N.M. Sept. 23, 1983, ASTM STP888, ASTM 1986
- [2.53] Igata, N., Miyahara, K., Uda, T., Asada, S.: Effects of specimen thickness and grain size on the mechanical properties of types 304 and 316 austenitic stainless steel, in [2.52], pp. 161-170, 1986
- [2.54] Rickerby, D.G., Fenici, P., Jung, P., Piatti, G., Schiller, P.: Comparison of mechanical properties in thin specimens of stainless steel with bulk material behavior, in [2.52], pp. 220-232, 1986

- [2.55] Kraaij, G.T.: Tensile tests of foil specimens of type 316 stainless steel in the temperature range of 20 to 900 °C (German), Kernforschungsanlage Jülich, Report Jül-Spez-94, ISSN 0343-7639, 1980
- [2.56] Matteazzi, S., Bernasconi, G., Piatti, G., Boerman, D.: Inelastic stress-strain relationship for AISI 316 stainless steel in the temperature range 20 – 800 °C, in *Transactions 6th Int. Conf. SMiRT*, vol. 4, paper L4/7, North Holland, Amsterdam 1981
- [2.57] Devos, J., Ritter, B., Auerkari, P., Dupas, P., Malmberg, T.: Reactor vessel integrity in severe accidents (REVISA), in: Proc. of mid-term symposium "FISA 97 – EU research on severe accidents" (Van Goethem, G., Keinhorst, G., Martin Bermejo, J., Zurita, A., ed.), EUR 18258 EN, pp. 113-122, 1998
- [2.58] Malmberg, T., Krompholz, K., Solomos, G., Aifantis, E.C.: Investigations on size effects in ferritic and austenitic materials, *15th Int. Conf. on Structural Mechanics in Reactor Technology (SMiRT-15)*, Seoul, Korea, Aug. 15-20, 1999, paper SMiRT-15-L1-B4-DE, 1999
- [2.59] Fridman, B.: Discussion of the effect of the size of objects on their mechanical properties (Deviations from similitude, model analysis and scale factor), *Industrial Laboratory (engl. transl. of Zavodskaya Laboratoriya)*, 26, 9, pp. 1179-1181, 1961
- [2.60] Shearin, P.E., Ruark, A.E., Trimble, R.M.: Size effects in steels and other metals from slow notch bend tests, *Fracturing of Metals*, A.S.M. Cleveland, pp. 167-188, 1948
- [2.61] Tsagrakis, I., Malmberg, T., Aifantis, E.C.: Gradient plasticity and size effects, *Proc. 5th National Cong. on Mechanics*, (Theocaris, P. S., Fotiadis, D. I., Massalas, C. V., ed.) Ioannina, Aug. 1998, vol. 2, pp. 953-960, The University of Ioannina Publ., 1998
- [2.62] Malmberg, T., Aktaa, J., Schlossmacher, P.: Personal communications, Forschungszentrum Karlsruhe, 1999

References Part I, Section 3

- [3.1] Aifantis, E.C.: On the microstructural origin of certain inelastic models, *J. Mat. Engng. Tech.*, vol.106, pp. 326-330, 1984
- [3.2] Aifantis, E.C.: The physics of plastic deformation, *Int. J. Plasticity*, vol. 3, pp. 211-247, 1987
- [3.3] Fleck, N.A., Hutchinson, J.W.: A phenomenological theory for strain gradient effects in plasticity, *J. Mech. Phys. Solids*, vol. 41, no.12, pp. 1825-1857, 1993
- [3.4] Mühlhaus, H.B., Aifantis, E.C.: A variational principle for gradient plasticity, *Int. J. Solids Structures*, vol. 28, no.7, pp. 845-857, 1991
- [3.5] Zbib, H.M., Aifantis, E.C.: A gradient-dependent flow theory of plasticity: Application to metal and soil instabilities, *Appl. Mech. Rev.*, vol. 42, pp. 295-304, 1989
- [3.6] Zbib, H.M.: Size effects and shear banding in viscoplasticity with kinematic hardening, In: *Material Instabilities: Theory and Applications* (Batra, R.C., Zbib, H.M., eds.), ASME AMD-Vol.183/MD-Vol.50, pp. 19-33, 1994
- [3.7] Vardoulakis, I., Sulem, J.: Second-grade plasticity theory for geomaterials, In: *Bifurcation Analysis in Geomechanics* (Vardoulakis, I., Sulem, J., eds.), Blackie Academic & Professional, New York, pp. 382-425, 1995
- [3.8] Sulem, J., Vardoulakis, I., Papamichos, E.: Microstructure and scale effect in granular rocks, In: *Continuum Models for Materials with Microstructure* (Mühlhaus, H.B., ed.), John Wiley & Sons, New York, pp. 201-237, 1995
- [3.9] de Borst, R., Mühlhaus, H.B.: Gradient-dependent plasticity: Formulation and algorithmic aspects, *Int. J. Numer. Meth. Eng.*, vol. 35, pp. 521-539, 1992
- [3.10] Sluys, L.J., de Borst, R., Mühlhaus, H.B.: Wave propagation, localization and dispersion in a gradient dependent medium, *Int. J. Solids Structures*, vol. 30, pp. 1153-1171, 1993
- [3.11] Li, Xikui, Cescotto, S.: Finite element method for gradient plasticity at large strains, *Int. J. Num. Meth. Engng.*, vol. 39, pp. 619-633, 1996
- [3.12] Altan, B.S., Aifantis, E.C.: On some aspects in the special theory of gradient elasticity, *J. Mechanical Behavior*, vol. 8, pp. 231-282, 1997

Tables

Table 2.1: Measured upper yield stresses in mild steel beams under pure bending; specimen dimensions in Fig. 2.7; based on Richards (1950, [2.20])

Series	B 1	B 2	B 3	B 4	B 5
Specimen number in each series	$(\sigma_u)_{ij}$, (psi)				
1	51450	48530	45010	35890	36980
2	44520	51760	45140	41300	37720
3	52470	53120	39570	46220	36980
4	49360	47500	42590	34460	36510
5	46940	46910	35030	30450	32815
6	49270	51260	44700	42930	33460
7	49190	49910	45800	39400	36540
8	52020	48430	43590	31540	35180
9	41600	53500	46670	37930	35200
10	50000	51930	43570	36790	33360
Mean (psi)	48680	50280	43170	37690	35470
value (MPa)	335.75	346.78	297.74	295.95	244.64
Standard (psi)	3262.9	2236.4	3296.5	4700.6	1659.9
deviation(MPa)	22.5	15.42	22.74	32.42	11.45

Note: $(\sigma_u)_{ij}$ = Maximum stress at yield

Table 2.2: Dimensions and proportions of tension test specimens in common use (1918); from Moore (1918, [2.32])

Specimens	Gage length l	Cross-section	l/\sqrt{a}	\sqrt{a}/l
A.S.T.M. Standard Round	2 in.	0.500 in. diameter	4.52	0.222
British, Short, Round	2 in.	0.564 in. diameter	4.00	0.250
French, Round	100 mm	13.8 mm diameter	8.17	0.122
German, Round	200 mm	20 mm diameter	11.3	0.089
Flat	8 in.	1.5 by 0.25 in.	13.05	0.077
Flat	8 in.	1.5 by 0.75 in.	7.54	0.132

Tab. 2.3: Dimensions and test data of almost geometrically similar flat tension specimens of three aluminium sheet metals (selected data from Templin (1926, [2.34])).

Soft aluminium sheet – 2S0							
Uniform length (in.)	Nominal width w (in.)	Actual thickness t (in.)	$\frac{w}{t}$	Area (sq.in.)	Yield stress (lb./sq.in.)	Ultimate stress (lb./sq.in.)	Elongation in 2 inch (%)
2.25	0.375	0.1260	2.98	0.0472	4000	12870	35.0
2.25	0.375	0.0630	5.95	0.0236	4800	12960	33.0
2.25	0.375	0.0305	12.30	0.0114	4900	12870	33.3
2.25	0.375	0.0155	24.19	0.00581	4600	12460	30.5
4.5	0.750	0.2473	3.03	0.1852	4400	12950	44.3
4.5	0.750	0.1248	6.01	0.0937	4000	12970	41.5
4.5	0.750	0.0640	11.72	0.0481	4600	12770	40.5
4.5	0.750	0.0300	25.00	0.0225	4500	12850	39.7
Hard aluminium – 2SH							
2.25	0.375	0.1255	2.99	0.0472	20800	23160	7.67
2.25	0.375	0.0645	5.81	0.0242	19500	21890	7.33
2.25	0.375	0.0307	12.22	0.0115	19500	21250	5.00
2.25	0.375	0.0155	24.19	0.0058	20900	22530	3.00
4.5	0.750	0.2475	3.03	0.1859	19900	22410	12.0
4.5	0.750	0.1250	6.00	0.0938	20100	23000	10.3
4.5	0.750	0.0655	11.45	0.0491	19100	21710	8.50
4.5	0.750	0.0300	25.00	0.0225	19000	21700	5.33
Heat-treated duralumin – 17S-T							
2.25	0.375	0.1245	3.01	0.0467	42800	62560	20.7
2.25	0.375	0.0640	5.86	0.0240	41800	61400	19.0
2.25	0.375	0.0315	11.91	0.0118	41500	58680	18.5
2.25	0.375	0.0170	22.06	0.00637	39000	57150	17.5
4.5	0.750	0.2560	2.99	0.1882	36300	59770	22.3
4.5	0.750	0.1238	6.06	0.0929	41200	61690	23.8
4.5	0.750	0.0638	11.76	0.0480	42000	60990	22.2
4.5	0.750	0.0310	24.20	0.0233	44000	59540	19.2

Table 2.4: Influence of cross-sectional shape and size on the tensile properties of a carbon steel; all specimens produced from a 1 inch plate. Each value is the average of three tests; selected data from Lyse et al. (1934, [2.35])

Dimension of cross-section	Johnson's limit (lb./sq.in.)	Ultimate stress (lb./sq.in.)	Elongation in 2 inches (%)	Area reduction (%)
circles				
¼ in.	31280	59760	30	65
½ in. diameter	29900	58290	43	67
1 in.	30570	58440	51	62
squares				
¼ x ¼ in.	25250	58850	36	63
½ x ½ in.	27650	58050	41	61
1 x 1 in.	31500	58100	55	62
rectangles				
¼ x ½ in.	26020	58250	39	62
½ x 1 in.	26750	58570	46	57
1 x 2 in.	31430	58910	62	58
¼ x ¾ in.	26000	58160	41	57
½ x ¾ in.	25500	58510	49	55
1 x 3 in.	32300	58580	67	54
¼ x 1 in.	27280	58380	47	55
½ x 2 in.	32200	58840	55	54
1 x 4 in.	31800	56770	71	50

Table 2.5: Materials and dimensions of geometrically similar specimens (static testing); extracted from Wood et al. (1943, [2.36])

Metal	Gage Length L (in./mm)	Diameter D (in./mm)	L/D	Scale Factor λ
Copper ½-in. bar annealed (480 °C, 1 h)	7/177.8	0.35/8.89	20	3.5
	2/50.8	0.10/2.54	20	1
Copper 1-in. bar annealed (480 °C, 1 h)	16/406.4	0.60/15.24	26.6	4
	8/203.2	0.30/7.62	26.6	2
	4/101.6	0.15/3.81	26.6	1
SAE 1020 cold rolled	7/203.2	0.30/7.62	26.6	2
	4/101.6	0.15/3.81	26.6	1
SAE 1020 annealed (875 °C, 1 h)	8/203.2	0.30/7.62	26.6	2
	4/101.6	0.15/3.86	26.6	1

Table 2.6: Results of static tests of geometrically similar tensile specimens, from Wood et al. (1943, [2.36])

Metal	Specimen Size Length x Diameter (inch)	Specimen No.	Ultimate Strength (lb./in. ²)	Prop. Limit (lb./in. ²)	Energy per Unit Volume (ft. lb./in. ³)	Elongation in Gage Length (percent)	Reduction Area (percent)	Hardness Rockwell
Annealed copper, ½ in. bar	7 x 0.35	2	29000	4000	820	41.4	71	74.8 F
	7 x 0.35	3	29500	4000	845	42.4	70	73.0 F
	2 x 0.10	11	29000	4000	670	32.8	68	31.5 F
	2 x 0.10	12	29200	4000	600	31.5	69	31.3 F
Annealed copper, 1 in. bar	16 x 0.6	1	28400	4000	756	38.0	69	38.0 F
	16 x 0.6	2	28200	4000	768	39.6	70	40.0 F
	8 x 0.3	1	29400	4000	756	37.6	75	65.6 F
	8 x 0.3	2	29300	4000	670	34.0	70	64.3 F
	4 x 0.15	1	29700	4000	715	34.6	72	39.5 F
4 x 0.15	2	29500	4000	706	34.8	75	38.0 F	
SAE 1020 cold-rolled steel	8 x 0.3	L1	85500	65000	361	5.4	66	94.4 B
	8 x 0.3	L2	82500	64000	442	6.6	66	92.8 B
	4 x 0.15	S1	95500	70000	256	3.5	63	95.0 B
	4 x 0.15	S2	94500	71500	253	3.4	64	91.1 B
SAE 1020 annealed steel	8 x 0.3	L9	66800	40800	1070	21.6	68	73.3 B
	8 x 0.3	L10	67000	40400	1050	21.4	67	74.2 B
	4 x 0.15	S10	73000	43000	747	14.1	58	72.3 B
	4 x 0.15	S11	74000	44000	773	14.2	55	73.0 B

Table 2.7: Percentage change of characteristic tensile data when the specimen size is reduced from 8.0 in. length x 0.3 in. diameter to 4.0 in. length x 0.15 in. diameter; based on Tab. 2.6

Material- SAE 1020	Proportional Limit	Ultimate stress	Elongation at fracture	Area reduction
cold rolled	+ 9.7 %	+ 13.1 %	- 43 %	- 3.8 %
annealed	+ 7.1 %	+ 9.7 %	- 34.2 %	- 16.3 %

Table 2.8: Diameter of specimens of low carbon steel FA-17 and neck dimensions after fracture (extracted from McAdam et al. (1948, [2.37, Tab. 2]))

Gage Diameter d_0 (in./mm)	Minimum Neck Diameter $d = 2b'$ (in./mm)	Meridional Neck Radius r' (in./mm)	Area Reduction ψ (%)	Meridional Radius
				Gage Radius $r'/(d_0/2)$ (-)
0.101 / 2.57 ⁽¹⁾	0.0522/1.33	0.021/0.53	73.3	0.416
0.133 / 3.38	0.0688/1.75	0.027/0.69	73.2	0.406
0.167 / 4.24 ⁽¹⁾	0.0908/2.31	0.049/1.24	70.4	0.587
0.250 / 6.35 ⁽¹⁾	0.1356/3.44	0.073/1.85	70.6	0.584
0.501 / 12.73 ⁽¹⁾	0.278/7.06	0.152/3.86	69	0.607
1.000 / 25.40	0.576/14.63	0.290/7.37	67	0.58
1.297 / 32.94	0.758/19.25	0.447/11.35	66	0.69

⁽¹⁾ The recorded data are the averages of two or more tests

Table 2:9: Uniform engineering strain ϵ_g and true stress S_u at maximum load; annealed low carbon steel FA-17 (extracted from McAdam et al. (1948, [2.37]))

Gage Diameter d_0 (in.)	$\left(\frac{A_0}{A}\right)_g$ (-)	ϵ_g (-)	S_u (lb./sq. in.)
0.101 ⁽¹⁾	~1.24	0.24	~71
0.133 ⁽¹⁾	- ⁽³⁾	- ⁽³⁾	- ⁽³⁾
0.167 ^{(1), (2)}	~1.22, 1.29	~0.22, 0.29	71, 75
0.250 ⁽¹⁾	~1.21	~0.21	67.5
0.501 ^{(1), (2)}	~1.24, - ⁽³⁾	~0.24, - ⁽³⁾	71, - ⁽³⁾
1.000 ⁽²⁾	~1.24	~0.24	71 (↓) ⁽⁴⁾
1.297 ⁽²⁾	- ⁽³⁾	- ⁽³⁾	- ⁽³⁾

(1) Axis of specimen at half-radial distance from axis of original 2¼ in. diameter bar
 (2) Co-axial with original bar
 (3) Data not marked in stress-strain curves
 (4) The arrow indicates how the value should be corrected (decreased: ↓)

Table 2:10: Ultimate stress, engineering fracture stress and fracture elongation of a medium carbon steel and as influenced by geometry; from Miklowitz (1948, [2.38, Fig. 4 and Tab. 1])

Specimen No.	h_0 (inch)	b_0/h_0	Ultimate-load stress (Psi)	Fracture-load stress (Psi)	Fracture elongation ϵ_1 (in scaled gage length l_0) (-)
10A	3/4	10	62500	53300	0.25
7A		7	62500	53300	0.27
6A		6	62000	53300	0.30
5A		5	65000	53300	0.30
3A		3	66500	52500	0.31
1A		1	68000	50000	0.41
10B	3/8	10	65400	56600	0.25
7B		7	65900	56000	...
6B		6	66900
5B		5	64700	52000	...
3B		3	63700	49200	0.33
1B		1	70300	51800	0.36
10C	3/16	10	63600	54000	...
7C		7	64300	53000	...
6C		6	66000	54700	0.32
5C		5	69500	56900	0.31
3C		3	65200	50500	0.35
1C		1	71400	50600	0.42

Table 2.11: Influence of geometry and size of medium carbon steel specimens on maximum strain values in the neck of flat tension bars at fracture; from Miklowitz (1948, [2.38])

Specimen No.	h_0 inch	b_0/h_0	Maximum ϵ_1	Maximum ϵ_2	Maximum ϵ_3
10A	3/4	10	1.84	-0.299	-0.497
7A		7	1.61	-0.300	-0.453
6A		6	1.60	-0.297	-0.454
6A		5	1.58	-0.300	-0.450
3A		3	1.72	-0.312	-0.467
1A		1	2.43	-0.447	-0.473
10B	3/8	10	1.54	-0.275	-0.457
7B		7	1.70	-0.283	-0.483
6B		6	1.78	-0.305	-0.482
5B		5	1.92	-0.335	-0.487
3B		3	2.05	-0.360	-0.487
1B		1	2.46	-0.453	-0.471
10C	3/16	10	2.09	-0.332	-0.516
7C		7	2.14	-0.322	-0.528
6C		6	1.81	-0.310	-0.483
5C		5	2.03	-0.340	-0.500
3C		3	2.16	-0.343	-0.517
1C		1	2.92	-0.513	-0.477

Table 2.12: Size influence on the true ultimate stress and stresses and strains in the minimum section of the neck after fracture of tension specimens of a medium carbon steel; compiled from Miklowitz (1950, [2.39])

Specimen No.	Diameter (in./mm)	Average True Stress at Ultimate Load (psi)		Average True Stress at Fracture (psi)		Maximum True Stress at Fracture (psi)		Axial Strain in the Minimum Neck Section after Fracture (-)	
		measured	averaged	measured	averaged	measured	averaged		
5 6	3/16 / 4.76	81600 82600	82100	144000 ^{↑(4)} 150000 [↑]	147000	173000 ^{↑(4)} 178000	175500	1.70 [↑] 1.80 [↑]	1.75 [↑]
A ⁽¹⁾ B ⁽¹⁾	0.357 / 9.07	- -	-	137000 140000	-	155500 162000	-	1.58 1.80	-
3 4	3/8 / 9.52	78700 78700	78700	137000 ^{↓(4)} 134500	135800	162500 [↓] 157500	160000 [↓]	1.83 [↓] 1.76	1.80 [↓]
1 2	3/4 / 19.05	83700 85200	84500	136000 [↓] 133000 [↓]	134500 [↓]	159500 [↓] 157000 [↓]	158300 [↓]	1.58 [↓] 1.46 [↓]	1.52 [↓]
7 8	3/2 / 38.1	80200 80700	80500	- ⁽³⁾ 113000 [↑]	113000	- ⁽³⁾ 127000 [↑]	127000 [↑]	- ⁽³⁾ 1.05 [↑]	1.05 [↑]
9 10	3 / 76.2	79800 80300	80100	90500 [↑] 90500 [↑]	90500 [↑]	93200 [↑] 93200 [↑]	93200 [↑]	0.47 [↑] 0.45 [↑]	0.46 [↑]
11 ⁽²⁾ 12 ⁽²⁾	3 / 76.2	84500 84500	84500	133800 (97800)	133800	155500 (144200)	155500	1.28 1.26	1.27
(1) Group III (2) Group II (3) Specimen 7 was not broken (4) The arrows indicate necessary corrections (increase [↑] and decrease [↓]) if the inhomogeneity in the cross-section is accounted for (see specimen A & B)									

Table 2.13: Influence of the specimen diameter on the tensile characteristics (turning data $v = 15$ m/min, $t = 0.2$ mm, $s = 0.14$ min/turn), from Plechanova et al. (1954, [2.41])

Material and Heat Treatment	d (mm)	σ_{pro} (kp/mm ²)	$\sigma_{0.2}$ (kp/mm ²)	σ_u (kp/mm ²)	S_R (kp/mm ²)	ψ (%)
(1) Copper	5	3.63	8.16	21.9	74.2	82.2
	10	2.20	6.53	22.3	78.7	83.6
	20	1.33	4.46	22.6	81.5	83.7
	40	1.18	3.21	21.9	76.5	82.9
(2) Aluminium	5	2.70	3.20	8.0	27.6	79.0
	10	2.50	3.05	8.5	26.0	79.0
	20	2.00	3.03	8.1	28.0	80.0
	40	1.60	2.70	8.2	25.5	80.7
(3) Steel 30 X ГСА	5	78.7	81.2	93.3	164	62
	10	69.3	74.8	87.7	156	63
	20	65.8	75.4	91.5	151	58
(4) Steel 30 X ГЧА	5	42.3	84.0	122	252	52.3
	10	35.9	78.0	121	207	49.7
	20	34.0	73.6	119	195	45.8
	40	32.8	71.8	119	186	40.4
(5) Steel 18 X HBA	5	69.6	103	114	195	64.6
	10	68.5	104	115	200	61.7
	20	62.4	97.5	113	182	59.5
	40	53.1	95.0	111	177	49.1
(6) Steel 40 X HMA	5	78.2	88.1	103	171	55.7
	10	71.3	85.2	103	171	52.6
	40	68.7	82.0	100	152	49.2

Table 2.14: Relative change of tensile characteristics with increase in size; e.g. $(\sigma_{pro})_{d=20}/(\sigma_{pro})_{d=5}$ & $(\sigma_{0,2})_{d=20}/(\sigma_{0,2})_{d=5}$; calculated from Tab. 2.13

Material and Heat Treatment	Ratios of				
	σ_{pro}	$\sigma_{0,2}$	σ_u	S_R	ψ
(1) Copper					
$\lambda = 20/5 = 4$	0.37	0.55	1.03	1.1	1.02
$\lambda = 40/5 = 8$	0.32	0.39	1.00	1.0	1.01
(2) Aluminium					
$\lambda = 4$	0.74	0.94	1.01	1.01	1.01
$\lambda = 8$	0.59	0.84	1.02	0.93	1.02
(3) Steel 30 X ГСА					
$\lambda = 4$	0.83	0.93	0.98	0.92	0.93
$\lambda = 8$	-	-	-	-	-
(4) Steel 30 X ГЧА					
$\lambda = 4$	0.81	0.88	0.97	0.78	0.88
$\lambda = 8$	0.78	0.85	0.97	0.74	0.78
(5) Steel 18 X HBA					
$\lambda = 4$	0.89	0.94	0.99	0.93	0.92
$\lambda = 8$	0.76	0.93	0.97	0.91	0.76
(6) Steel 40 X HMA					
$\lambda = 4$	-	-	-	-	-
$\lambda = 8$	0.88	0.93	0.97	0.88	0.88

Table 2.15: Tensile characteristics of Cu-specimens with different surface properties; extracted from Plechanova (1954, [2.41])

Production Process	σ_{pro} (kp/mm ²)	$\sigma_{0,2}$ (kp/mm ²)	σ_u (kp/mm ²)	S_R (kp/mm ²)	Ψ (%)	Micro-hardness 20 p
(α) Annealing, 600 °C, 2 h Specimen fabrication: 5 mm \varnothing Turning $v = 15$ m/min $t = 0.2$ mm, $s = 0.14$ mm/turn ref. [2.41] Tab. 3	3.63	8.16	21.9	74.2	82.2	-
(β) Annealing, 600 °C, 2 h Specimen fabrication: 5 mm \varnothing Turning $v = 84$ m/min $t = 0.2$ mm, $s = 1.4$ mm/turn ref. [2.41] Tab. 5	3.6	8.2	22	74.2	82	115
(γ) Specimen fabrication: 5 mm \varnothing Annealing, 600 °C grinding with grinding cloth ref. [2.41], Tab. 5	1.4	2.8	22	73.9	82	70
(δ) Annealing, 600 °C, 2 h Specimen fabrication: 5 mm \varnothing shot peening: $v = 43.5$ mm/s duration 3 min, ball diam. 0.6 – 0.7 mm ref. [2.41], Tab. 5	4.7	11.2	22	74.6	82	144
(ϵ) Annealing, 600 °C, 2 h Specimen fabrication: 40 mm \varnothing Turning $v = 15$ m/min $t = 0.2$ mm, $s = 0.14$ mm/turn ref. [2.41] Tab. 3	1.18	3.21	21.9	76.5	82.9	-
(ζ) Annealing, 600 °C, 2 h Specimen fabrication: 40 mm \varnothing Turning $v = 8,4$ m/min $t = 0.2$ mm, $s = 1.4$ mm/turn ref. [2.41] Tab. 5	1.2	3.2	22	76.5	82.9	-

Table 2.16: Comparison of tension tests on 3-mm diameter (not ruptured) and 15-mm diameter (ruptured) tensile specimens; 37XH3A-steel with three different heat treatments; from Chechulin (1961, [2.44])

Hardness H _v	Diameter mm	Mechanical characteristics ¹⁾				No. of tests
		σ_B (kg/mm ²)	$\sigma_{0.2}$ (kg/mm ²)	δ (%)	ϕ (%)	
<u>380–386</u> 383	15.0	<u>122.5–124.8</u> 123.6	<u>108.5–111.0</u> 109.0	<u>11.7–13.1</u> 13.2	<u>53.4–56.4</u> 54.4	5
<u>373–380</u> 378	3.0	<u>120.2–127.2</u> 123.9	<u>109.0–114.5</u> 111.1	<u>10.0–12.5</u> 11.9	<u>53.4–56.0</u> 54.7	5
<u>300–310</u> 304	15.0	<u>95.6–100.0</u> 97.9	<u>79.2–80.6</u> 80.0	<u>15.2–18.4</u> 17.2	<u>63.0–64.4</u> 64.0	5
<u>298–306</u> 302	3.0	<u>96.3–98.2</u> 97.1	<u>65.9–81.0</u> 79.0	<u>15.6–15.8</u> 15.7	<u>62.0–65.7²⁾</u> 64.1	3
<u>258–279</u> 268	15.0	<u>82.5–85.5</u> 83.5	<u>68.4–73.5</u> 70.5	<u>18.6–22.5</u> 20.4	<u>69.0–69.5</u> 69.1	4
<u>260–272</u> 265	3.0	<u>79.2–86.3</u> 84.0	<u>63.7–69.3</u> 68.7	<u>17.8–20.5</u> 19.1	<u>66.3–69.4</u> 68.1	4

¹⁾ The range of variation of the results is shown above the line and the average value is below the line

²⁾ The specimen had a microscopic crack in the neck.

Table 2.17: Test results obtained from tension tests on specimens of carbon steel Ck15 of different diameters d_0 ; from Schneeweiß (1966, [2.45])

Characteristic Data	Units	d_0 (mm)						
		3.5	3.5	6	10	14	14	30
Test series		1	2	3	4	5	6	7; 8
Young's modulus	kp/mm ²	-	-	21535	20840	21240	21290	-
Upper yield stress	kp/mm ²	28.06	27.30	28.02	27.16	26.21	28.88	28.58
Lower yield stress	kp/mm ²	-	-	23.76	24.81	23.08	24.76	28.33
Ultimate tensile stress	kp/mm ²	42.72	41.96	42.42	41.73	41.62	41.71	41.10
True stress at maximum load	kp/mm ²	53.78	53.21	53.83	52.56	52.53	52.47	51.05
Uniform strain, type I δ_g'	%	25.32	26.05	26.81	26.25	26.34	26.02	24.45
Uniform strain, type II δ_g''	%	25.46	27.56	26.97	25.65	26.08	25.55	23.97
Average axial neck strain $\approx \delta_{10} - \delta_{gm}$	%	8.68	9.72	7.80	8.07	8.34	7.64	8.11
Number of tests		12	11	21	9	9	9	4
Position in the bar		7	8	3	6	4	1	2; 5

Table 2.18: Effect of the diameter on the mechanical properties of the longitudinal (L) and the traverse specimens (Q) of two melts of different impurity contents of the 36CrNiMo4-steel (K; E) and of the X20Cr13-steel (I; II); from Buch (1969, [2.46])

Specimen Type	d (mm)	σ_B (kp/mm ²)	δ_5 (%)	ψ (%)	σ_R (kp/mm ²)	$\frac{\psi_Q}{\psi_L}$	$\frac{\sigma_{RQ}}{\sigma_{RL}}$
KL	5	92	18.0	59.9	170		
	3	102	19.5	61.5	212		
KQ	5	91	14.9	36.5	138	0.61	0.81
	3	102	17.3	47.4	165	0.77	0.78
EL	5	104	17.9	63.3	180.0		
	3	103	19.0	66.2	236.5		
EQ	5	105	17.9	59.8	181.0	0.94	1.0
	3	102	17.8	59.4	199.5	0.90	0.84
KL	4	234	12.2	43.1	328		
KQ	4	224		7.0	242	0.16	0.74
EL	4	218	9.9	40.5	301		
EQ	4	219	7.3	20.8	275	0.52	0.92
IL	5	78.3	21.0	69.9	157.0		
	4	78.3	21.3	70.3	158.5		
	3	79.0	20.1	70.3	191.0		
IQ	5	80.3	20.0	62.5	147	0.89	0.94
	4	79.3	19.5	62.5	154	0.94	0.97
	3	79.8	19.9	67.5	181	0.96	0.95
IIL	5	80.8	18.9	65.4	149		
	4	77.5	19.0	65.9	144		
	3	75.8	19.0	67.3	175		
IIQ	5	75.8	14.9	36.3	104.0	0.53	0.70
	4	76.8	14.9	42.6	114.0	0.65	0.79
	3	76.8	16.0	46.6	122.5	0.69	0.70

K: conventional costs, E: electrode-slug remelting
 impurity content (K) > impurity content (E)
 impurity content (II) > impurity content (I)

Tab. 2.19: Round specimens (Japanese Industrial Standard); from Sato et al. (1971, [2.47])

Specimen No.	D (mm)	L ₀ (mm)	L _c	L_0/\sqrt{A}	L_c/\sqrt{A}	L _c /D	R (mm)	R/D	Remarks
10	12.5	50	60	4.51	5.42	4.8	20	1.6	
4	14	50	60	4.03	4.83	4.3	20	1.43	
14A1	14	70	77	5.65	6.20	5.5	20	1.43	L ₀ = 5D, L _c = 5.5 D
14A2	14	70	98	5.65	7.90	7.0	20	1.43	L ₀ = 5D, L _c = 7 D
14A3	18	90	128	5.65	8.03	7.1	20	1.11	L ₀ = 5D, L _c = 7 D
14A4	22	110	155	5.65	7.95	7.0	30	1.36	L ₀ = 5D, L _c = 7 D

Diameter of grip section = 1.5 D
 D-diameter of cross-section
 L₀ – gage length, L_c – length of reduced section, A – sectional area, R – fillet radius

Table 2.20: Chemical composition (%) of three aluminium alloys; from Sato et al. (1971, [2.47])

Material	Si	Fe	Cu	Mg	Mn	Zn	Ti
1100	0.10	0.16	<0.01	<0.01	<0.01	<0.01	0.005
2017	0.11	0.34	5.1	0.03	0.62	0.02	0.011
5056	0.06	0.17	0.02	4.5	0.68	0.01	0.008

Table 2.21: Ratio L_0/d_0 of a family of tensile specimens; extracted from Matic et al. (1988, [2.48])

d_0 (mm)	L_0 (mm)			
	(a) 12.7	(b) 25.4	(c) 38.1	(d) 50.8
(a) 7.6	$\frac{12.7}{7.6} = 1.67$	$\frac{25.4}{7.6} = 3.342$	$\frac{38.1}{7.6} = 5.01$	$\frac{50.8}{7.6} = 6.68$
(b) 12.7	$\frac{12.7}{12.7} = 1$	$\frac{25.4}{12.7} = 2$	$\frac{38.1}{12.7} = 3$	$\frac{50.8}{12.7} = 4$
(c) 17.8	$\frac{12.7}{17.8} = 0.713$	$\frac{25.4}{17.8} = 1.427$	$\frac{38.1}{17.8} = 2.14$	$\frac{50.8}{17.8} = 2.854$

Table 2.22: Comparison of the elongation at fracture ϵ_f of HY-100 steel for almost geometrically similar specimens; extracted from Matic et al. (1988, [2.48])

Specimen type (d_0, L_0)	(c, b) & (a, a)	(b, b) & (c, c)	(e, d) & (b, c)
L_0/d_0	1.427 & 1.67	2 & 2.14	2.854 & 3
λ_d	2.34	1.4	1.4
ϵ_f	0.4 & 0.4	0.342 & 0.31	0.25 & 0.265

Figures

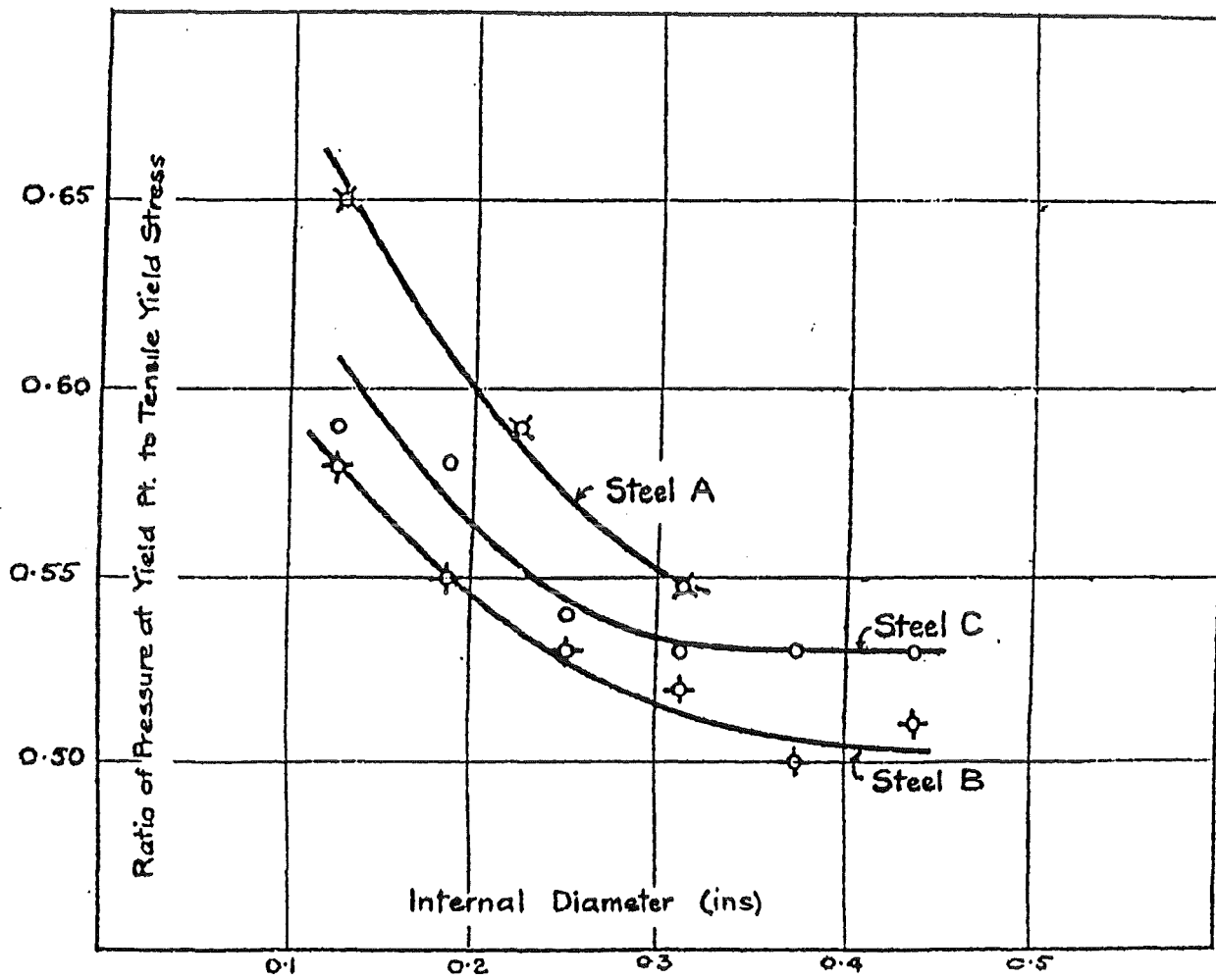


Fig. 2.1 Size effect observed at initial yield point in steel cylinders. Ratio external-to-internal diameter: 3; from Cook (1931, [2.7]).

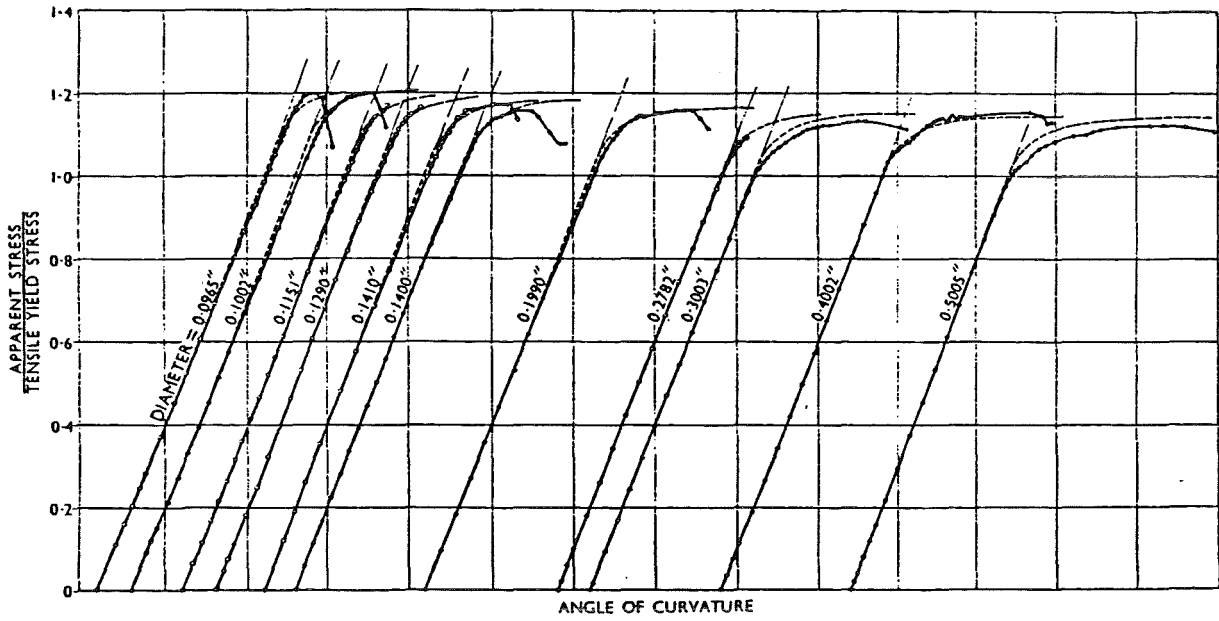


Fig. 2.2 Size effect in flexure: moment-angle curves
 ○—○ Intermittent strain: experimental curves. ●—● Continuous strain: experimental curves. ---- Curves calculated; from Morrison (1939, [2.14]).

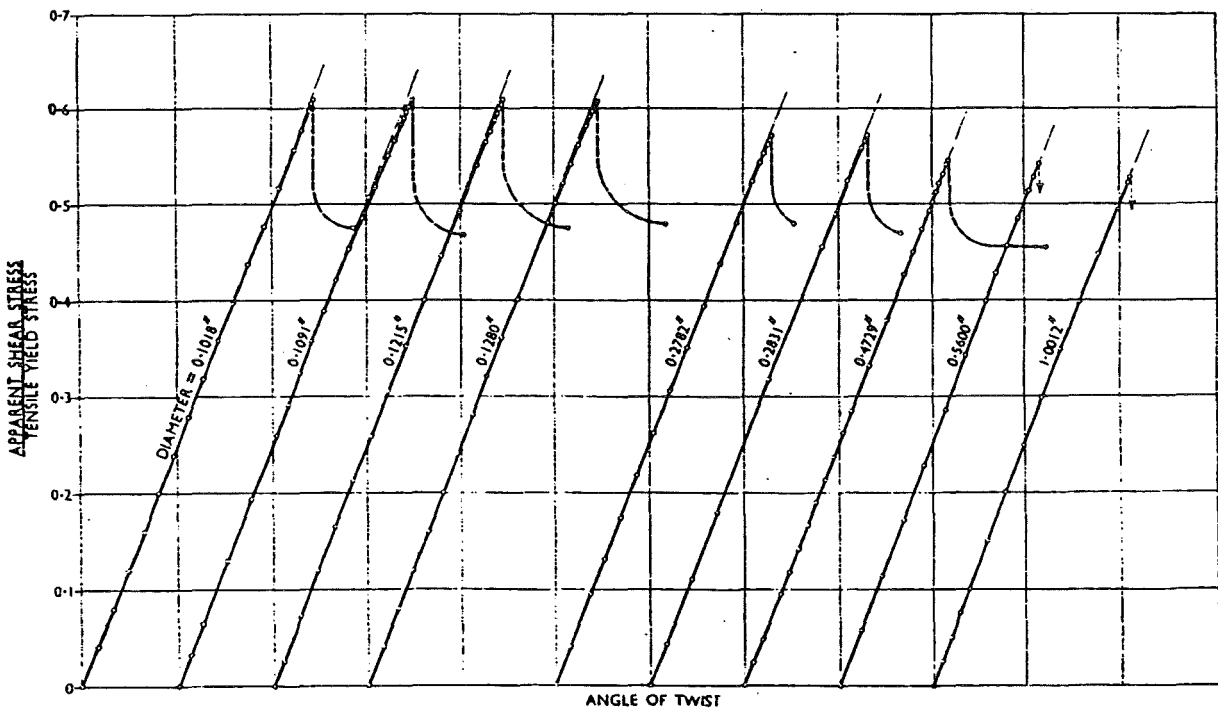


Fig. 2.3 Size effect in torsion: torque-angle curves; from Morrison (1939, [2.14]).

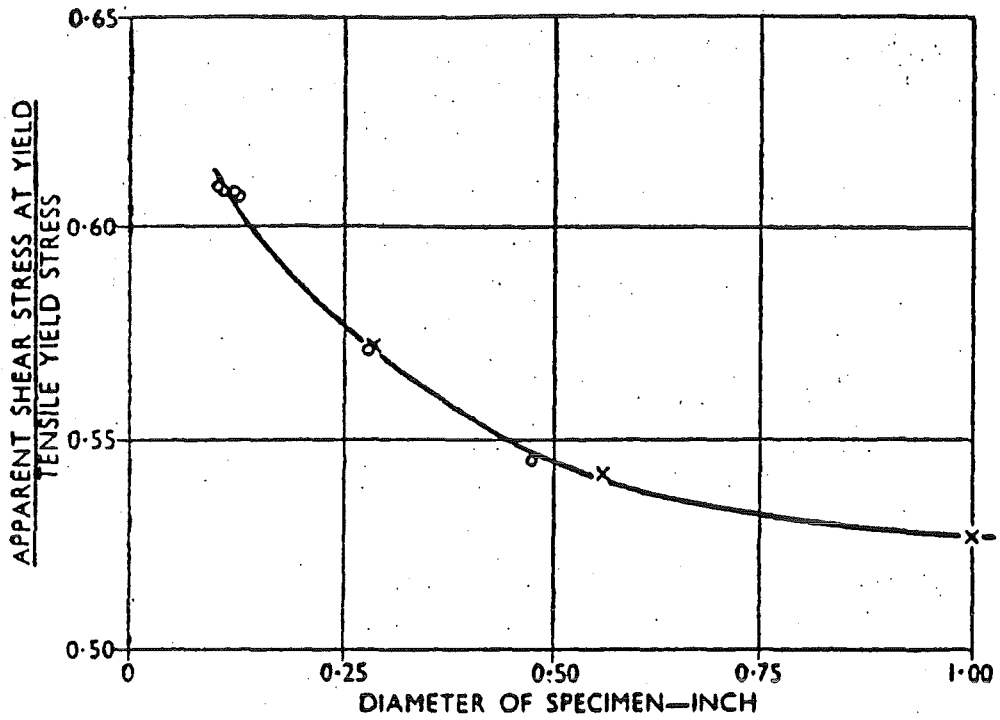


Fig. 2.4 Size effect in torsion. x First series. o Second series; from Morrison (1939, [2.14]).

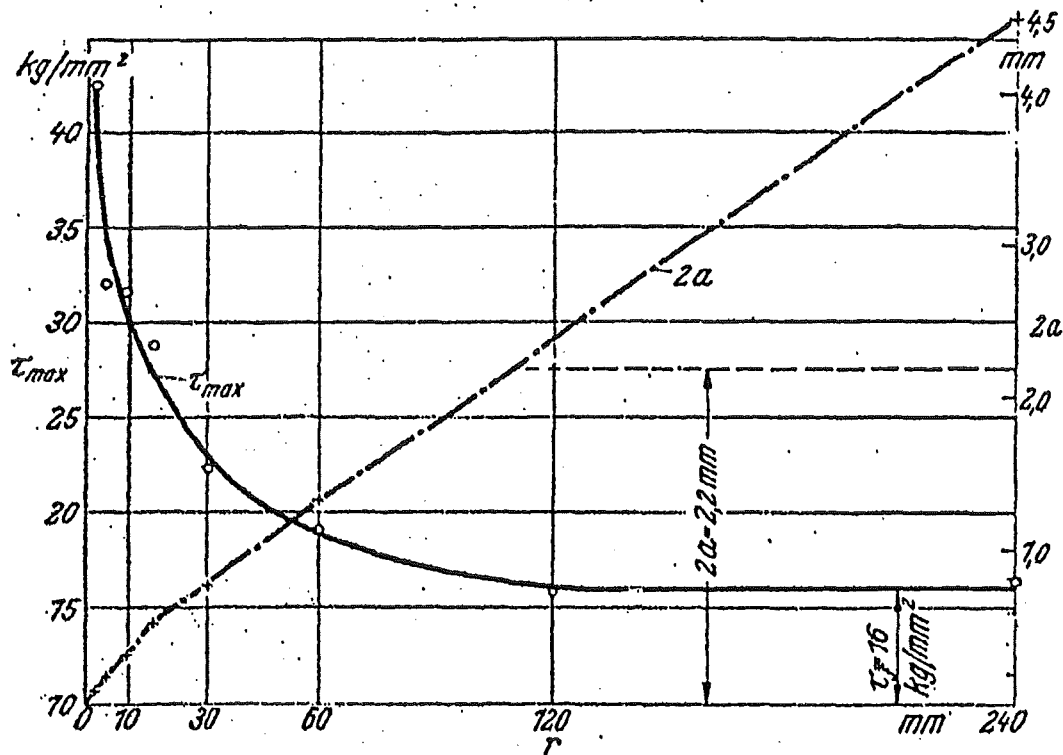


Fig. 2.5 Size effect in indentation: maximum shear stress and width of the contact area versus roll-radius at initiation of flow lines in steel St37; from Föppl and Huber (1941, [2.16]).

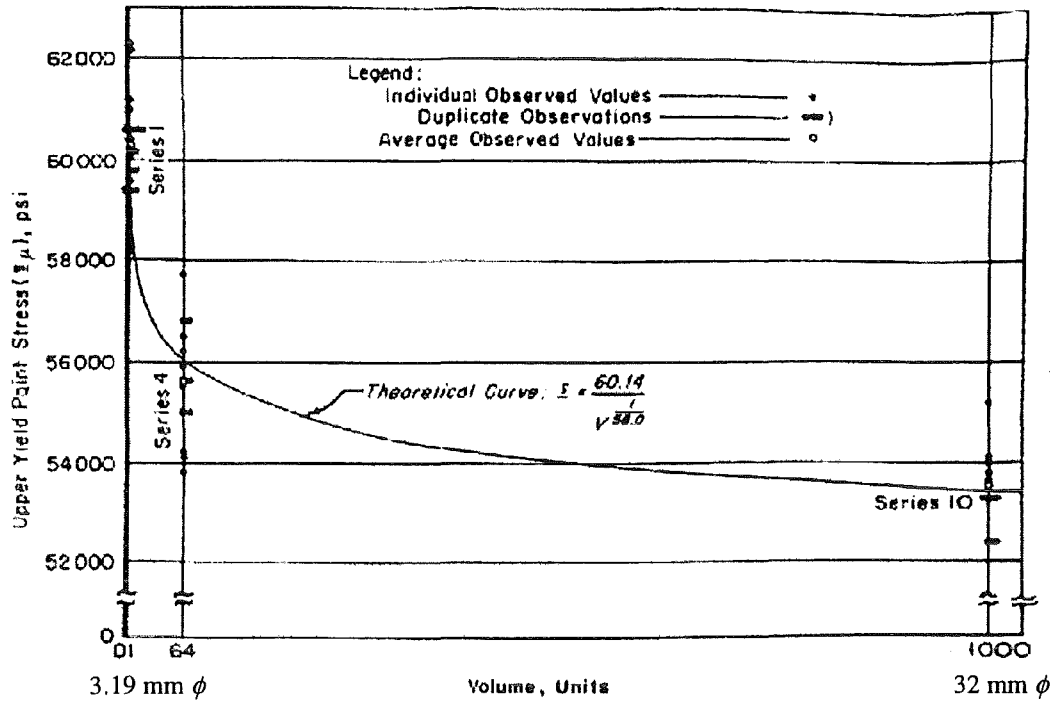


Fig. 2.6 Size effect in tension of a mild steel: Variation of upper yield point stress with volume; from Richards (1954, [2.19]).

BEAM DIMENSIONS.

Series (Bj)	Width, <i>b</i> , (in.)	Depth, <i>h</i> , (in.)	Span, <i>g</i> , (in.)	Mo-ment Arm, <i>e</i> , (in.)	Roller Diam., <i>d</i> , (in.)	$\log_{10} 10h$
B1 ...	0.0635	0.1585	1.840	0.460	0.161	0.2
B2 ...	0.1005	0.251	2.912	0.728	0.250	0.4
B3 ...	0.1590	0.398	4.615	1.154	0.391	0.6
B4 ...	0.2525	0.631	7.32	1.83	0.625	0.8
B5 ...	0.4000	1.000	11.6	2.90	1.000	1.0

Note. $b = 0.4h$ $e = 0.25g = 2.9h$
 $g = 11.6h$ $d \cong h$

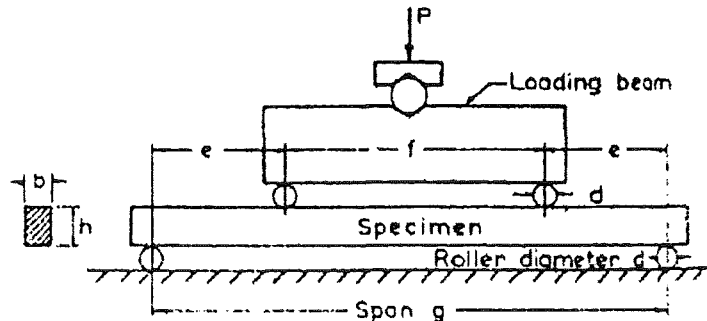


Fig. 2.7 Pure bending loading arrangement and beam dimensions; from Richards (1958, [2.20]).

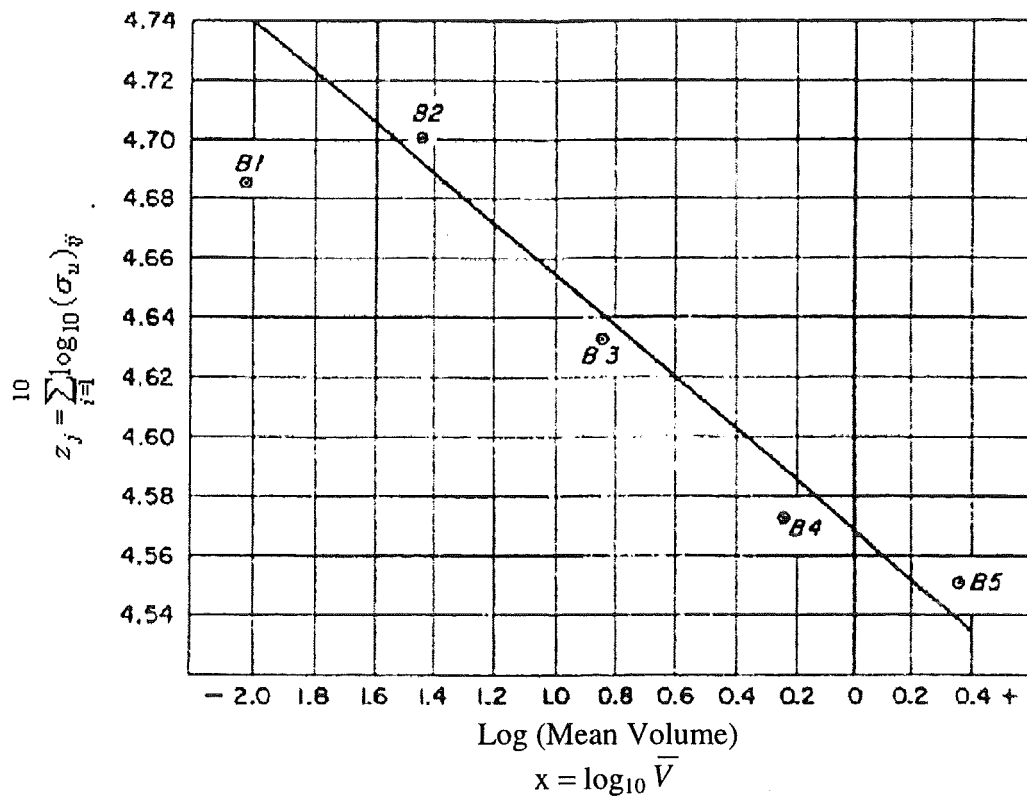


Fig. 2.8 Size effect of yield initiation in pure bending of mild steel beams: variation of upper yield point stress with volume; from Richards (1958, [2.20]).

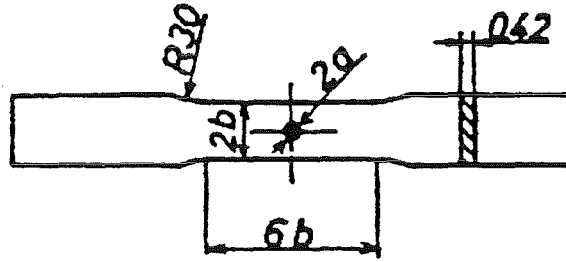


Fig. 2.9 Geometry of specimen; from Imamura and Sato (1986, [2.22]).

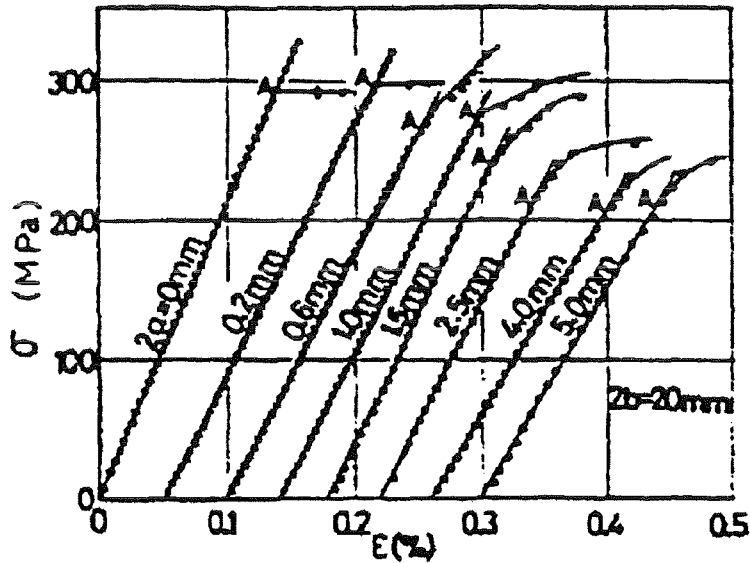


Fig. 2.10 Stress-strain diagram for the perforated tensile strip with varying hole diameters; from Imamura and Sato (1986, [2.22]).

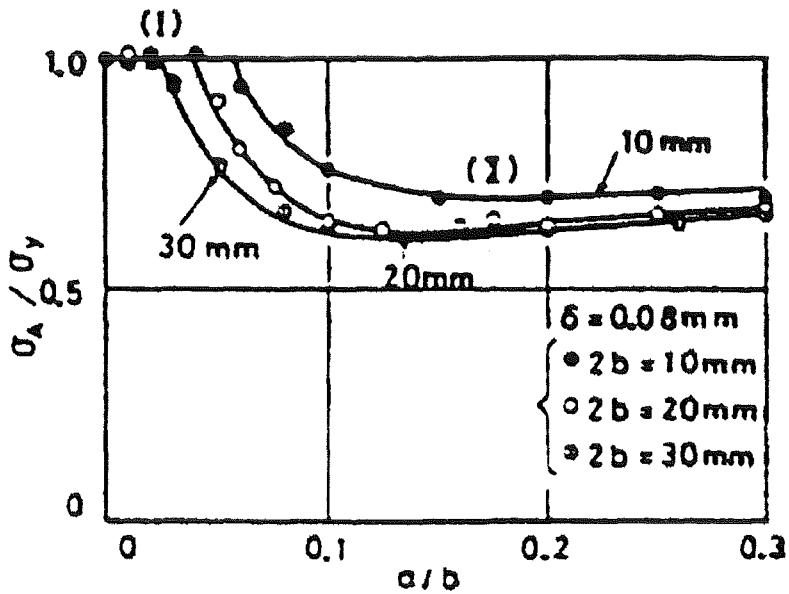
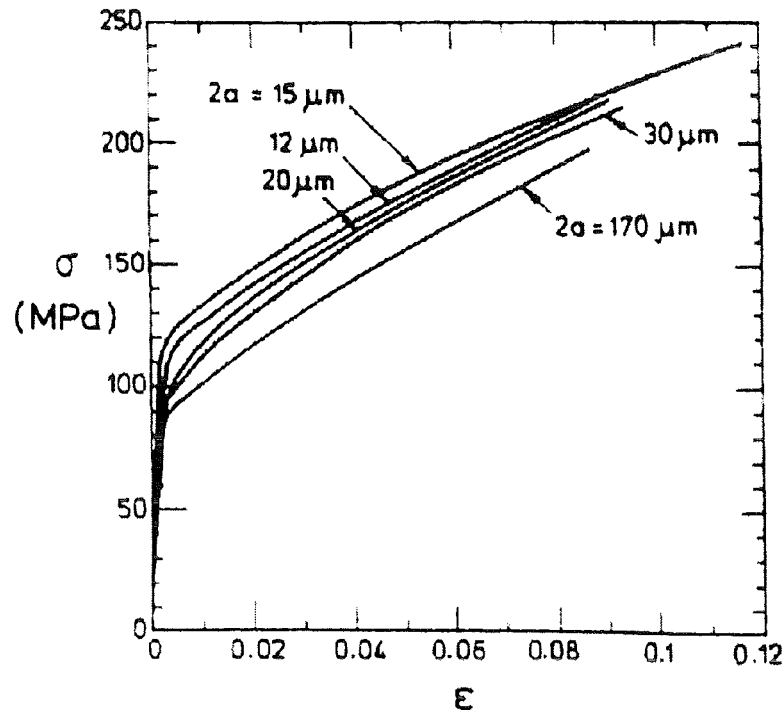
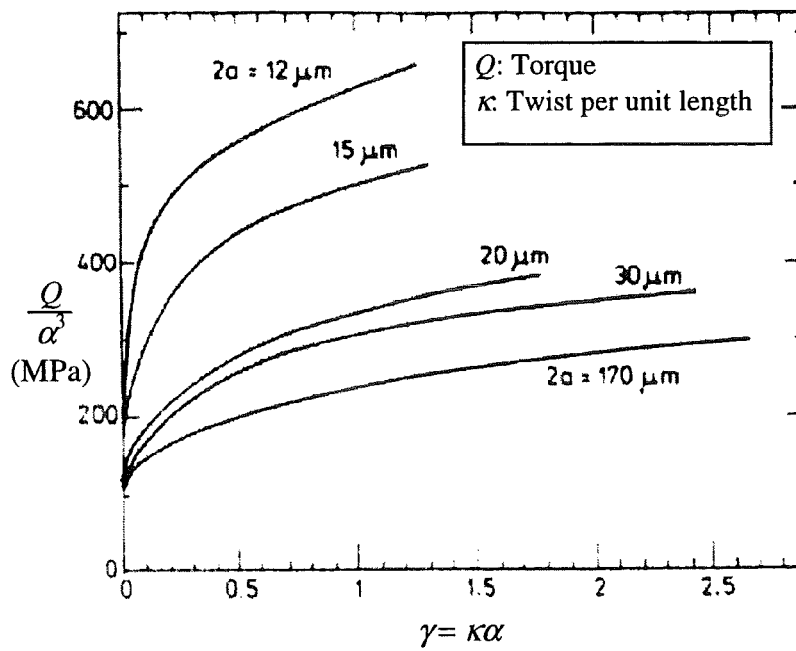


Fig. 2.11 Normalized yield stress versus relative hole diameter; parameter: specimen width (size); from Imamura and Sato (1986, [2.22]).



(a) True stress σ vs logarithmic strain ϵ tension data; strain rate $\dot{\epsilon} \sim 10^{-3}/s$.



(b) Torsional response of copper wires of diameter 2α in the range 12-170 μm ; shear strain rate $\dot{\gamma} \sim 10^{-3}/s$.

Fig. 2.12 Size effect in tension and torsion of thin copper wires of diameter 2α in the range 12-170 μm ; from Fleck et al. (1994, [2.26]).

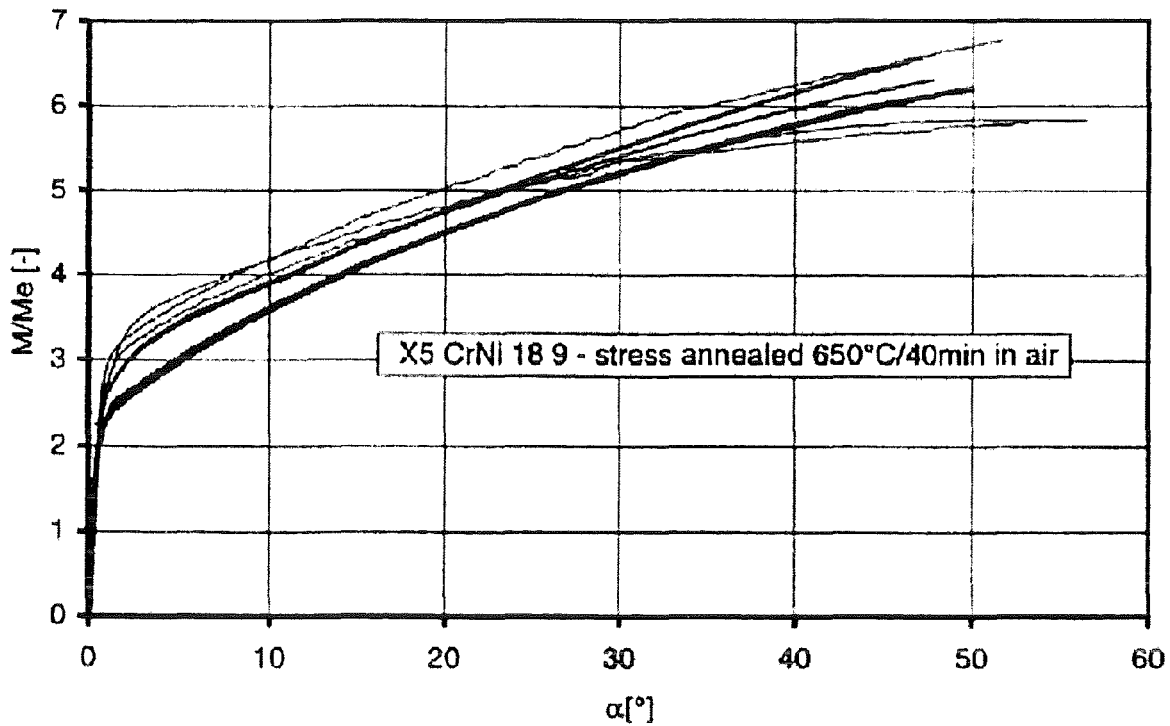


Fig. 2.13 Size effect in cantilever bending of tapered stainless steel beams: normalized bending moment versus angle of rotation; three nominally identical tests for each size; the line thickness refers to the minimum diameter D of the bending joints: Thin $\rightarrow D = 1$ mm, Medium $\rightarrow D = 4$ mm, Thick $\rightarrow D = 10$ mm; from Stach (1997, [2.27]) and Jordan and Malmberg (1998, [2.28]).

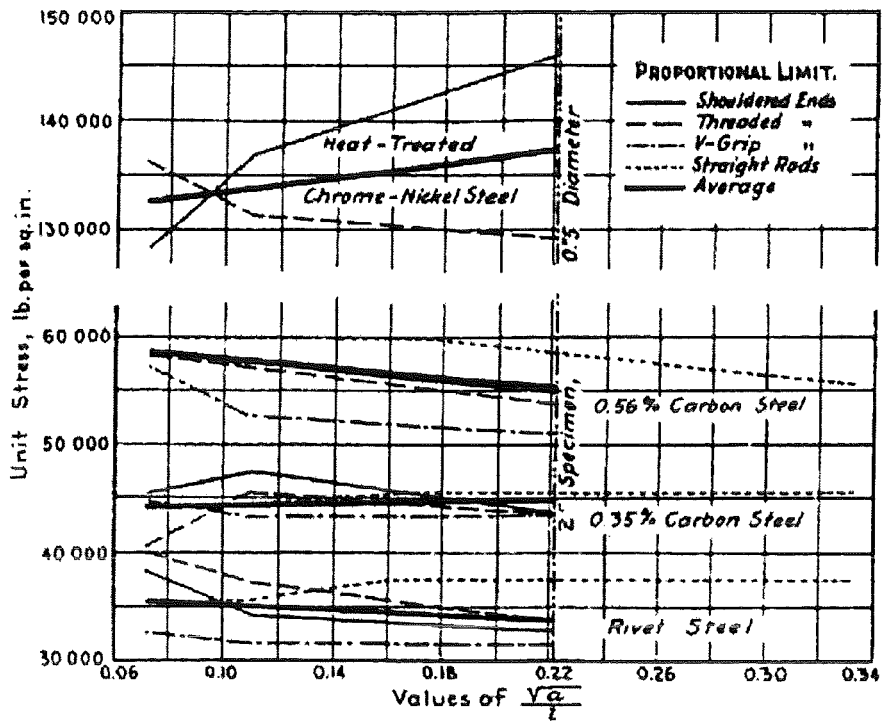


Fig. 2.14 Dependence of the proportional limit of four grades of steel on the stoutness $\sqrt{\alpha}/l$ using different specimen types; from Moore (1918, [2.32]).

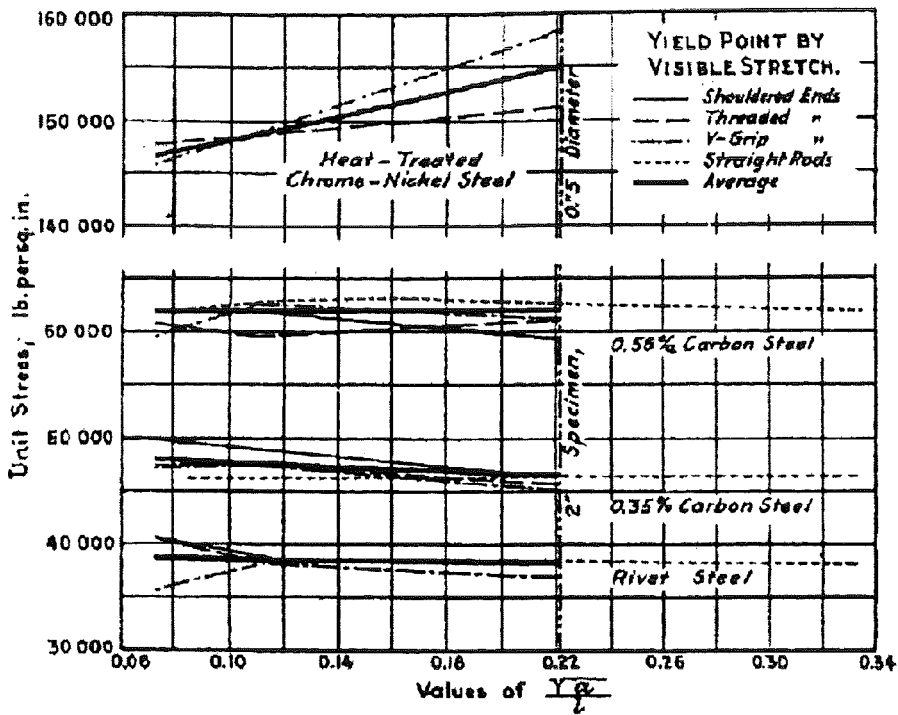


Fig. 2.15 Dependence of yield point (at 0.5% strain) of four grades of steel on the stoutness $\sqrt{\alpha}/l$, using different specimen types; from Moore (1918, [2.32]).

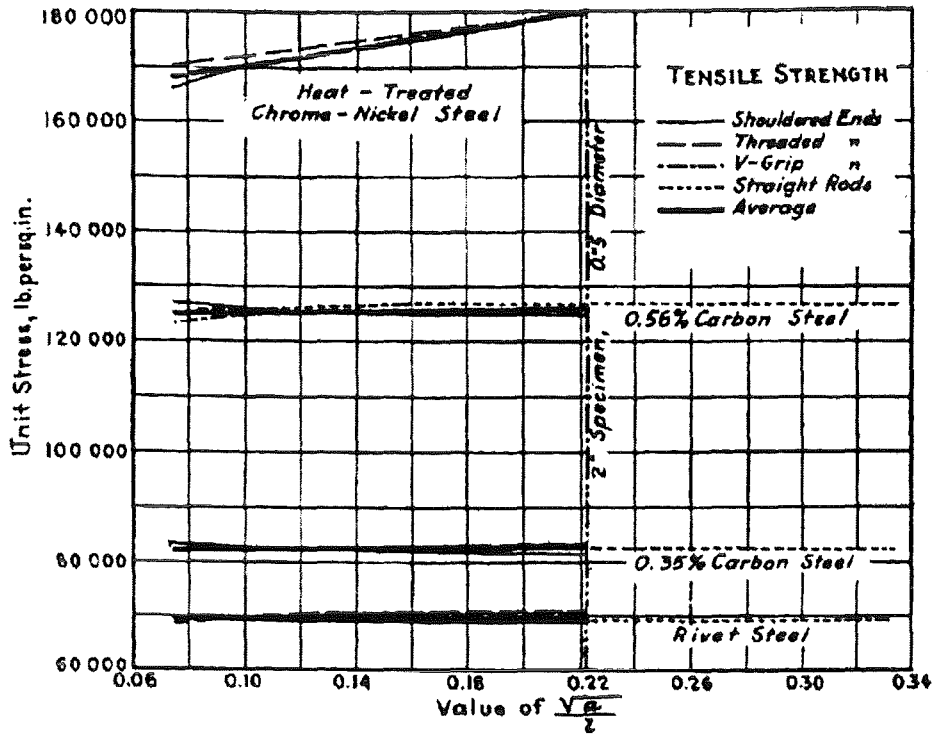


Fig. 2.16 Relation between tensile strength and \sqrt{a}/l ; from Moore (1918, [2.32]).

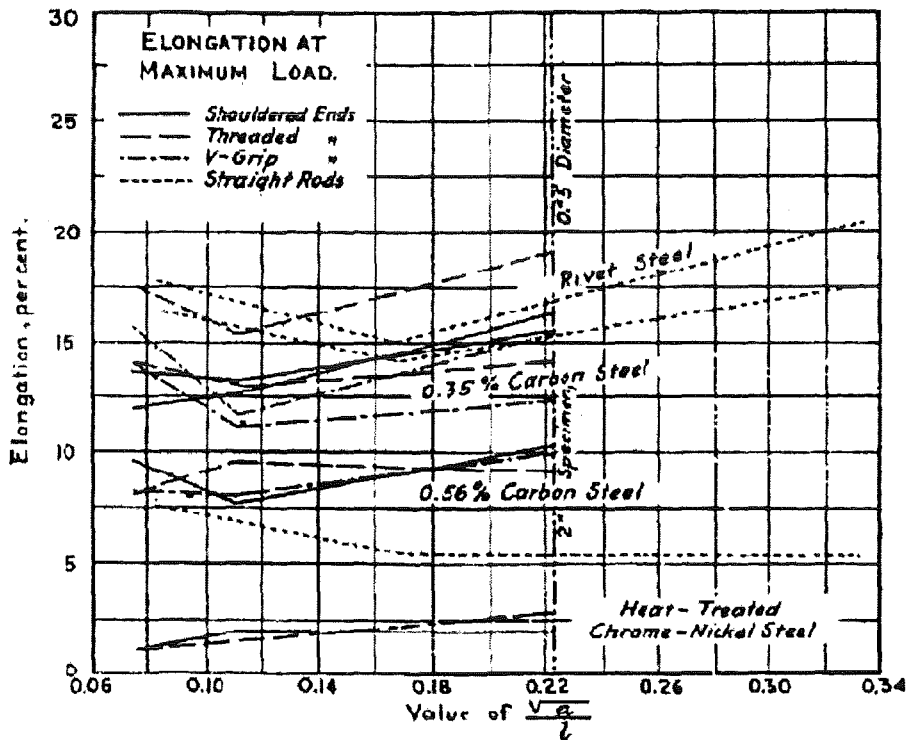


Fig. 2.17 Relation between elongation at maximum load and \sqrt{a}/l ; from Moore (1918, [2.32]).

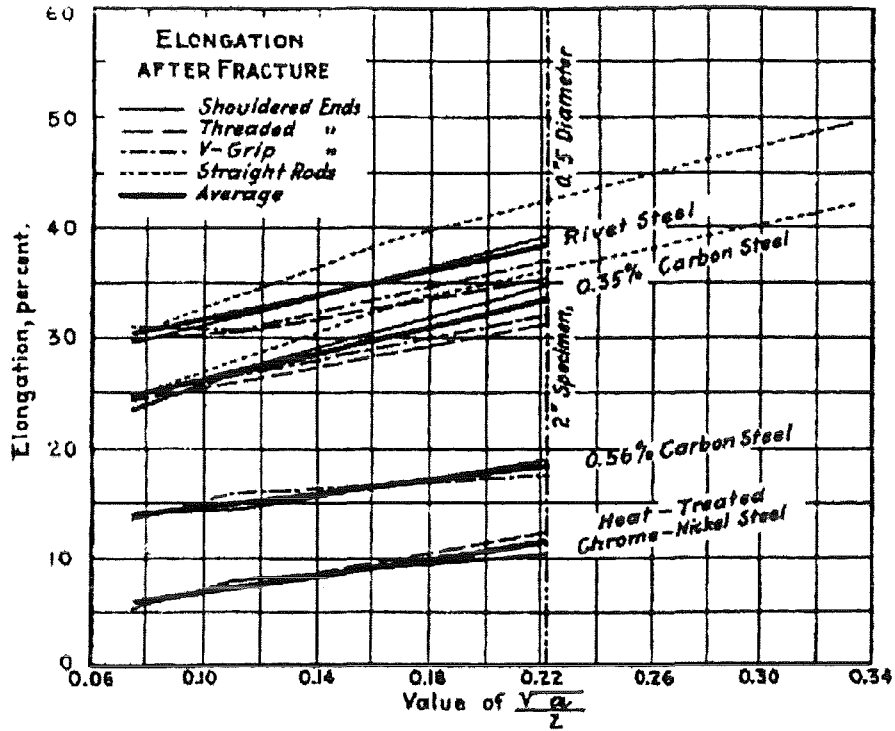


Fig. 2.18 Relation between elongation after fracture and $\sqrt{\alpha/l}$; from Moore (1918, [2.32]).

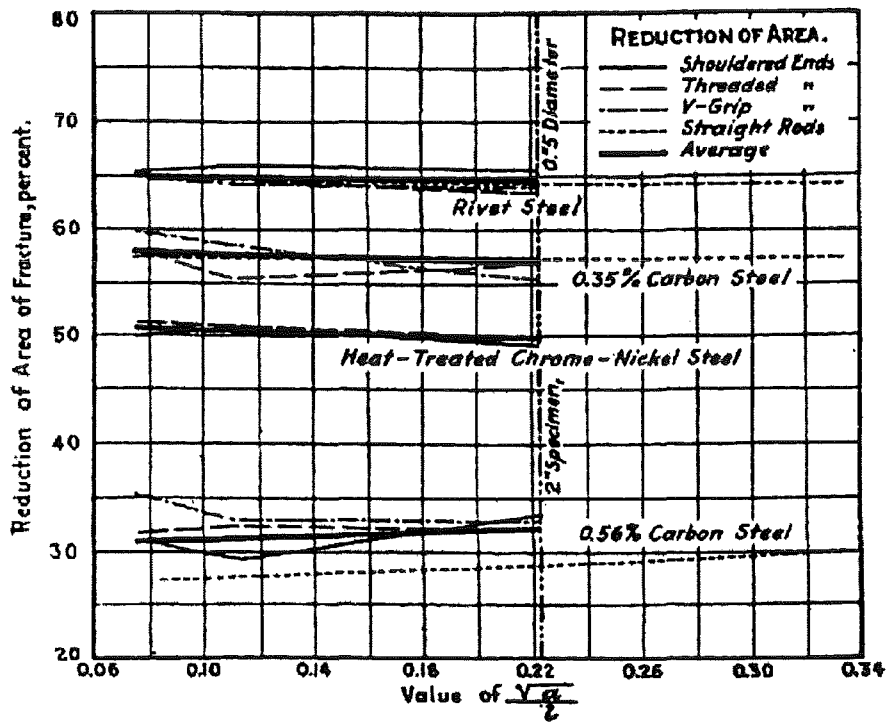


Fig. 2.19 Relation between reduction of area and $\sqrt{\alpha/l}$; from Moore (1918, [2.32]).

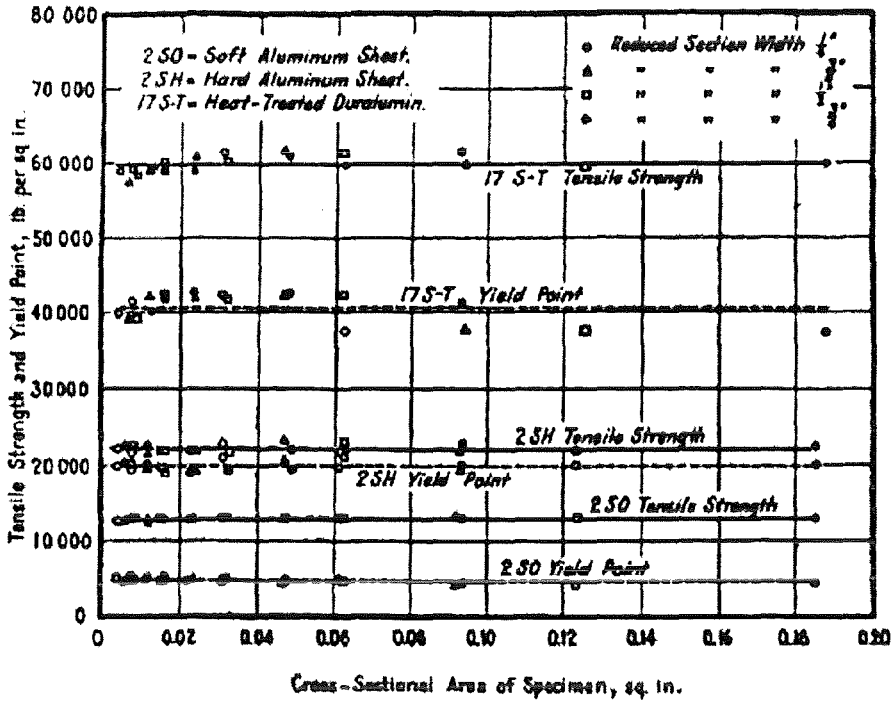


Fig. 2.20 Dependence of tensile strength and yield stress on the cross-section area of three aluminium alloys; from Templin (1926, [2.34]).

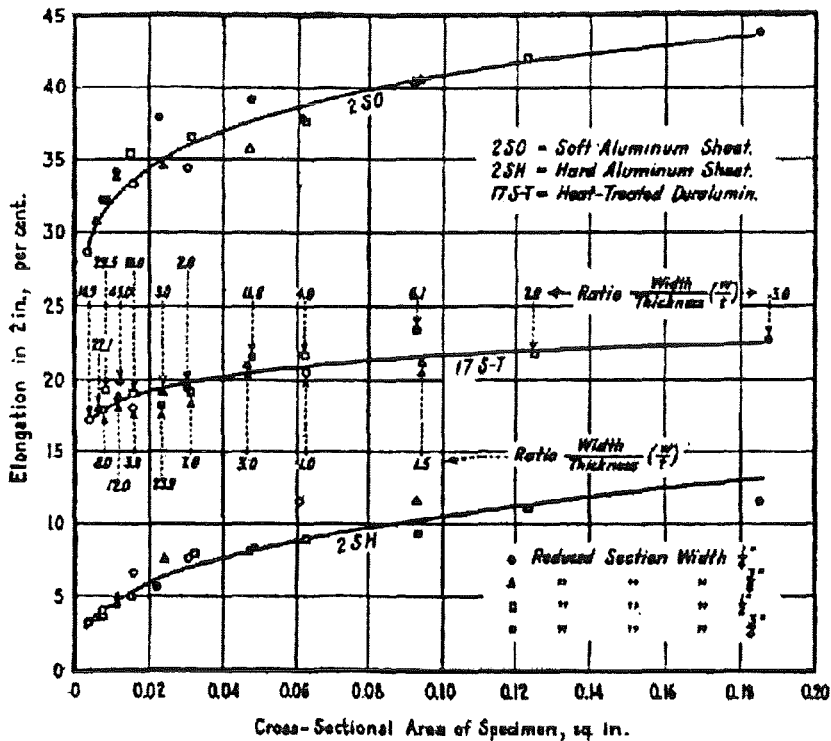


Fig. 2.21 Dependence of fracture elongation in a 2 inches gage length on the cross-section area of three aluminium alloys; from Templin (1926, [2.34]).

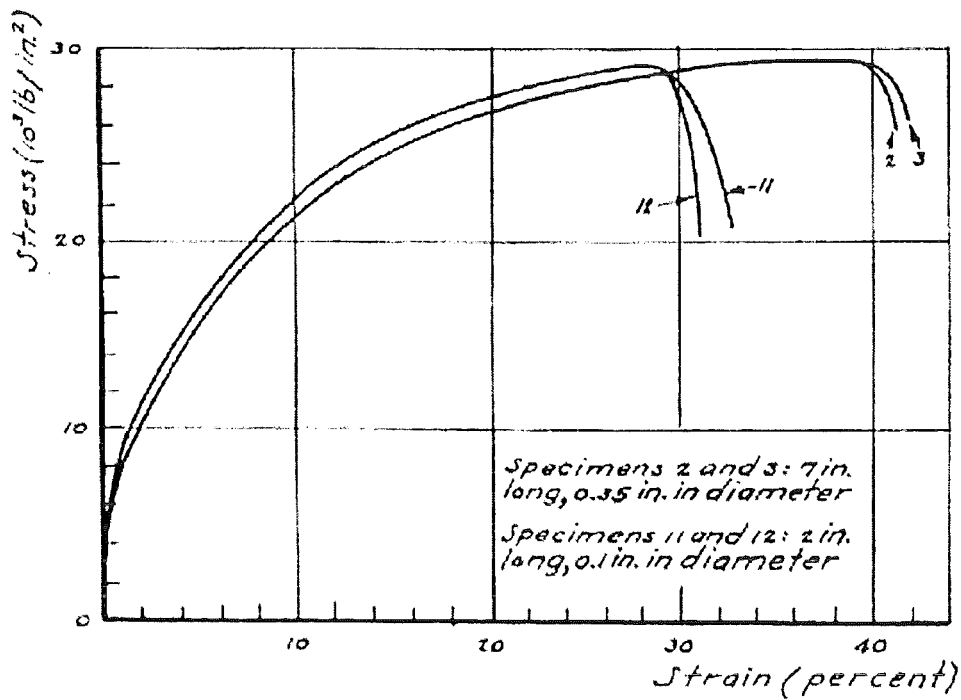


Fig. 2.22 Static stress-strain curves for annealed copper specimens machined from 1/2-in. round bar; from Wood et al. (1943, [2.36]).

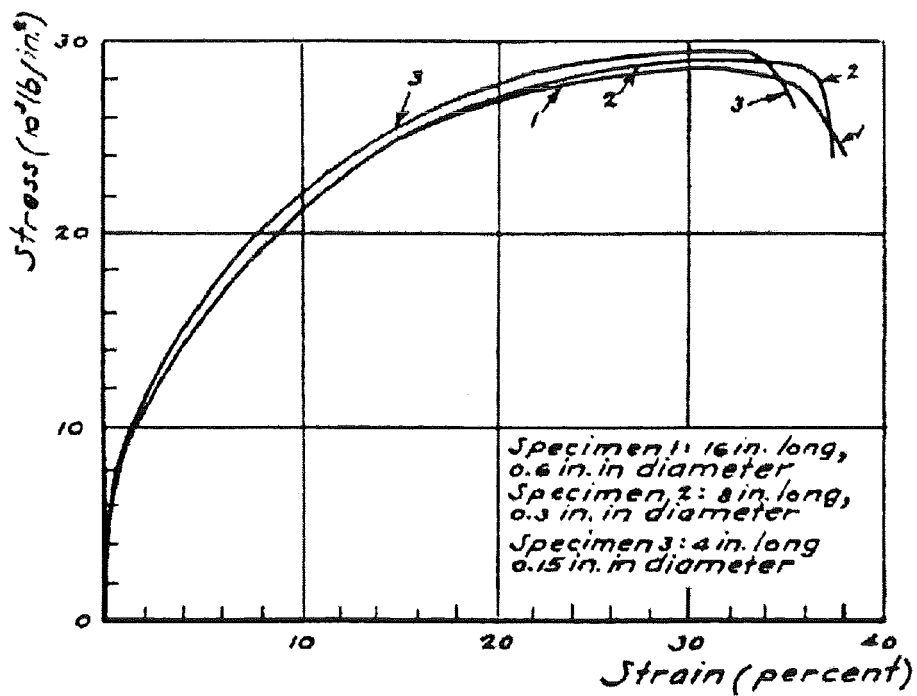


Fig 2.23 Static stress-strain curves for annealed copper specimens machined from 1-in. round bar; from Wood et al. (1943, [2.36]).

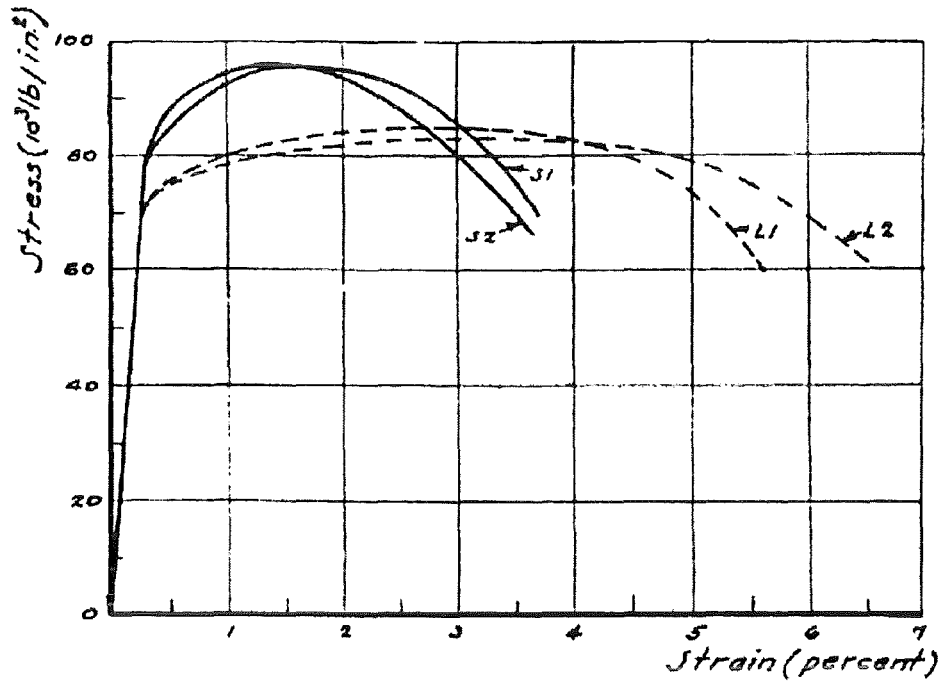


Fig. 2.24 Static stress-strain curves for cold-rolled steel SAE 1020;
 ——— short specimens; ----- long specimens;
 specimen numbers indicated on curves; from Wood et al. (1943, [2.36]).

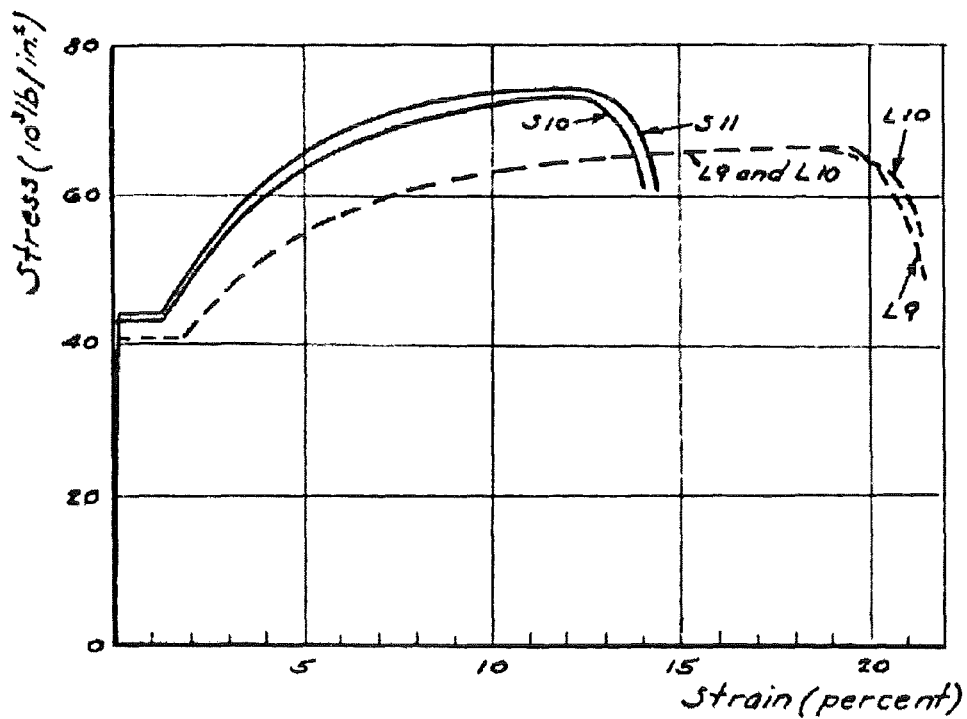


Fig. 2.25 Static stress-strain curves for annealed steel SAE 1020;
 ——— short specimens; ----- long specimens;
 specimen numbers indicated on curves; from Wood et al. (1943, [2.36]).

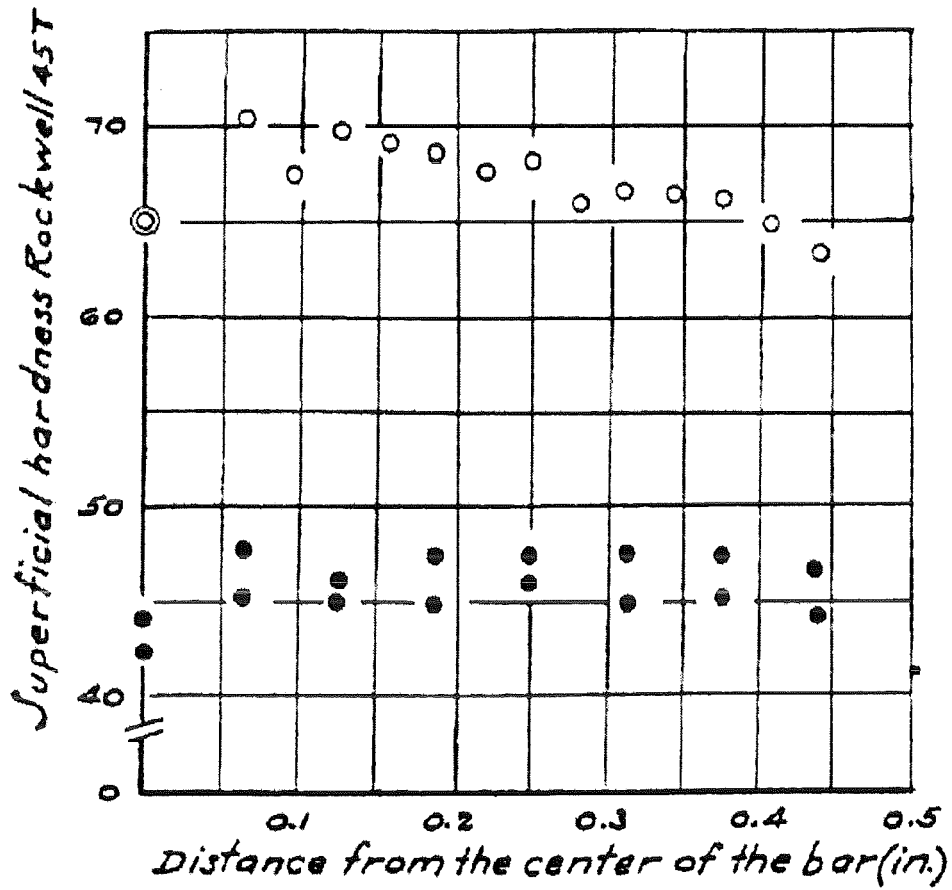


Fig 2.26 Variation of superficial hardness in a cross-section of a bar of cold-rolled (o) and annealed (•) steel SAE 1020; from Wood et al. (1943, [2.36]).

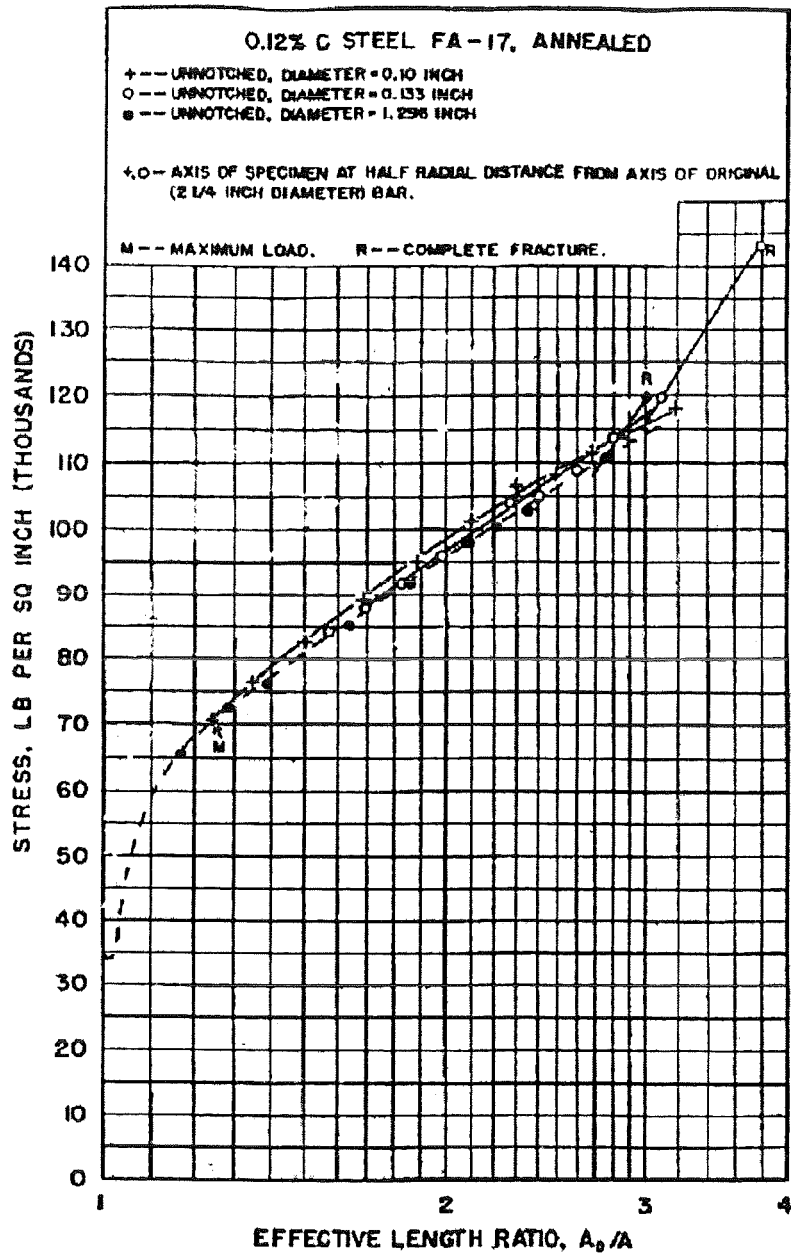
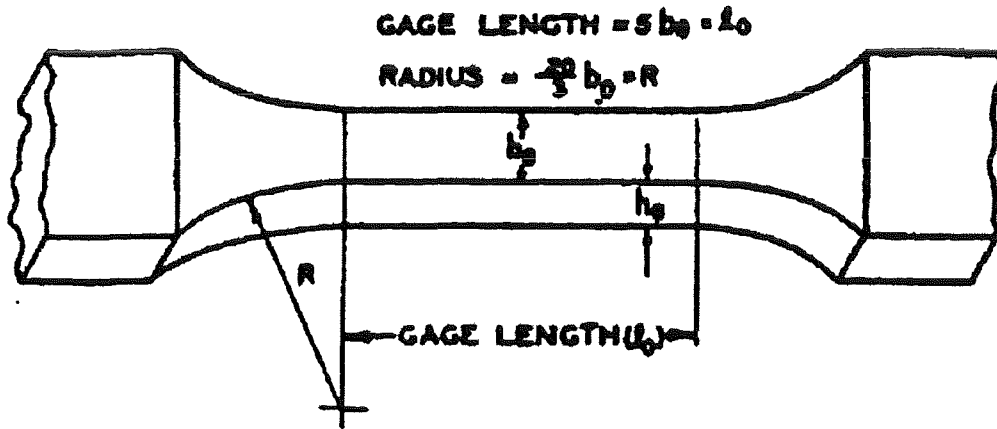
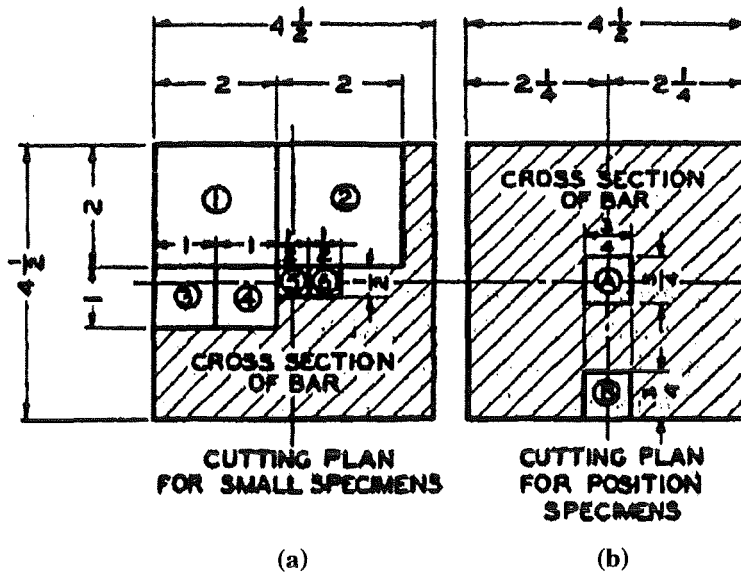


Fig. 2.27 Flow and fracture of unnotched tensile specimens of different size; from McAdam et al. (1948, [2.37]).



SERIES	SPEC. NO.	DIMENSION (INCHES)				b_0/h_0	l_0/h_0
		h_0	b_0	l_0	R		
A	10 A	0.750	7.500	37.50	50.00	10	50
	7 A	↓	5.250	26.25	35.00	7	35
	6 A		4.500	22.50	30.00	6	30
	5 A		3.750	18.75	25.00	5	25
	3 A		2.250	11.25	15.00	3	15
	1 A		0.750	3.75	5.00	1	5
B	10 B	0.375	3.750	18.75	25.00	10	50
	7 B	↓	2.625	13.13	17.50	7	35
	6 B		2.250	11.25	15.00	6	30
	5 B		1.875	9.38	12.50	5	25
	3 B		1.125	5.63	7.50	3	15
	1 B		0.375	1.88	2.50	1	5
C	10 C	0.188	1.875	9.38	12.50	10	50
	7 C	↓	1.313	6.56	8.75	7	35
	6 C		1.125	5.63	7.50	6	30
	5 C		0.938	4.69	6.25	5	25
	3 C		0.563	2.81	3.75	3	15
	1 C		0.188	0.94	1.25	1	5

Fig 2.28 Dimensions of flat bars used in size effect tensile tests; from Miklowitz (1948, [2.38]).



DIMENSIONS IN INCHES

Fig. 2.29 Cutting plans for small specimens; from Miklowitz (1950, [2.39]).

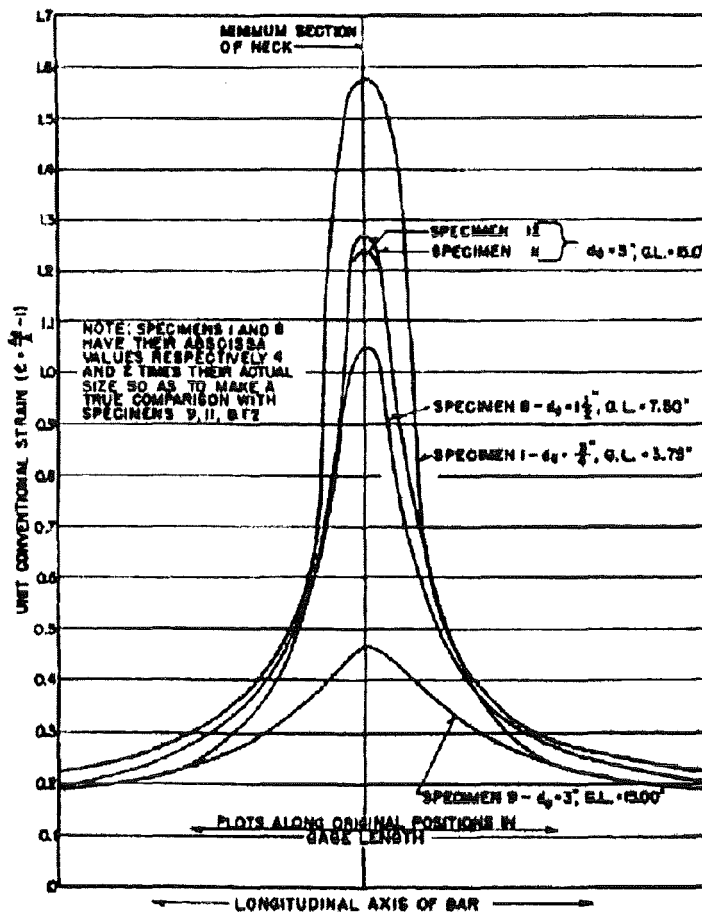


Fig. 2.30 Distribution of axial strain in neck after fracture of round tension specimens of different sizes; scaled abscissa of specimen 1 and 8; Miklowitz (1950, [2.39]).

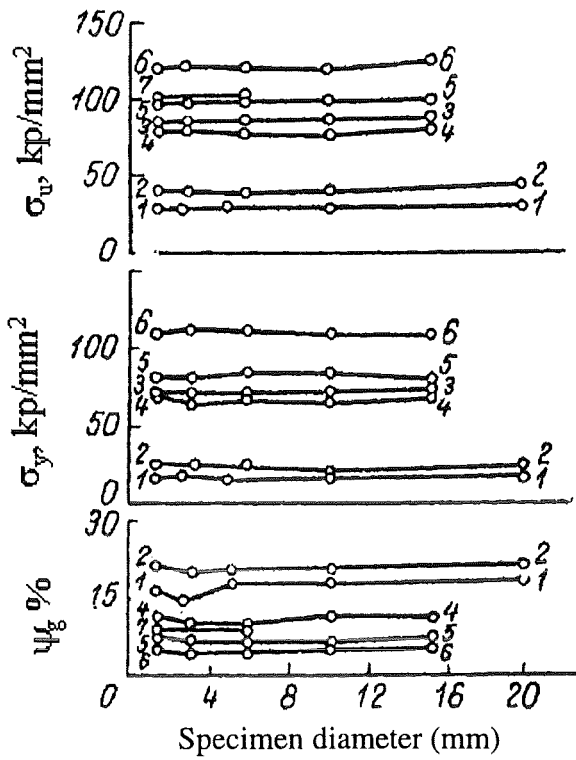


Fig. 2.31 Size dependence of ultimate stress σ_u , yield stress σ_y , uniform area reduction ψ_g ; from Chechulin (1954, [2.42]).

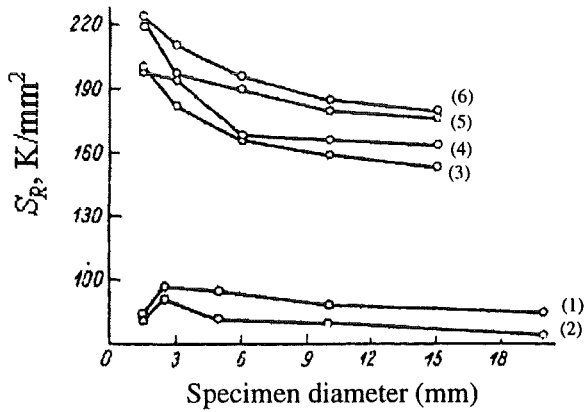


Fig. 2.33 Size dependence of average true fracture stress S_R ; from Chechulin (1954, [2.42]).

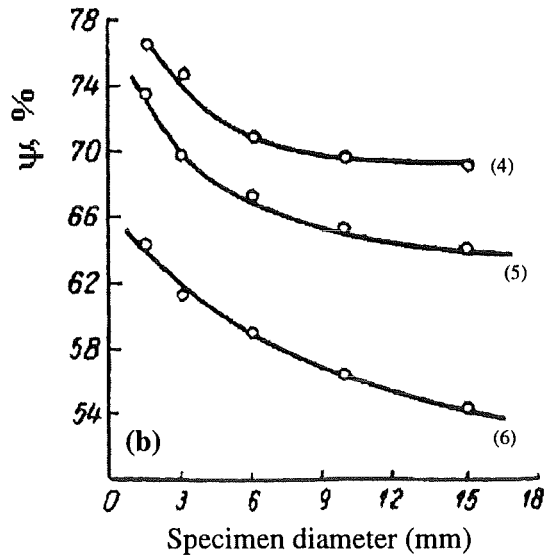
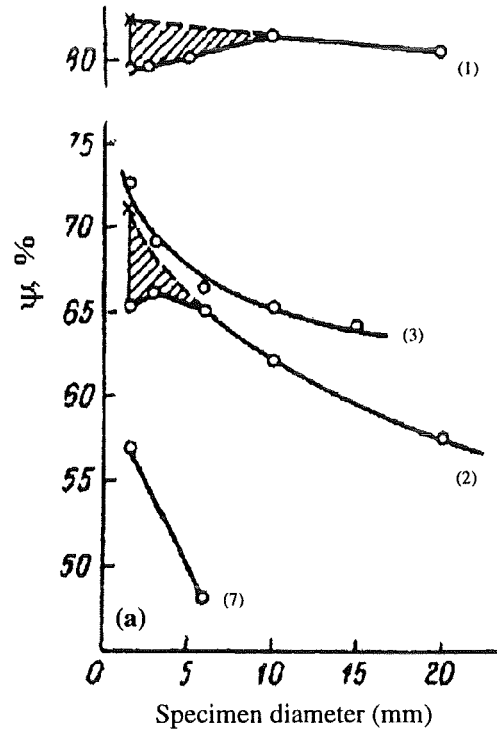


Fig. 2.32 Size dependence of area reduction ψ at fracture; from Chechulin (1954, [2.42]).

Legend:

- (1) Pure iron (Armco type)
- (2) Low carbon steel St3
- (3) CrNi steel (30 ChN3-GOST)
- (4) CrNi steel (37 ChN3A-GOST), $H_B=241$
- (5) CrNi steel (37 ChN3A-GOST), $H_B=293$
- (6) CrNi steel (37 ChN3A-GOST), $H_B=352$
- (7) CrNi steel (40 ChN-GOST)

- ψ percentage reduction in area after rupture
- s_R, s_R^* true fracture stress, test results
- σ_B ultimate tensile strength
- $\delta_s; \delta_{10}$ elongation at rupture
- σ_{So} upper yield point
- δ_{gm} strain at maximum load

$$\delta_{gm} = (\delta'_g + \delta''_g) / 2$$

$$s''_R = s_B [(1 + \psi) - (1 - \psi) \delta_{gm}]$$

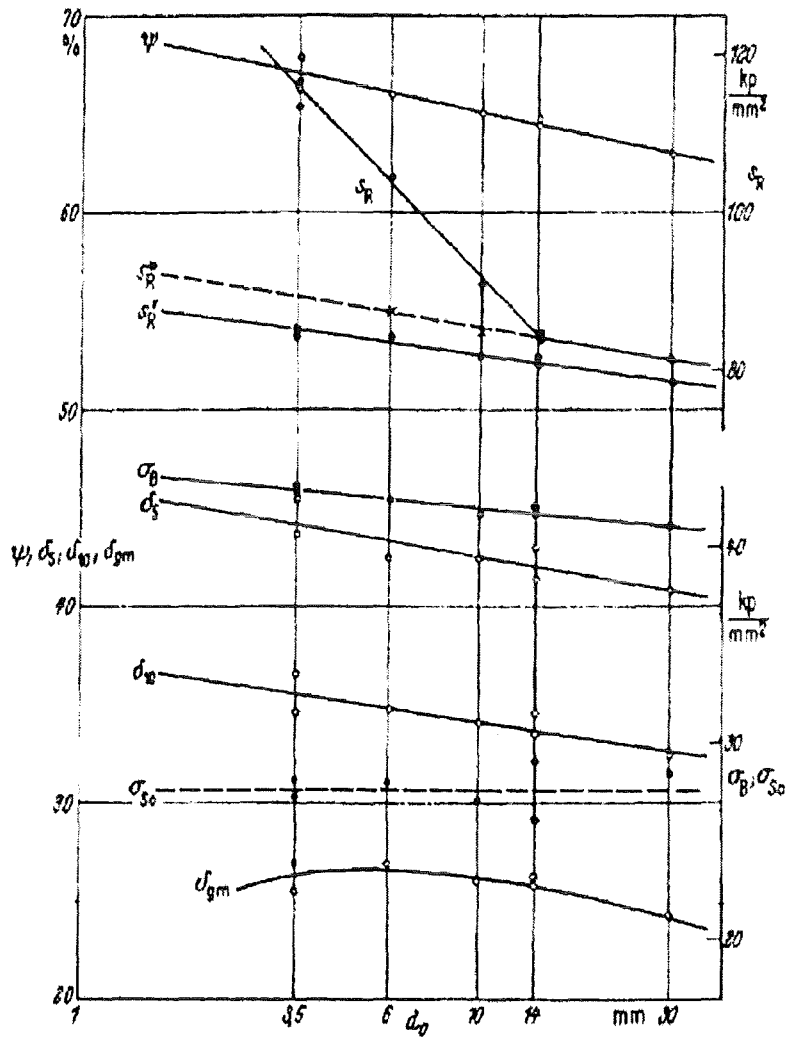


Fig. 2.34 Effect of specimen diameter d_0 on the tensile characteristics of the carbon steel Ck15; from Schneeweiss (1966, [2.45]).

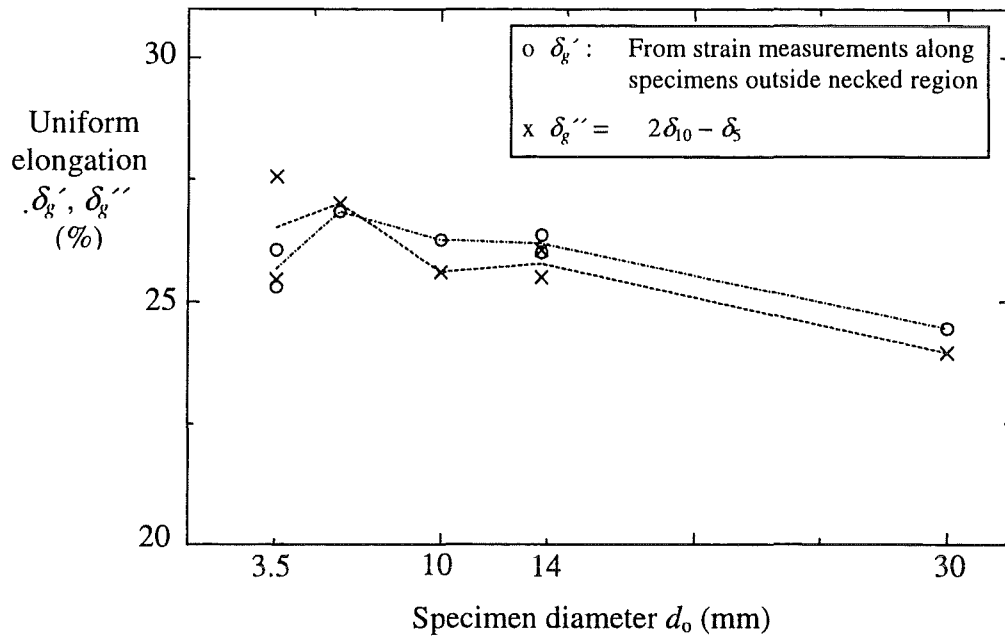


Fig. 2.35 Effect of specimen size on uniform elongation; from Schneeweiss (1966, [2.45]).

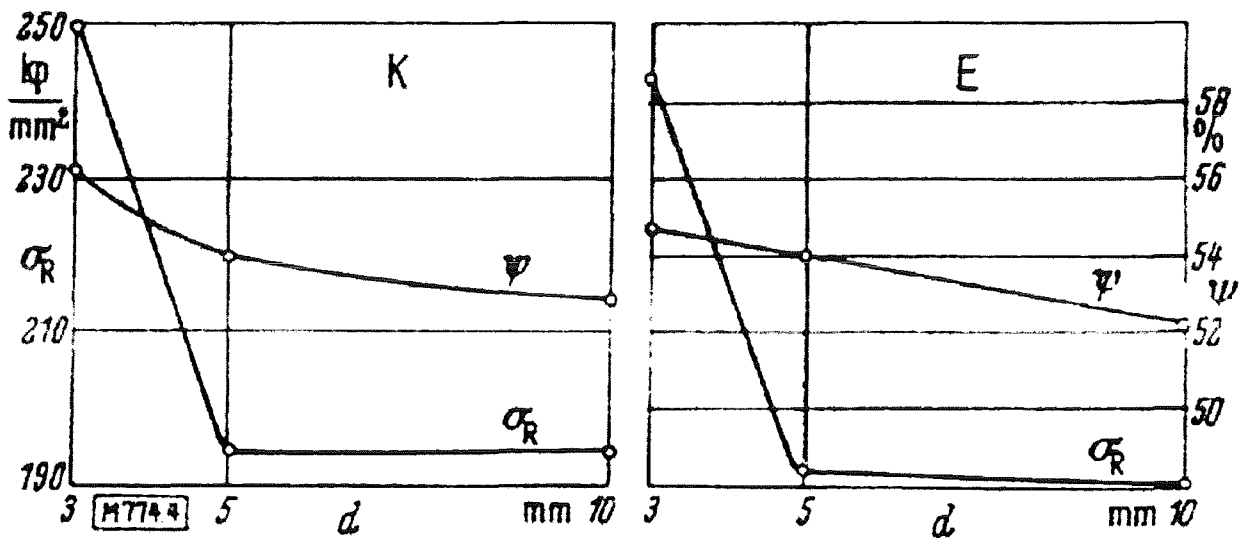


Fig. 2.36 Effect of specimen diameter on reduction of area and true rupture stress of ball bearing steel 100 Cr6; from Buch (1969, [2.46]).

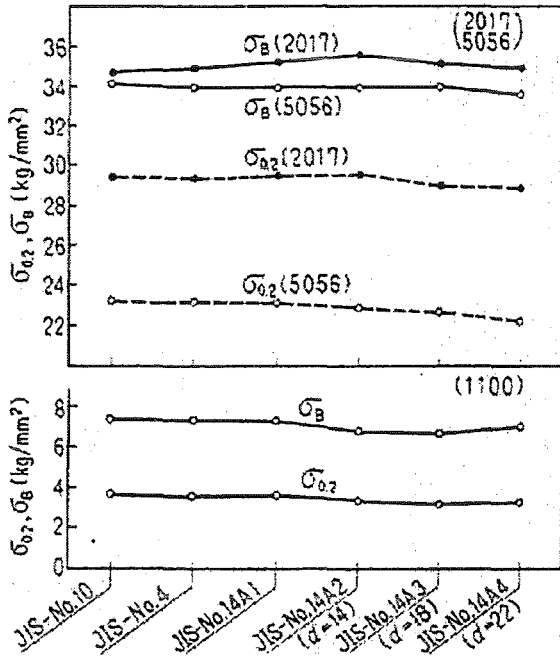


Fig. 2.37 Ultimate stress σ_B and 0.2 %-proof stress $\sigma_{0.2}$ for various JIS round specimens; from Sato and Terazawa (1971, [2.47]).

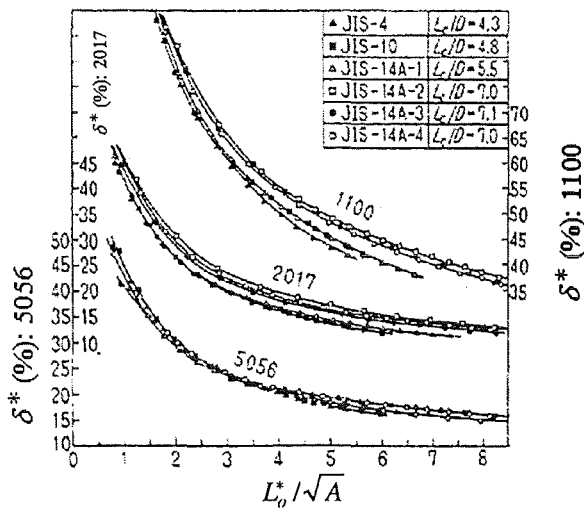


Fig. 2.39 Percent elongation at fracture versus L_o^*/\sqrt{A} ; from Sato and Terazawa (1971, [2.47]).

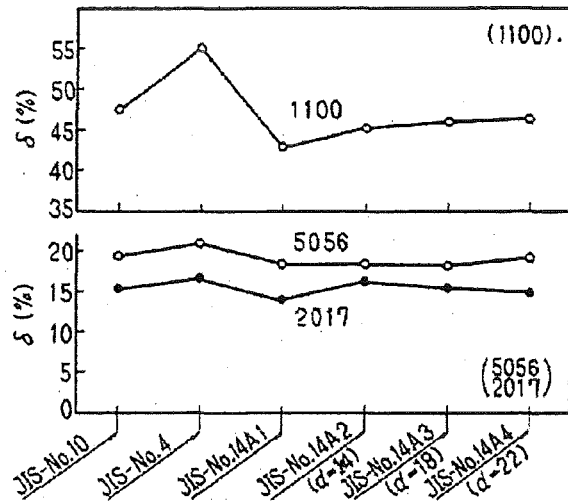


Fig. 2.38 Percent elongation at fracture for various JIS round specimens; from Sato and Terazawa (1971, [2.47]).

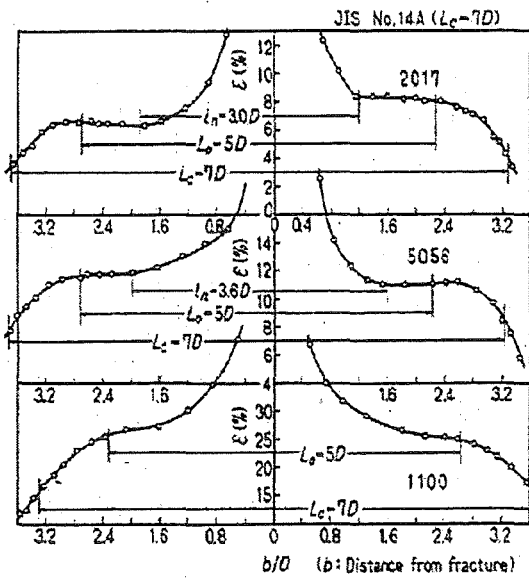


Fig. 2.40 Axial strain distribution after fracture along undeformed JIS No. 14A ($L_c = 7D$) specimens of three aluminium alloys; l_n : undeformed length of necked specimen region; from Sato and Terazawa (1971, [2.47]).

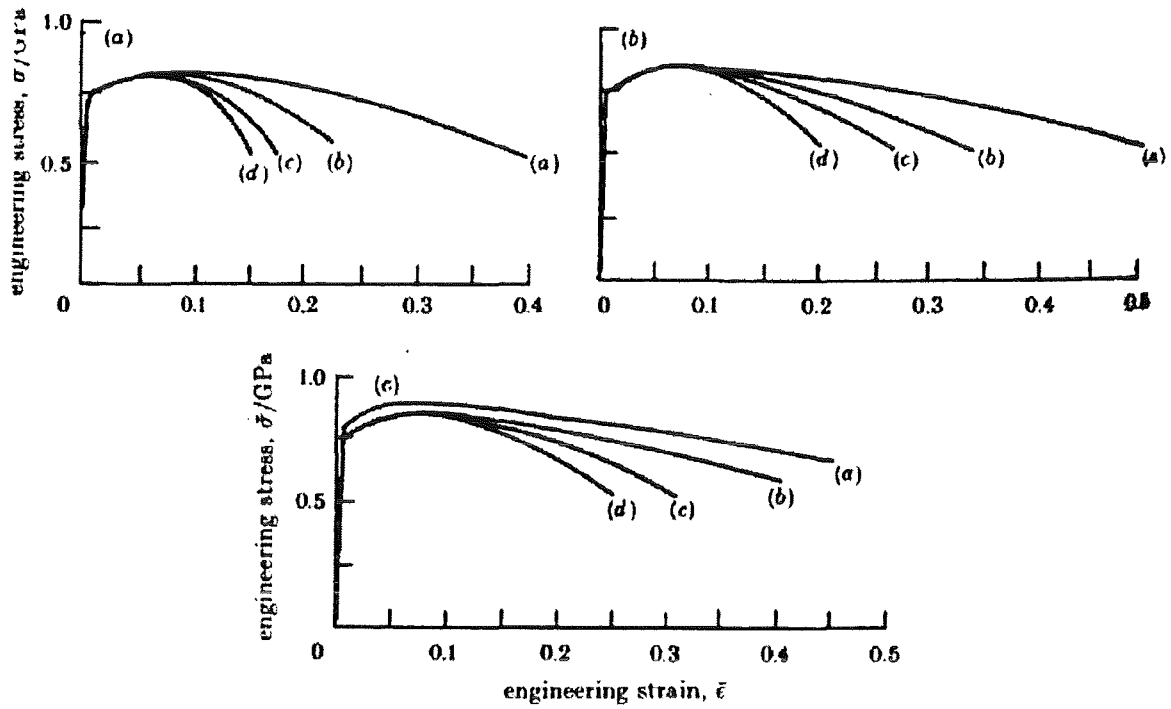


Fig. 2.41 Engineering stress- engineering strain curves from experiments (steel HY-100). Curves *a*, *b*, *c* and *d* refer to specimen gage length L_0 of 12.7, 25.4, 38.1, and 50.8 mm, respectively. Figs. (a) to (c) correspond to different specimen diameters D_0 : 7.6, 12.7, and 17.8 mm; from Matic et al. (1988, [2.48]).

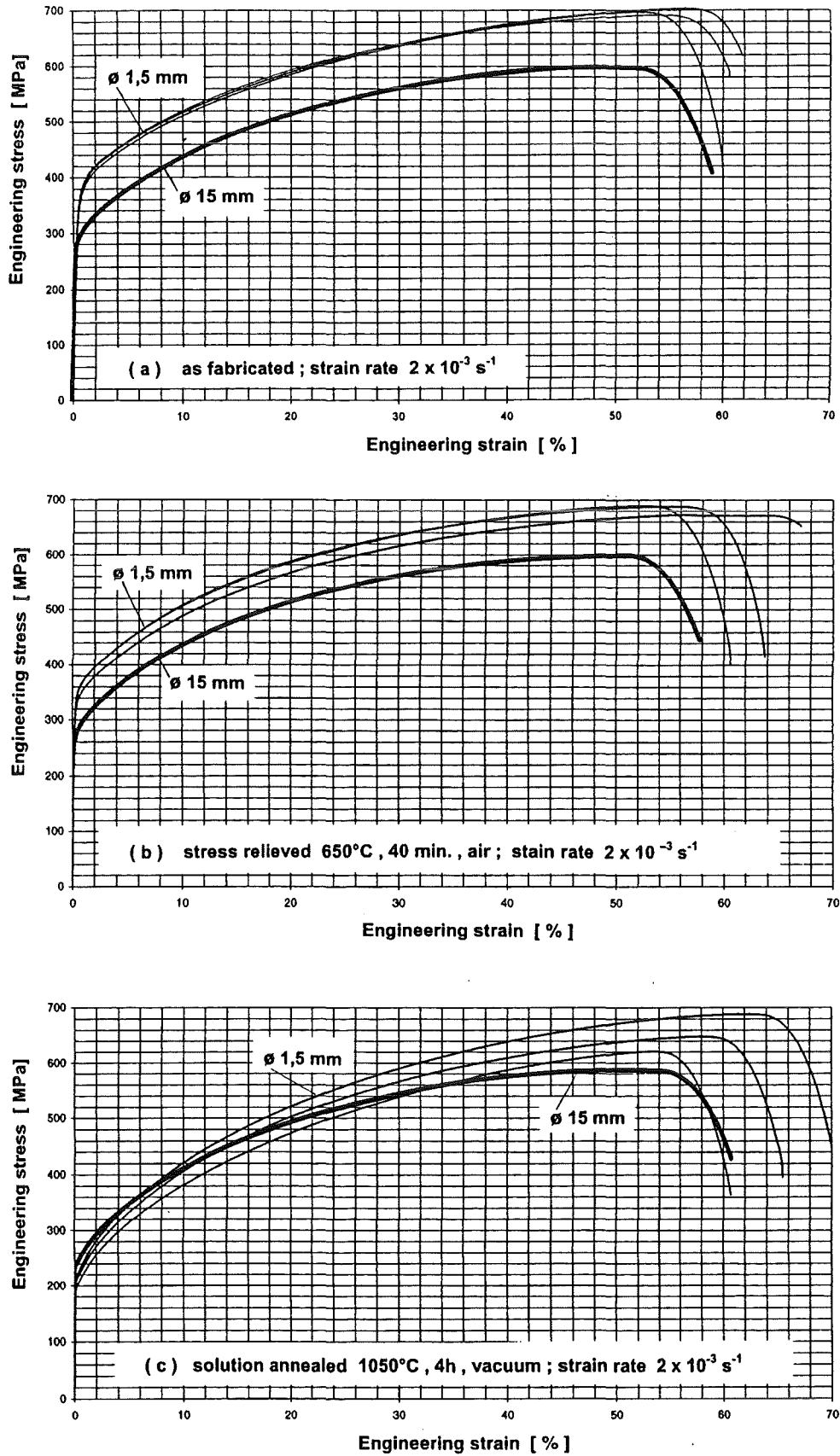


Fig. 2.42 Engineering stress-strain curves of 1.5 and 15 mm diameter tensile specimens of the austenitic steel X5CrNi189 for three different states: (a) as fabricated, (b) stress annealed for 40 min. at 650°C in air, and (c) solution annealed for 4 h at 1050°C in vacuum, from Malmberg et al. (1999, [2.62]).

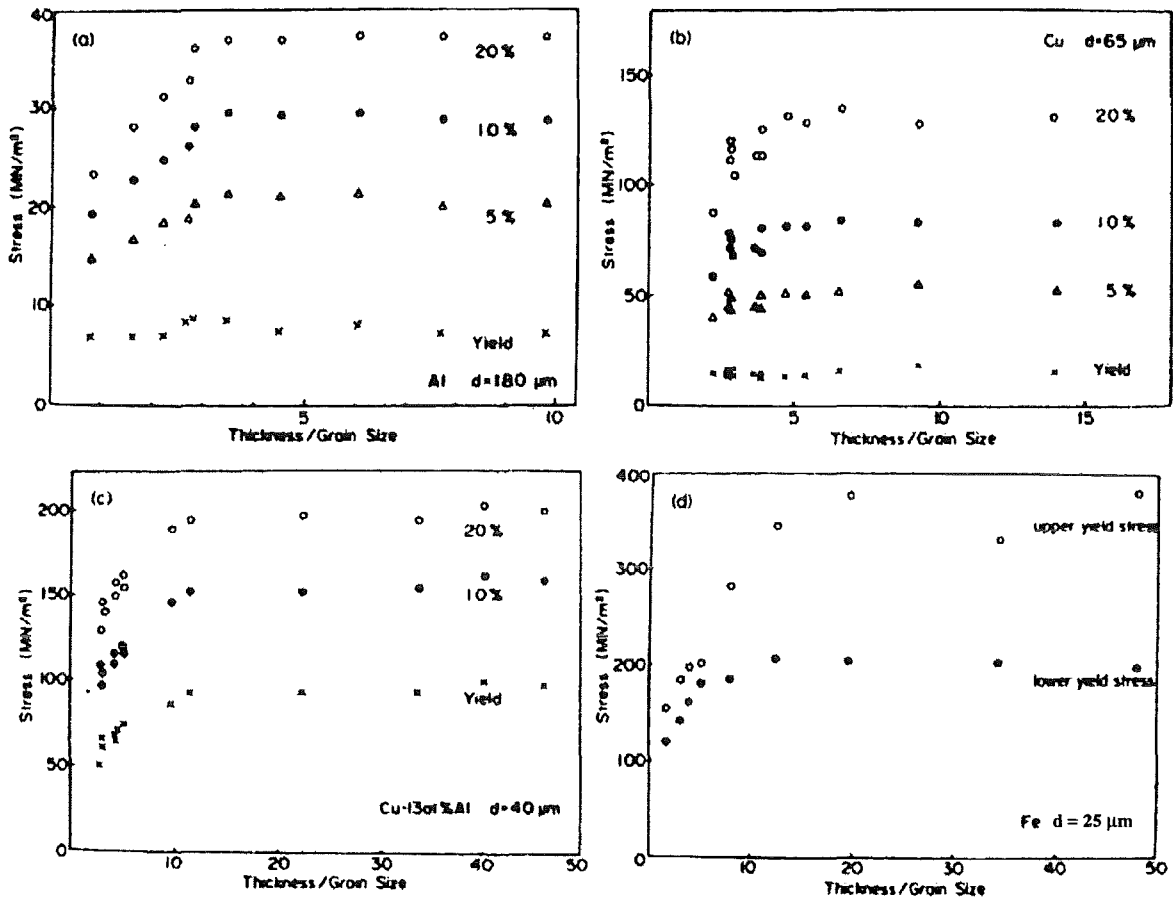


Fig. 2.43 Thickness effect on the flow stress at various strains in polycrystalline (a) Al, (b) Cu, (c) Cu-13 at % Al and (d) Fe; from Miyazaki et al. (1979, [2.51]).

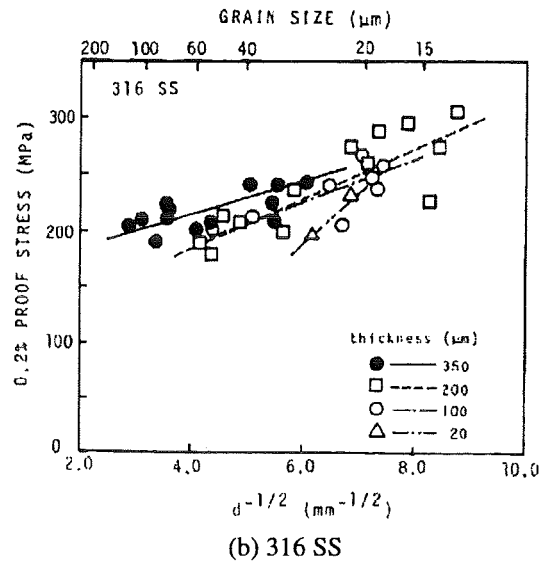
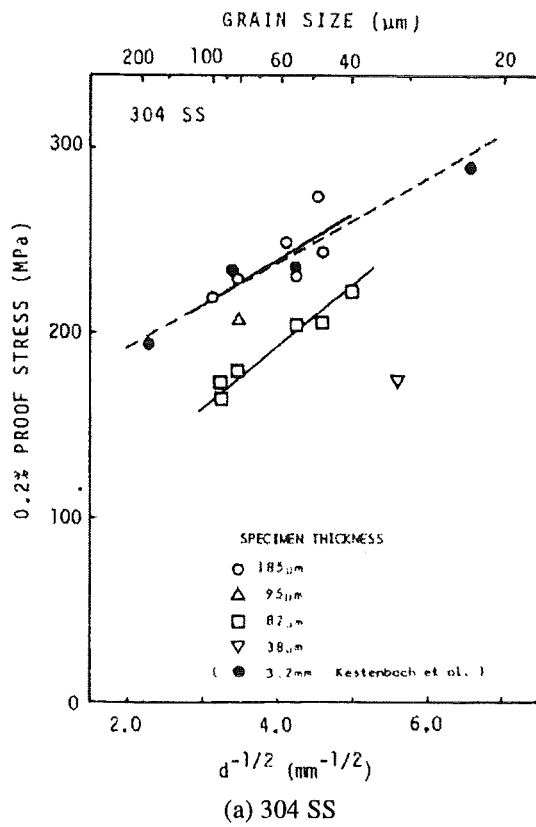


Fig. 2.44 Dependence of the 0.2% proof stress of 304 and 316 stainless steel on grain size d and thickness t ; from Igata et al. (1983, [2.53]).

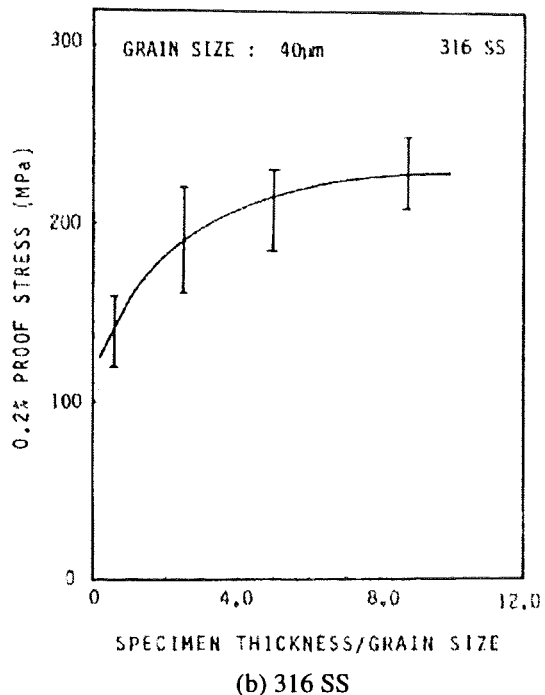
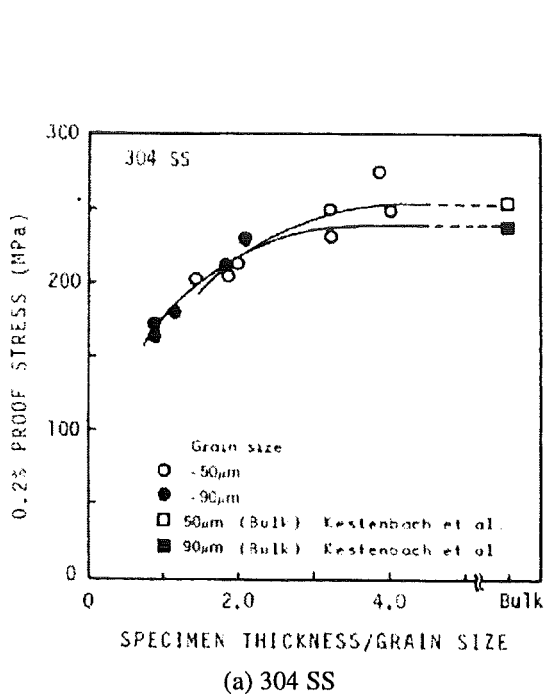
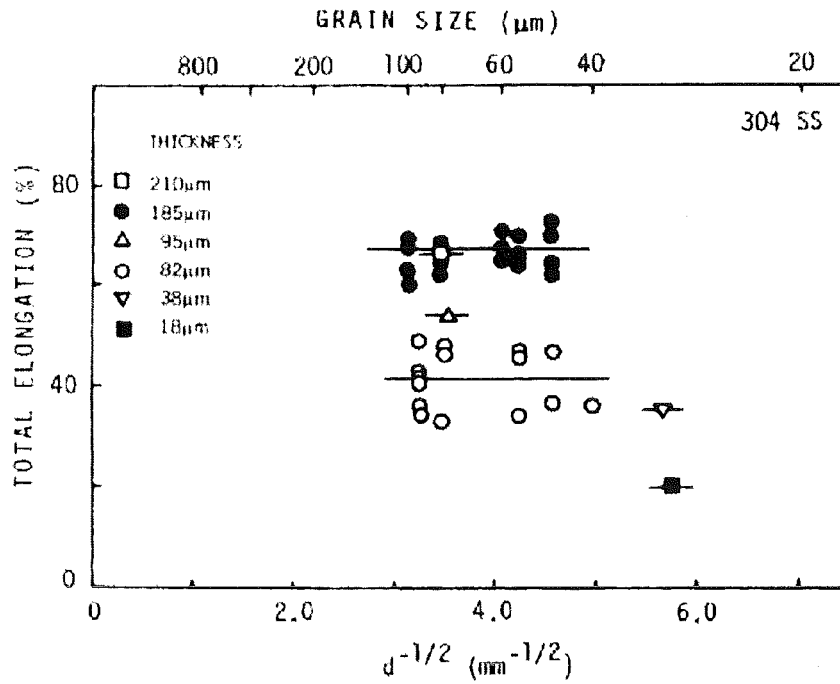
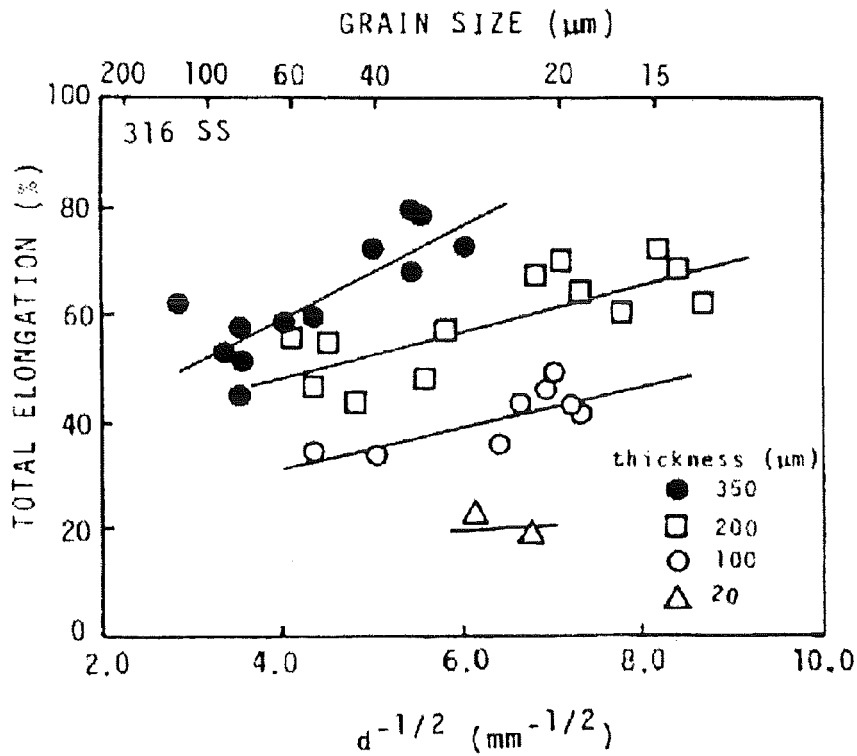


Fig. 2.45 Dependence of the 0.2% proof stress on number of grains per thickness t/d at different grain sizes of 304 and 316 stainless steel; from Igata et al. (1983, [2.53]).



(a) 304 Stainless steel



(a) 316 Stainless steel

Fig. 2.46 Grain size and thickness dependence of the total elongation at fracture of 304 and 316 stainless steel; from Igata et al. (1983, [2.53]).

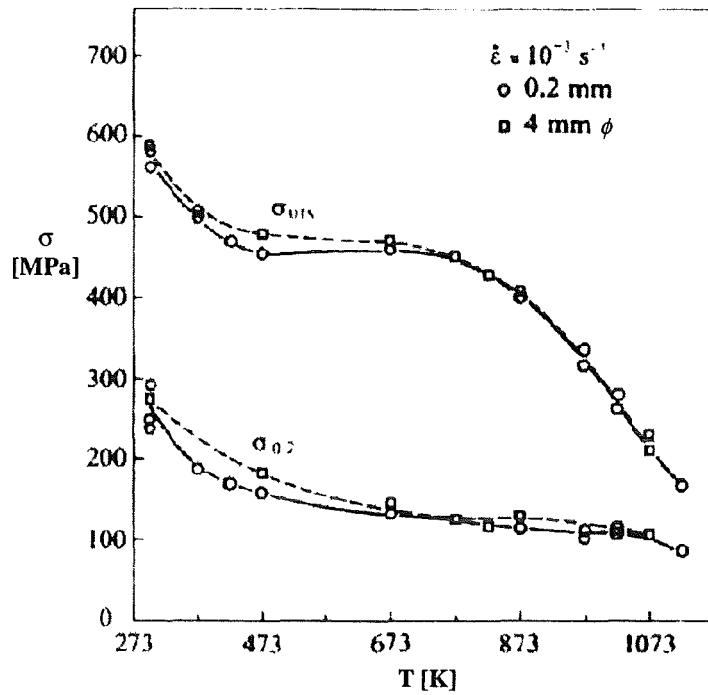


Fig. 2.47 Variation of 0.2% proof stress and ultimate stress with temperature and flat specimen thickness or diameter; from Rickerby et al. (1979, [2.54]).

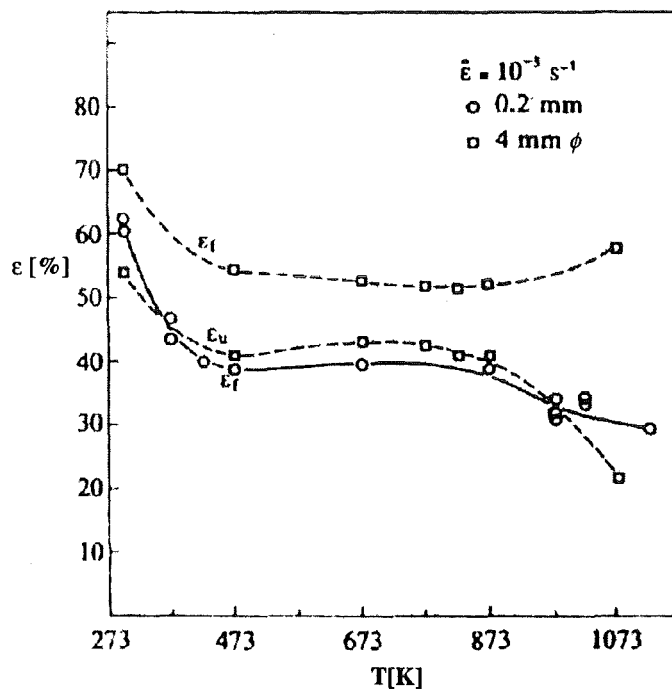


Fig. 2.48 Variation of uniform elongation and elongation at fracture with temperature and flat specimen thickness or diameter; from Rickerby et al. (1979, [2.54]).

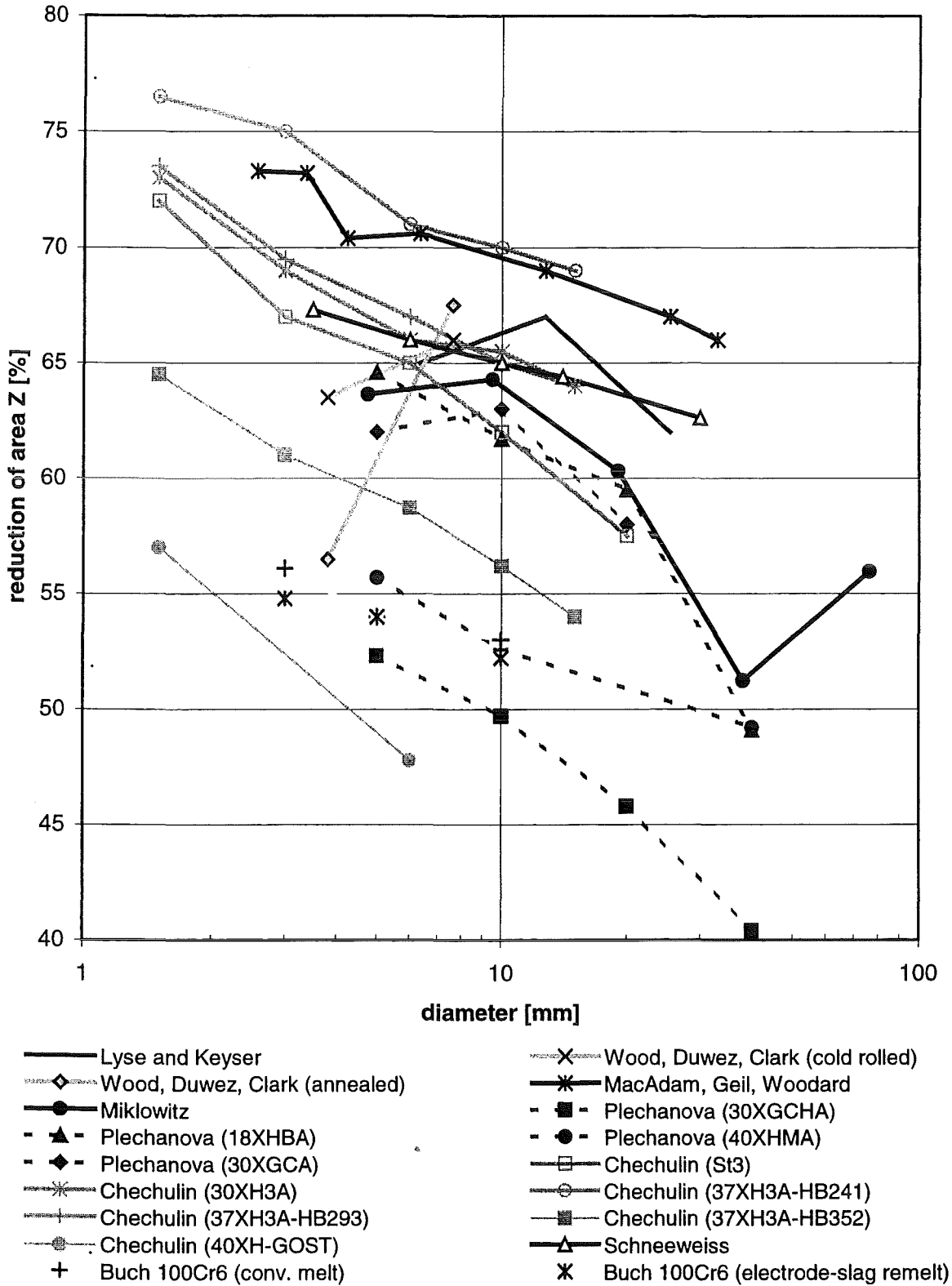


Fig. 2.49: Size dependence of the reduction of area for circular tension specimens